Analysis, modeling and numerical simulation of complex plasmas
under microgravity conditions

Eduardo Rodrigo Gonzalez Tapia

München 2006

Analysis, modeling and numerical simulation of complex plasmas
under microgravity conditions

Eduardo Rodrigo Gonzalez Tapia

Dissertation
an der Fakultät für Physik
der Ludwig–Maximilians–Universität
München

vorgelegt von
Eduardo Rodrigo Gonzalez Tapia
aus Santiago de Chile

München, den 27. Juli 2006

Erstgutachter: Prof. Dr. Dr.h.c. G. Morfill
Zweitgutachter: Prof. Dr. H. Zohm
Tag der mündlichen Prüfung: 16. November 2006

...the electric tension first overcomes the insulation of the dielectric, and proceeds from that point, in an apparently irregular path, so as to take in other weak points, such as particles of dust floating in air...

...These, and many other phenomena of electrical discharge, are exceedingly important, and when they are better understood they will probably throw great light on the nature of electricity as well as on the nature of gases...

J. C. Maxwell

Zusammenfassung

Diese Dissertation hat sich mit dem Prozess der Implementierung numerischer Simulationen auf komplexe Plasmen auseinandergesetzt, aufbauend auf ein Set gekoppelter Partielle Differentialgleichungen. Die Dynamik komplexer Plasmen ist durch die Wechselwirkung ihrer unterschiedlichen Komponenten auf mikroskopischen und mesoskopischen Ebenen charakterisiert worden. Diese Wechselwirkungen resultieren in einer Mischung elektrodynamischer und strömungsdynamischer Effekte. Dieses Differentialgleichungssystem ist mit der Methode der finiten Elemente gelöst worden, die die Verkuppelung verschiedener physikalischer Phänomene in beschränkten Bereichen ermöglicht.

Die Sturm-Liouville Theorie ist als mathematisches Gerüst verwendet worden, um Maxwellsche Gleichungen in beschränkten Hohlraumresonatoren mit inhomogenen Randbedingungen zu lösen. Die Profile der elektrischen Energiedichte sind kalkuliert worden, sowohl für den elektrostatischen Fall, als auch für die ersten sechs Eigenresonanzfrequenzen der elektromagnetischen Wellen. Es hat sich herausgestellt, dass die angelegte Hochfrequenz niedriger als die erste Eigenfrequenz der HF-Plasmakammer ist.

Es hat sich erwiesen, dass sich die elektromagnetische Energie innerhalb der HF-Plasmakammer unter den Eigenfrequenzen aufspaltet, und dass die Rahmenbedingungen bestimmte Resonanzen erzeugen. Die Form und Verteilung dieser elektromagnetischen Energie korrelieren mit den Eigenfunktionen der respektiven Eigenresonanzfrequenzen.

Um eine makroskopische Beschreibung der Dynamik komplexer Plasmen zu erreichen, ist die kinetische Theorie für Modellierung der Strömungsdynamik verwendet worden. Die Kopplung zu den elektromagnetischen Feldern ist auf der kinetischen Ebene durchgeführt worden. Dieses Herangehen überbrückt den Sprung von der mikroskopischen Beschreibung der Boltzmann Gleichung zu einer makroskopischen Beschreibung.

Wir haben festgestellt, dass sowohl die dielektrischen Partikel als auch der Dielektrikumfluss einen "Elektrodruck" empfinden. Hohe Gradienten der elektrischen Energiedichte können die komplexen Plasmen zum Wirbeln bringen. Diese Herangehensweise ist neu, denn die gegenwärtige Theorie betrachtet das Neutralgas im Ruhezustand, dabei wird der Reibungswiderstand auf die komplexen Plasmen ausüben. Die beobachteten Wirbel in dem PK-3 Plus Experiment können durch die Stromlinien dieser Gradienten erklärt werden.

Wir haben herausgefunden, dass der partikelfreie Raum in dem PK-3 Plus Experiment erklärt werden kann, wenn man sowohl die Elektrostatik als auch die erste Eigenresonanzfrequenz der elektrischen Energiedichte der HF-Plasmakammer berücksichtigt. Dies ist durch ein dreidimensionales Modell visualisiert worden. Dieses Model erklärt auch die Bildung sekundürer Räume, die durch die Einführung metallischer Tastkopfe in die HF-Plasmakammer hervorgebracht werden.

Die Hypothese der elektrischen Energiedichte als Quelle der partikelfreien Räume kann durch die Trennung der Partikel in den Plasmakristall-Experimenten geklärt werden. Dielektrophoretische Kräfte stoßen Partikel mit höheren Permittivität (oder größere Partikel, falls alle aus demselben Material sind) in die Richtung der Regionen mit höherer elektrischer Energiedichte. Die Grenze zwischen Partikeln unterschiedlicher Permittivität (oder Größe) ist durch Isoflächen dieser Energiedichte geformt.

Die Erklärung dieser Phänomene (die auf der Distribution elektrischer Energiedichte beruht) bietet einen neuen Standpunkt zur aktuellen Theorie, die auf der Reibungskraft der Ionenströmung basiert.

Contents

Introduction 1

The field of *complex plasmas*[1] has experienced a rapid growth since the theoretical prediction of the "Coulomb crystals" in 1986 and its experimental discovery (in a capacitive coupled low-pressure radio-frequency discharge) almost simultaneously in several laboratories in 1994.[2] Since then, there have been more than 3000 publications in the subject,[3] with almost a new published paper every day.[4]

Even though most of the theoretical and experimental work has focused on the understanding of the basic physics behind these phenomena; there is, however, still a lack of research on the theory of complex plasmas simulations.

This monograph deals with the process of implementing a three dimensional complex plasma model in a computer. Through a classical mechanics description, the forces acting on each one of the complex plasmas components have been derived. These forces are then used within a kinetic theory approach, in order to obtain the macroscopic behavior of complex plasmas under microgravity conditions.

The numerical implementation of this model follows the finite element method (FEM).

1.1 Complex plasmas

"Pure" plasmas are complex systems: electrons, ions and neutral molecules interact with each other via collisions, chemical reactions and with the surroundings via the electromagnetic fields. In this sense, dust particles just introduce another degree of complexity in the dynamics of plasmas. To understand the behavior of such particles is a hot topic for fusion plasma, semiconductor industry and plasma production.

In plasma discharge chambers, dust particles can be produced due to chemical processes among the different plasma components. They can also be etched from the walls of the chamber, or they can be arbitrarily intro-

[1] Also called *dusty plasmas* (PACS number 52.27.Lw).
[2] See Refs. 1-8.
[3] See the reviews in Refs. 64-75.
[4] See Ref. 9.

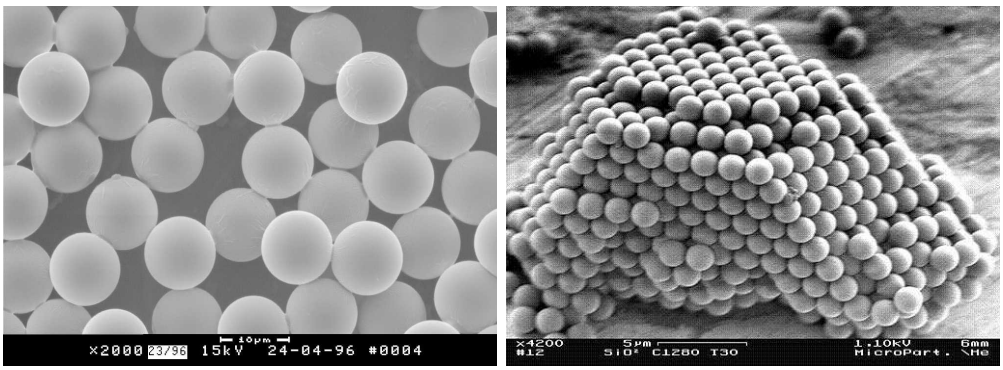

(a) (b)

Figure 1.1: Scanning electron micrograph images of monodisperse spherical particles. (a) Melamine particles of 1 μm in diameter. (b) Silica particles of 1.5 μm in diameter.

duced, like in complex plasmas experiments. In these experiments, sphere (or rod-like particles) of few micrometers in diameter, are intentionally introduced in a plasma chamber in order to observe *plasma crystals*. Most of these experiments use latex, melamine or silica particles. Figure 1.1 shows a scanning electron micrograph of dust particles used in complex plasmas experiments.[5]

The different masses and electric properties of each component, and the diverse length and time-scales associated to the dynamic of their interactions, make complex plasmas simulations a very complicated task.

- While electrons are small, light and fast, the dust particles are much bigger, chubbier and slower.[6]

- Electrons have opposite electric charge than positive ions, the neutral atoms of argon have a polarizability (in unit volume) of 1.5 Å^3. Inside the chamber, there will be approximately 10^{22} neutral atoms per cm^3, 10^{11} ions and electrons, and 10^5 dust particles.

- Ions and neutrals have roughly the same mass and temperature, but the proportion of each component may vary from high temperature[7]

[5] http://www.microparticles.de.

[6] The mass of electrons is 9.11 10^{-31} kg, the mass of argon atoms 6.68 10^{-22} kg and the typical mass of dust particle in complex plasma experiments is 10^{-12} kg.

[7] The temperature in fusion devices is around 10^8 K, and almost all the neutrals are ionized.

till low-temperature plasmas, where the degree of ionization is less than 10^{-8} at room temperature.

- Where the neutrals can be modeled by the kinetic theory of gases, the electrons obey quantum dynamic effects. The dust particles can, however, almost be observed with an unaided eye, and their positions and velocities can be recorded with high resolution video cameras.

- While electrons and ions feel the Lorentz force, paramagnetic particles will feel the magnetic fields, and dielectric particles will be pushed by dielectrophoretic forces. In the laboratory, gravity forces can be neglected for neutral, electrons and ions, but not for micrometer-size particles.

- Laboratory plasmas are contained in vessels or observed in short distance sparks and thrusters (with length-scales ranging from millimeters to meters); atmospheric and astronomical plasmas (lightning, fireballs, auroras and Alfvén waves) have length-scales of kilometers or even longer.

- Further degrees of complexity are also introduced by temperature gradients, convection, viscosity, etc.

Boundary conditions make laboratory plasmas a completely different phenomenon than space plasmas, which can "freely" move around. Boundary conditions force the electromagnetic fields to behave in such a way that the dynamics of the plasma depends on the topology of the cavity.

1.2 Simulating complex systems

Complex plasmas (also called *dusty plasmas*) are complex systems. The presence of electrons, ions, neutrals and dust particles provides a wide range of time, length and mass scales for these phenomena, making it very hard to find the right level of description. Dust particles can be of different materials, sizes and shapes. Metallic dust behaves different than dielectric, paramagnetic or ferromagnetic dust. Moreover, the shape of the dust particles seems to be an important parameter in the dynamic of complex plasmas.[8]

When the model of a physical system contains different time scales, ranging from very fast to very slow, implementing a numerical solution can be

[8] Microrods align in a different way than spherical particles. See Refs. 10-13.

"computationally" very expensive. Computational resolution of the fast time-scales would be outrageously expensive because of the small time steps required, since the needed numerical time-step has to be at least as small as the fastest time-scale of the system.

In order to extract physical knowledge from a complex system, one must focus on the right level of description. A N-body simulation, based on the interaction of particles with each other (molecular dynamics, PIC codes, etc.), is useful for microscopic or mesoscopic scales (of time and length). Nevertheless, to simulate three-dimensional models at macroscopic scales with these techniques demands an extraordinary computational effort, since the computational cost increases with the square of the number of particles used in the simulation.[9]

Further numerical problems arise from the calculation of N(N-1)/2 distances (and the unavoidable use of square-root algorithms) in every time-step. Most of the time, the problem under study has interesting properties at a coarse level of description. So after intensive calculations, one still has to calculate averages in order to get temperatures, densities, mean velocities, or any other macroscopic quantity of interest.

The dynamics of complex systems in biology, economics and physics is dictated by the behavior of each one of their components and their collective interaction. Therefore, finding the right connection between the microscopic and the macroscopic scales seems to be the key issue in order to obtain a good model. Furthermore, the use of the right level of description will help to catch the phenomena of interest: "Don't model bulldozers with quarks".[10]

The complex behavior of fluids and gases is also caused by molecular interactions. One way of achieving a macroscopic description of their dynamics is to proceed from the atomistic equations of motion to a continuum description via the kinetic theory of gases or some other coarse-graining theory.

1.3 Complex plasmas under microgravity

Complex plasmas formed under microgravity conditions have been intensively investigated in radio-frequency discharges during the last ten years. The first attempts to create plasma crystals in weightless environments (parabolic flights and Texus rockets) were reported by Morfill *et al.* in 1996.[11]

The PKE-Nefedov experiment was launched to the International Space Station (ISS) in February 2001, and finished its operation in December 2005.

[9] See for instance Ref. 14.
[10] See Ref. 15.
[11] See Refs. 16-24.

It carried out 13 experimental missions, with the result of more than 50 hours of microgravity experiments.[12] It was the first long term experiment on complex plasmas in space. Since January 2006, the PK-3 Plus laboratory is in operation onboard the ISS. This second generation project was created within the framework of a Russian-German scientific cooperation program, as well as its predecessor PKE-Nefedov.

One of the most interesting phenomena observed in the PKE experiment was the formation of a void, a dust-free region in the center of the plasma chamber. It appeared already with few particles, and it was present in a wide region of parameters of the plasma discharge. This phenomenon has been observed both on ground-based[13] as well as in gravity-free experiments.[14] The causes of this phenomenon have also been intensively analyzed and different theories have been proposed.[15]

The most believed theory of void formation is attributed to the ion-drag force.[16] Yet, this approach has not been exempt of controversies.[17] Other interesting observed phenomenon is the formation of vortices close to the electrode edges.[18]

The internal structure of the PKE chamber made the attempts of making three-dimensional simulations a very complicated task. The new PK-3 Plus chamber consists of an improved geometry, which avoids the inhomogeneities of the first chamber. It also includes new electronics, pumps, extra video cameras, and further technical advances.

All of these improvements have not only resulted in a more reliable control of the plasma parameters and a more homogeneous discharge, but have also made the implementation of a computational model a much easier task.

1.4 Outlook

This monograph offers a description of the formation of voids, vortices and the separation of dust particles of different sizes in complex plasma experiments, alternative to the ion-drag theory.

This point of view is based on the distribution of the electromagnetic energy inside the PK-3 Plus plasma chamber. It allows to describe the forma-

[12] http://www.mpe.mpg.de/theory/plasma-crystal.
[13] See Refs. 17-23.
[14] See Refs. 24-31.
[15] See Refs. 32-48.
[16] See Refs. 18, 49-58.
[17] See Refs. 52-54.
[18] See Refs. 59-63.

tion of voids and vortices, and the de-mixing of particles in three-dimensional cavities.

The proposed interpretation is based in a three-dimensional computational model, which makes it possible to simulate the non-homogeneities of the electric fields. This model is based on the finite element method, a numerical method which is optimal while minimizing the error of the computed solution. This approach also allows managing non-uniform grids in complex geometries, like the PK-3 Plus chamber.

A clear picture of the electromagnetic fields inside the chamber is crucial for understanding the macroscopic behavior of complex plasmas dynamics. For instance, the knowledge (with a certain degree of accuracy) of the direction of the electric lines of force, allows us "to see" the forces acting on the complex plasma components. Only an accurate three dimensional model of the chamber will let us reach this goal. Also, the implementation of an appropriate numerical scheme is a must.

By means of the finite element method, it is possible to create a virtual prototype of the chamber. In order to obtain a macroscopic description of the whole process, these electromagnetic fields are coupled with the dynamics of the complex plasmas components at the kinetic level. Complex plasmas experiments offer the possibility to study the kinetics of each dust grain, and also to study the collective behavior of the whole system. This thesis explores how microscopic properties are extrapolated in the macroscopic formation of voids and vortices.

As a first step, the density of the electromagnetic energy has been calculated, both in the dc regime (or zero frequency) and when the first resonant mode of the cavity is exited. The Sturm-Liouville theory is used in order to find a mathematical description of this electromagnetic *boundary value problem* (BVP). Both, the PKE and the PK-3 Plus experiments can be modeled as boundary value problems. Indeed, without providing the required energy (in order to ionize the neutral gas), it is not possible to observe any kind of complex plasma. In these experiments, the required energy is provided through external power supplies, which force the electrodes at a certain radio-frequency voltage.

This monograph will show how the formation of voids and vortices is correlated with the way in which the electromagnetic energy distributes inside the chamber. The computational model allows us to estimate the profile of the electric energy density, and in this way imagining how this energy may influence the dynamics of complex plasmas.

The following chapter describes the necessary mathematical background in order to numerically calculate electric fields in complex geometries. This implementation will allow us to visualize the way in which the electromag-

netic energy distributes, both in the electrostatic case and when the fields are time-dependent.

Chapter 3 describes how electromagnetic forces impel the motion of point charges, point dipoles and polarized particles. This classical mechanics derivation uses the electromagnetic fields previously described in Chap. 2, and settles the starting point for a macroscopic description of complex plasmas.

A macroscopic description of complex plasmas is obtained in Chap. 4. Starting from a microscopic description of it constituents, the kinetic theory is used in order to obtain a macroscopic description of great amounts of particles of different types. The macroscopic forces are obtained from the interaction of the electromagnetic fields with the microscopic components of complex plasmas.

Chapter 5 gives a brief introduction to the PK-3 Plus experiment. This chapter describes the main technical details of this second generation complex-plasma facility onboard the International Space Station ISS.

Chapter 6 presents the main results of this monograph, and Chap. 7 discusses its future implications. There is also an appendix which briefly describes the finite element method.

Maxwell equations in cavities

2

Maxwell equations describe how electric charges produce electric fields (Gauss law), the experimental absence of magnetic charges, how changing magnetic fields produce electric fields (Faraday law of induction) and how currents produce magnetic fields (Ampère law).

Maxwell put these partial differential equations together and applied a correction to the Ampère law: alternating electric fields act like currents, and therefore act like a source of magnetic fields. Later, O. Heaviside and W. Gibbs reformulated the original quaternion representation of Maxwell by using vector analysis.[1] Nowadays this mathematical formulation is the most used, although there are other representations.[2]

The importance of Maxwell work is that the four equations plus his correction, predict waves of oscillating electric and magnetic fields:

> *This velocity is so nearly that of light, that it seems we have strong reason to conclude that light itself (including radiant heat, and other radiations if any) is an electromagnetic disturbance in the form of waves propagated through the electromagnetic field according to electromagnetic laws.*[3]

The hyperbolic behavior of the electromagnetic fields is crucial while implementing numerical methods capable to describe how electromagnetic fields distribute inside resonant cavities.

The following sections will give a brief introduction to the field of computational electromagnetism. These concepts will then be used for estimating the distribution of electromagnetic energy inside a plasma chamber.

2.1 Maxwell equations

Let us denote the *electric field* as $\mathbf{E}(\mathbf{x}, t)$, the *magnetic field* as $\mathbf{B}(\mathbf{x}, t)$, the *charge density* as $\rho(\mathbf{x}, t)$ and the *current density* as $\mathbf{J}(\mathbf{x}, t)$. By using this

[1] O. Heaviside called this vectorial representation the *duplex equations* in a paper to *The Electrician* in 1885. See Refs. 76-77.

[2] See Ref. 78.

[3] See Ref. 79 p. 535.

notation,[4] the Maxwell equations in SI units read[5]

$$\nabla \cdot \mathbf{E} = \frac{\rho}{\epsilon_0} \tag{2.1}$$

$$\nabla \cdot \mathbf{B} = 0 \tag{2.2}$$

$$\nabla \times \mathbf{E} + \frac{\partial \mathbf{B}}{\partial t} = 0 \tag{2.3}$$

$$\nabla \times \mathbf{B} - \frac{1}{c^2}\frac{\partial \mathbf{E}}{\partial t} = \mu_0 \mathbf{J} \tag{2.4}$$

where ϵ and μ are the permittivity and permeability of the media, and $c = \sqrt{1/\epsilon\mu}$ is the speed of the electromagnetic waves.[6]

By taking the curl of Eq. (2.3), using the vector identity (B.1) with the gradient of Eq. (2.1) and the time derivative of Eq. (2.4), we obtain the wave equation for the electric field

$$-\nabla^2 \mathbf{E} + \frac{1}{c^2}\frac{\partial^2 \mathbf{E}}{\partial t^2} = -\frac{1}{\epsilon_0}\nabla\rho - \mu_0 \frac{\partial \mathbf{J}}{\partial t}. \tag{2.5}$$

In the same way, by taking the curl of Eq. (2.4), and using the vector identity (B.2) with Eq. (2.2) and the time derivative of Eq. (2.3), we get the wave equation for the magnetic field

$$-\nabla^2 \mathbf{B} + \frac{1}{c^2}\frac{\partial^2 \mathbf{B}}{\partial t^2} = \mu_0 \nabla \times \mathbf{J}. \tag{2.6}$$

The expressions on the *r.h.s.* of Eqs. (2.5) and (2.6) represent the sources of the electromagnetic fields.

2.1.1 Electric and magnetic potentials

Maxwell equations, as outlined in the previous section, conform a set of six inhomogeneous hyperbolic partial differential equations (one PDE per each component of $\mathbf{E}$ and $\mathbf{B}$). It is possible to reduce the number of PDEs by expressing these equations in terms of the electric and magnetic potentials.

Let us consider the definitions of electric and magnetic fields, and the

[4] For simplicity, we will indistinctly use $\mathbf{E}$, $\mathbf{B}$, etc. instead of $\mathbf{E}(\mathbf{x}, t)$, $\mathbf{B}(\mathbf{x}, t)$.

[5] See Ref. 80 Chap. 18.

[6] The subindex "0" denotes vacuum properties.

Lorenz[7] gauge

$$\mathbf{E} = -\nabla\phi - \frac{\partial \mathbf{A}}{\partial t} \tag{2.7}$$

$$\mathbf{B} = \nabla \times \mathbf{A} \tag{2.8}$$

$$\frac{1}{c^2}\frac{\partial \phi}{\partial t} = -\nabla \cdot \mathbf{A} \tag{2.9}$$

where $\phi(\mathbf{x}, t)$ represents the *electric potential* and $\mathbf{A}(\mathbf{x}, t)$ the *magnetic potential*.

By taking the divergence of Eq. (2.7) together with Eq. (2.9), one obtains the wave equation for the electric potential

$$\nabla \cdot \mathbf{E} = -\nabla^2\phi + \frac{1}{c^2}\frac{\partial^2 \phi}{\partial t^2}. \tag{2.10}$$

On the other hand, by deriving Eq. (2.7) with respect to the time variable and then dividing it by c^2, it becomes

$$\frac{1}{c^2}\frac{\partial \mathbf{E}}{\partial t} = -\frac{1}{c^2}\frac{\partial \nabla\phi}{\partial t} - \frac{1}{c^2}\frac{\partial^2 \mathbf{A}}{\partial t^2} \tag{2.11}$$

together with the gauge condition and the vector identity (B.3), we obtain

$$\frac{1}{c^2}\frac{\partial \mathbf{E}}{\partial t} = \nabla\nabla \cdot \mathbf{A} - \frac{1}{c^2}\frac{\partial^2 \mathbf{A}}{\partial t^2} = \nabla \times \mathbf{B} + \nabla^2\mathbf{A} - \frac{1}{c^2}\frac{\partial^2 \mathbf{A}}{\partial t^2}. \tag{2.12}$$

These formulations (Eq. (2.10) together with Eq. (2.1) and Eq. (2.12) with Eq. (2.4)) lead to expressions of the wave equation for the electric and magnetic potentials,[8] subject to charge and current density sources

$$-\nabla^2\phi + \frac{1}{c^2}\frac{\partial^2 \phi}{\partial t^2} = \frac{\rho}{\epsilon_0} \tag{2.13}$$

$$-\nabla^2\mathbf{A} + \frac{1}{c^2}\frac{\partial^2 \mathbf{A}}{\partial t^2} = \mu_0\mathbf{J} \tag{2.14}$$

2.2 Maxwell equations in cavities

In empty space, the solution of the Maxwell equations (either for the potentials ϕ and $\mathbf{A}$, or for the fields $\mathbf{E}$ and $\mathbf{B}$) is a planar wave traveling with the speed of light. The planar behavior drastically changes when the traveling

[7] See Ref. 81 p. 240.
[8] See Ref. 80 Chap. 18, Ref. 81 p. 240.

waves are forced inside a cavity. The walls of the cavity will impose *boundary conditions* on these partial differential equations.

From a mathematical point of view, Maxwell equations conform a well-posed set of PDEs (in the sense of Hadamard[9]) regarding that they are provided with suitable boundary conditions.

Let us consider a vacuum cavity Ω enclosed by conducting and insulating walls. The behavior of the electromagnetic fields inside this cavity will be solely dictated by the boundary conditions. These boundary conditions may be of the Dirichlet, Neumann or Robin type. For instance, conducting walls might be forced (by an external source, which can also be time-dependent) to be at a certain fixed potential (*Dirichlet boundary conditions*); insulating walls might be modeled by *Neumann* or *Robin boundary conditions*, and a floating potential wall can be defined in terms of weak constrains.

For example, the boundary between a cavity (containing a medium of permittivity ϵ and permeability μ) and a perfect conductor (of infinite conductivity) is modeled as[10]

$$\epsilon \mathbf{E} \cdot \mathbf{n} = -\sigma_s \qquad \mathbf{E} \times \mathbf{n} = 0 \qquad \phi = \phi_0 \qquad \mathbf{B} \times \mathbf{n} = \mu \mathbf{J}_s \qquad \mathbf{B} \cdot \mathbf{n} = \mathbf{0}$$

where the normal $\mathbf{n}$ points outwards the cavity, σ_s is the surface charge density, $\mathbf{J}_s$ is the surface current density and ϕ_0 is the electric potential of the conductor.

When the external sources impose time-dependent boundary conditions, they will excite resonances where the electromagnetic energy is exchanged between the electric and magnetic fields.

Every cavity will have an infinite number of resonant frequencies[11] depending on its topology. Each of them will have a well defined structure for the associated electromagnetic energy, but only the excited modes will concentrate the energy in their respective electromagnetic fields. The resultant field pattern (either for the electric or magnetic fields) will primary be the sum of the field patterns associated to the exited modes.

When a dielectric material is placed inside a vacuum cavity the resonant frequencies of the normal modes will shift, and the respective resonance curves will stretch depending on the material's permittivity. Also, the bandwidth will be broadened depending on the energy losses (any kind of work done by the electromagnetic fields, or by losses of energy through the walls).

For complex geometries, the only way of estimating the resonant frequencies and the structure of their electromagnetic fields is to use numerical

[9] See Refs. 180-181. See also Appendix A.

[10] See Ref. 85 Chap. 9. The normal $\mathbf{n}$ points towards the perfect conductor.

[11] The lowest resonant frequency is called the *fundamental frequency*.

simulations. The following section will provide the necessary mathematical background in order to numerically obtain the resonant frequencies of a three-dimensional cavity.

2.3 Sturm-Liouville theory

Let Ω be a simple bounded domain in $\mathbb{R}^3$ with boundary $\Gamma \equiv \partial\Omega$ and unit outward normal $\mathbf{n}$. Let us assume that there will be two kind of boundaries, i.e. $\Gamma = \Gamma_1 \cup \Gamma_2$. The Dirichlet (essential) boundary condition is represented as $\phi(\mathbf{x}, t) = g(\mathbf{x}, t)$ on Γ_1 and the Neumann (natural) boundary condition as $\nabla\phi(\mathbf{x}, t) \cdot \mathbf{n} = h(\mathbf{x}, t)$ on Γ_2. The electric potential $\phi(\mathbf{x}, t)$ will be defined in every point $\mathbf{x} \in \Omega$ at every time $t \in (0, T)$ by solving (2.13) in $\Omega \times (0, T)$ with the boundary conditions imposed on $\Gamma \times (0, T)$. We can write this problem in a compact form

$$\begin{aligned} -\nabla^2\phi + \frac{1}{c^2}\frac{\partial^2\phi}{\partial t^2} &= \frac{\rho}{\epsilon_0} \quad && \text{in } \Omega \times (0, T) \\ \phi &= g \quad && \text{on } \Gamma_1 \times (0, T) \\ \nabla\phi \cdot \mathbf{n} &= h \quad && \text{on } \Gamma_2 \times (0, T). \end{aligned} \tag{2.15}$$

This inhomogeneous hyperbolic partial differential equation turns to be homogeneous for a vacuum cavity, since $\rho = 0$. This PDE is also well-posed.

Let us consider the most general case, which is the inhomogeneous wave equation representing either the potential ϕ or each component of the vectors $\mathbf{A}$, $\mathbf{E}$ or $\mathbf{B}$ (from equations (2.13), (2.14), (2.5) or (2.6)) subject to general Dirichlet and Neumann boundary conditions.[12] We can also write this general problem in a compact form

$$\begin{aligned} -\nabla^2 u + \frac{1}{c^2}\frac{\partial^2 u}{\partial t^2} &= f \quad && \text{in } \Omega \times (0, T) \\ u &= g \quad && \text{on } \Gamma_1 \times (0, T) \\ \nabla u \cdot \mathbf{n} &= h \quad && \text{on } \Gamma_2 \times (0, T). \end{aligned} \tag{2.16}$$

The general solution to this problem can be split into the sum of the solutions to the *particular* and the *homogeneous problems*

$$u(\mathbf{x}, t) = u_P(\mathbf{x}, t) + u_H(\mathbf{x}, t).$$

The next subsections will describe the method for obtaining such solutions.

[12] It can easily be extended to boundary conditions of the Robin type.

2.3.1 The homogeneous solution

Let us first find the solution to the homogeneous problem

$$\begin{aligned} -\nabla^2 u_H + \frac{1}{c^2}\frac{\partial^2}{\partial t^2} u_H = 0 \qquad & \text{in } \Omega \times (0,T) \\ u_H = g \qquad & \text{on } \Gamma_1 \times (0,T) \\ \nabla u_H \cdot \mathbf{n} = h \qquad & \text{on } \Gamma_2 \times (0,T), \end{aligned} \tag{2.17}$$

and suppose that its solution can be separated into two functions, one of them depending on the time variable t, and the other depending on the space variable $\mathbf{x}$:

$$u_H(\mathbf{x},t) = \tau(t)\psi(\mathbf{x}).$$

It is easy to prove, by separation of variables (since the operator $-\nabla^2 + \frac{1}{c^2}\frac{\partial}{\partial t^2}$ is *linear* and *homogeneous*), that[13]

$$\frac{\nabla^2\psi(\mathbf{x})}{\psi(\mathbf{x})} = \frac{1}{c^2}\frac{\ddot{\tau}(t)}{\tau(t)}. \tag{2.18}$$

The *l.h.s.* only depends on the variable $\mathbf{x}$, and the *r.h.s.* only depends on the variable t. Thus, this equality must be equal to a constant independent on $\mathbf{x}$ and t

$$\frac{\nabla^2\psi(\mathbf{x})}{\psi(\mathbf{x})} = \frac{1}{c^2}\frac{\ddot{\tau}(t)}{\tau(t)} = -\lambda. \tag{2.19}$$

- The "electrostatic" case is achieved when $\lambda = 0$. The general solution of $\ddot{\tau} = 0$ is $\tau(t) = \alpha t + \beta$. Since the solution cannot linearly grow with time, it is concluded that $\tau(t) = \beta$ is constant in time. Then, we just have to solve $\nabla^2\psi = 0$ subject to the boundary conditions on Γ (see Sec. 2.4).

- On the other hand, if $\lambda < 0$, the time-dependent part $\tau(t)$ grows exponentially with time (as a linear combination of $\sinh(\sqrt{\lambda}ct)$ and $\cosh(\sqrt{\lambda}ct)$).

- When $\lambda > 0$ the solution of $\ddot{\tau} = -\lambda c^2\tau$ will be $\tau(t) = \alpha e^{j\omega t} + \beta e^{-j\omega t}$ with $\omega = \sqrt{\lambda}c$, (or equivalently $\tau(t) = a\sin(\omega t) + b\cos(\omega t)$) with constants α and β (or a and b) depending on the initial conditions $u_0 = u(\mathbf{x},0)$.

[13] If we normalize the space and time variables, so $\mathbf{x} = L\overline{\mathbf{x}}$ and $t = T\bar{t}$, this equality becomes

$$\frac{\overline{\nabla}^2\psi(\overline{\mathbf{x}})}{\psi(\overline{\mathbf{x}})} = \frac{1}{\bar{c}^2}\frac{\ddot{\tau}(\bar{t})}{\tau(\bar{t})} \qquad \text{where } \bar{c} = cT/L \text{ is also dimensionless (see Sec. 4.3.3).}$$

Eigenvalues and eigenfunctions

The solution of Eq. (2.19)

$$\nabla^2\psi + \lambda\psi = 0 \tag{2.20}$$

with $\lambda > 0$ give[14] rise to an *infinite* set of non-trivial solutions.

The eigenvalues $\lambda_n > 0$ are associated to their respective eigenfunctions by

$$\nabla^2\psi_n + \lambda_n\psi_n = 0, \tag{2.21}$$

and to the respective normal modes by

$$\ddot{\tau}_n = -\lambda_n c^2\tau_n = -\omega_n^2\tau_n, \tag{2.22}$$

where the eigenfrequencies are $\omega_n = \sqrt{\lambda_n}c$.

Multiplying Eq. (2.21) by τ_n and then using Eq. (2.22) it gives

$$\begin{aligned}\nabla^2\psi_n\tau_n + \lambda_n\psi_n\tau_n &= \nabla^2\psi_n\tau_n - \frac{1}{c^2}\psi_n\ddot{\tau}_n \\ &= \nabla^2 u_n - \frac{1}{c^2}\frac{\partial^2}{\partial t^2}u_n = 0\end{aligned}$$

Since $u_n(\mathbf{x},t) = \tau_n(t)\psi_n(\mathbf{x})$ satisfies the homogeneous equation (2.17), the solution to the homogeneous problem can be written as a linear combination of $u_n = \tau_n\psi_n$

$$u_H(\mathbf{x},t) = \sum_{n=1}^{\infty} a_n\tau_n(t)\psi_n(\mathbf{x}) = \sum_{n=1}^{\infty} A_n(t)\psi_n(\mathbf{x}), \tag{2.23}$$

where the functions $A_n(t) = a_n\tau_n(t)$ can be found by evaluating u_H on the boundary Γ, and by considering the initial conditions $u_H(\mathbf{x},0)$.

Let us introduce the concept of *inner product* between two functions $\phi(\mathbf{x})$ and $\varphi(\mathbf{x})$

$$(\phi,\varphi) \doteq \int_\Omega \phi(\mathbf{x})\varphi(\mathbf{x})d\mathbf{x}.$$

[14] If we multiply $\nabla^2\phi + \lambda\phi = 0$ by ϕ and then we integrate over the domain Ω, we obtain $\int\left(\phi\nabla^2\phi + \lambda\phi^2\right)d\mathbf{x} = 0$, and then by using the Green's identity together with homogeneous boundary conditions, we obtain

$$\int_\Omega \nabla\phi\cdot\nabla\phi d\mathbf{x} = \lambda\int_\Omega \phi^2 d\mathbf{x}, \qquad \text{since both integrals are positive, } \lambda \text{ must also be positive.}$$

This inner product defines the L^2-norm in Ω

$$\|\varphi\| \doteq \sqrt{\int_\Omega \varphi^2 d\mathbf{x}} = \sqrt{(\varphi,\varphi)},$$

and functions with finite L^2-norm define an infinite-dimensional *function space*

$$L^2(\Omega) = \left\{ \varphi : \int_\Omega \varphi^2 d\mathbf{x} < \infty \right\}.$$

The expansion of the homogeneous solution in terms of the eigenfunctions $\psi_n(\mathbf{x})$ is possible because this set is a generalized Fourier basis. The eigenfunctions form a *complete basis*,[15] meaning that any piecewise smooth function $f(\mathbf{x})$ (with $\mathbf{x} \in \Omega$) can be represented by the series (also called generalized Fourier series)

$$f(\mathbf{x}) = \sum_{n=1}^{\infty} f_n \psi_n(\mathbf{x})$$

by choosing the appropriated set of coefficients $f_n = (f(\mathbf{x}), \psi_n(\mathbf{x}))$.[16]

Also, the eigenfunctions are orthogonal and can be normalized

$$(\psi_n, \psi_m) = \begin{cases} 0 & \text{if } n \neq m \\ 1 & \text{if } n = m \end{cases} \tag{2.24}$$

and are related to the eigenvalues by[17]

$$(-\nabla^2\psi_n, \psi_m) = (\psi_n, -\nabla^2\psi_m) = \begin{cases} 0 & \text{if } n \neq m \\ \lambda_n & \text{if } n = m. \end{cases} \tag{2.25}$$

The eigenfunctions also satisfy homogeneous boundary conditions, i.e.

$$\begin{aligned} \psi_n &= 0 && \text{on } \Gamma_1 \\ \nabla\psi_n \cdot \mathbf{n} &= 0 && \text{on } \Gamma_2. \end{aligned}$$

[15] $V \subset L^2(\Omega)$ such $V = \left\{ v : \int_\Omega v^2 d\mathbf{x} < \infty;\ v = 0 \text{ on } \Gamma_1;\ \nabla v \cdot \mathbf{n} = 0 \text{ on } \Gamma_2 \right\}$.

[16] If we denote the error of the approximation as $e_N = f - \sum^N f_n\psi_n$, we can find that

$$\|e_N\|^2 = \left(f - \sum_{n=1}^{N} f_n\psi_n, f - \sum_{n=1}^{N} f_n\psi_n \right) = \|f\|^2 - \sum_{n=1}^{N} f_n^2 \qquad \text{and} \qquad \|e_N\|^2 \xrightarrow{N\to\infty} 0.$$

[17] Note that the operator $L(\psi) = -\nabla^2\psi = \lambda\psi$ is *self-adjoint*.

When the domain Ω is one-dimensional, Fourier series can represent any function in terms of orthogonal bases of sines and cosines (also, the eigenvalues λ_n can be analytically found). For three-dimensional problems (in complex geometries), the eigenfunctions ψ_n do not follow such a nice sinusoidal representation (neither the eigenvalues λ_n follow an analytical form), and in order to get an idea of their shape, we have to use a computational approach. The finite element method (FEM) have been used for obtaining the eigenfrequencies and eigenfunctions of the PK-3 Plus chamber.[18]

2.3.2 The particular solution

Let us now investigate the solution to the particular problem

$$\begin{aligned} -\nabla^2 u_P + \frac{1}{c^2}\frac{\partial^2}{\partial t^2} u_P &= f \qquad \text{in } \Omega \times (0,T) \\ u_P &= 0 \qquad \text{on } \Gamma_1 \times (0,T) \\ \nabla u_P \cdot \mathbf{n} &= 0 \qquad \text{on } \Gamma_2 \times (0,T). \end{aligned} \tag{2.26}$$

Since the eigenfunctions ψ_n form a complete set in Ω, any well-behaved function $f(\mathbf{x},t)$ (which can be separated into $f(\mathbf{x},t) = F(t)X(\mathbf{x})$) can be represented as the linear combination

$$f(\mathbf{x},t) = \sum_{n=1}^{\infty} f_n(t)\psi_n(\mathbf{x})$$

regarding that the functions f_n are properly chosen as $f_n(t) = (f(\mathbf{x},t), \psi_n(\mathbf{x}))$. Also, the particular solution can be written by using the *Ansatz*[19]

$$u_P(\mathbf{x},t) = \sum_{n=1}^{\infty} b_n(t)\psi_n(\mathbf{x}). \tag{2.27}$$

By using this Ansatz on Eq. (2.26)

$$\begin{aligned} -\nabla^2 u_P + \frac{1}{c^2}\frac{\partial^2}{\partial t^2} u_P &= f \\ \sum_{n=1}^{\infty}\left(-b_n\nabla^2\psi_n + \frac{1}{c^2}\ddot{b}_n\psi_n\right) &= \sum_{n=1}^{\infty} f_n\psi_n, \end{aligned}$$

[18] The expansion of the solution of a cold plasma in terms of eigenfunctions of the cavity was discussed in Refs. 82-83.

[19] The solution to the particular problem can be also found by means of the *Green's function* of the cavity. See Ref. 81 pp. 127-129.

and then multiplying this equation by $\psi_m(\mathbf{x})$ and integrating over Ω, we get a relationship for the functions $b_n(t)$

$$\sum_{n=1}^{\infty}\left(b_n(-\nabla^2\psi_n,\psi_m)+\frac{1}{c^2}\ddot{b_n}(\psi_n,\psi_m)\right)=\sum_{n=1}^{\infty}f_n(\psi_n,\psi_m).$$

Due to the properties of ψ_n (Eqs. (2.24) and (2.25)) we obtain

$$\lambda_n b_n+\frac{1}{c^2}\ddot{b_n}=f_n.$$

Using $\omega_n=\sqrt{\lambda_n}c$, the functions b_n can be found by solving the ordinary differential equation[20]

$$\ddot{b_n}(t)=-\omega_n^2 b_n(t)+c^2 f_n(t).$$

Finally, the total solution of the general problem (2.16) can be written as the sum of the solutions to the homogeneous (2.23) and particular (2.27) problems

$$u(\mathbf{x},t)=u_H+u_P=\sum_{n=1}^{\infty}a_n\psi_n+\sum_{n=1}^{\infty}b_n\psi_n=\sum_{n=1}^{\infty}u_n(t)\psi_n(\mathbf{x}),\tag{2.28}$$

where the functions $u_n(t)=a_n(t)+b_n(t)$ depend both on the boundary and initial conditions, and on the load f.

2.4 Electrostatic regime

Let us consider the case when the boundary conditions are functions independent of the time variable. Since the boundary conditions do not depend on the time, it is reasonable to assume that neither the electric nor the magnetic potential will do. So, the "static" electric field reaches $\mathbf{E}=-\nabla\phi$ and equation (2.13) becomes the (elliptic) Poisson equation for the electric potential. As an example, let us account for three kinds of boundaries: Γ_1 and Γ_2 perfect conductors (forced by an external source) at potentials ϕ_1 and ϕ_2 respectively. The third boundary will be considered to be a perfect insulator, i.e. $\nabla\phi\cdot\mathbf{n}=0$.

We can write this problem in the compact form

[20] With zero initial conditions, it gives $b_n(t)=\frac{c^2}{\omega_n}f_n(t)\otimes\sin(\omega_n t)$, where $\otimes$ denotes time-convolution.

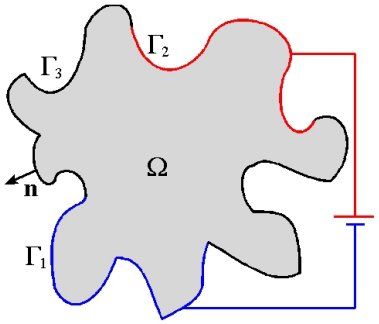

$$\begin{aligned} -\nabla^2\phi &= 0 \quad && \text{in } \Omega \\ \phi &= \phi_1 && \text{on } \Gamma_1 \\ \phi &= \phi_2 && \text{on } \Gamma_2 \\ \nabla\phi\cdot\mathbf{n} &= 0 && \text{on } \Gamma_3 \end{aligned} \tag{2.29}$$

Schematic representation of problem (2.29)

The electric energy density is defined as

$$u_e = \frac{1}{2}\epsilon_0\mathbf{E}^2 = \frac{1}{2}\epsilon_0\nabla\phi\cdot\nabla\phi$$

and the electric energy is the *functional* defined as[21]

$$U_e = \int_\Omega u_e d\mathbf{x} = \frac{1}{2}\epsilon_0(\nabla\phi,\nabla\phi).$$

By using the Green identity[22] we get

$$U_e = \int_\Gamma \frac{1}{2}\epsilon_0\phi\nabla\phi\cdot\mathbf{n}ds - \int_\Omega \frac{1}{2}\epsilon_0\phi\nabla^2\phi d\mathbf{x}$$

and we could use the definition of the problem (2.29) to find out that

$$U_e = -\int_{\Gamma_1}\frac{1}{2}\epsilon_0\phi_1\mathbf{E}\cdot\mathbf{n}ds - \int_{\Gamma_2}\frac{1}{2}\epsilon_0\phi_2\mathbf{E}\cdot\mathbf{n}ds.$$

Finally, by using the surface charge on the conductors $\sigma = -\epsilon_0\mathbf{E}\cdot\mathbf{n}$, and the fact that total charge on each surface must be equal (but of opposite sign), i.e. $\int_{\Gamma_1}\sigma_1 ds = -\int_{\Gamma_2}\sigma_2 ds = -Q$, the total stored energy in this cavity will be

$$U_e = \frac{1}{2}\phi_1\int_{\Gamma_1}\sigma_1 ds + \frac{1}{2}\phi_2\int_{\Gamma_2}\sigma_2 ds = \frac{1}{2}VQ,$$

where $V = \phi_2 - \phi_1$ is the difference of potential applied between the conducting surfaces. Note that the total charge Q on the electrodes depends on

[21] Existence and uniqueness was already demonstrated by Maxwell. See Ref. 84 pp. 135-137, Ref. 85 pp. 194-197.

[22] $\int_\Omega \nabla\psi\cdot\nabla\phi d\mathbf{x} = \int_\Gamma \psi\nabla\phi\cdot\mathbf{n}ds - \int_\Omega \psi\nabla^2\phi d\mathbf{x}$.

V, this give us an idea for defining the capacitance of the cavity as $Q = CV$, so we can estimate the stored energy as $U_e = CV^2/2$.

For this geometry (in general, for any cavity which is not an idealization) it is not possible to find an analytical expression for describing the electric field $\mathbf{E}$, the potential ϕ, the surface charge σ, or any other quantities of interest. The finite element method (FEM) have been used for getting a numerical representation of these quantities. This numerical method is based on variational principles, and it is optimal since it minimizes the error of the numerical approximation. It is particularly well suitable for solving physical problems derived from variational principles. For instance, in this problem the potential $\phi(\mathbf{x})$ inside the cavity Ω is such that the stored energy U_e is a minimum (and depends on the applied boundary conditions).

Figure 2.1 shows some results for the domain Ω used as example. Note that the electric energy density u_e distributes inside Ω in a different way than the the electric potential ϕ.

Note also, that the gradient of the potential ϕ defines the streamlines of electric field (that is, the lines perpendicular to equipotential contours). Charged particles inside this cavity will follow these streamlines. But a dielectric particle will follow the streamlines of the gradient of the electric energy density u_e. This issue will be addressed in the following chapter, while analyzing the forces acting on dipoles and dielectric particles.

2.5 Time-dependent regime

Let us now consider the most general case, which is when the boundary conditions depend also on the time variable t. Following Sec. 2.3, we could use the expansion of the electric field inside the cavity[23] in terms of the eigenfunctions ψ_n (as outlined in Eq. (2.28))

$$\mathbf{E}(\mathbf{x}, t) = \sum_n \mathbf{E}_n(t)\psi_n(\mathbf{x}).$$

This representation also leads to an expression for the electric energy density in terms of the eigenfunctions ψ_n (the term $\mathbf{E}^*$ denotes the *complex-conjugate* of the field)

$$u_e = \frac{1}{2}\epsilon_0|\mathbf{E}|^2 = \frac{1}{2}\epsilon_0 \sum_n^\infty \mathbf{E}_n\psi_n \cdot \sum_m^\infty \mathbf{E}_m^*\psi_m.$$

[23] For an intuitive approach see Ref. 80 Chap. 23.

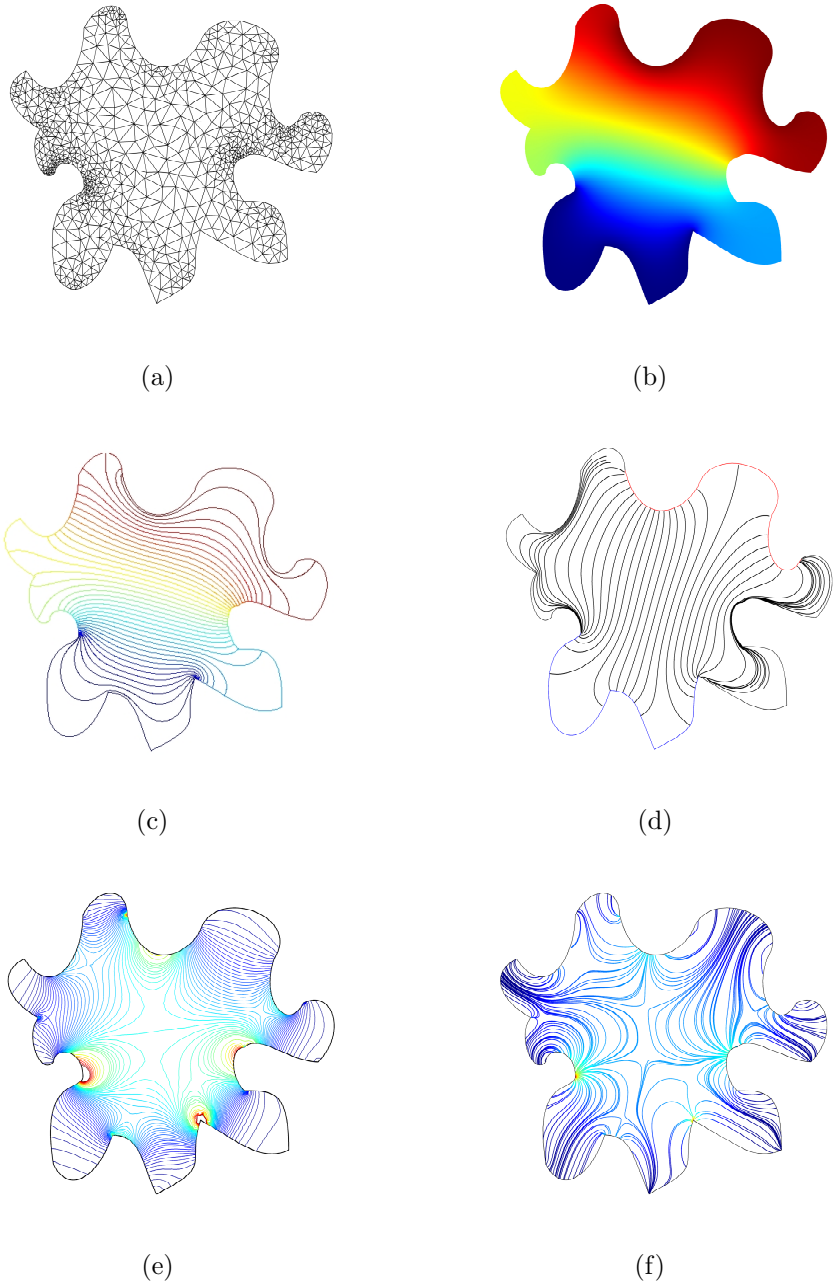

(a) (b)

(c) (d)

(e) (f)

Figure 2.1: (a) Computational mesh and (b) solution for the potential $\phi(\mathbf{x})$, (c) Contours of equipotential lines ϕ, (d) streamlines of electric field $-\nabla\phi$, (e) contours of electric energy density u_e and (f) streamlines of gradient of electric energy density ∇u_e.

We can find the total electric energy U_e by using the properties defined in Eq. (2.24)

$$U_e = \int_\Omega u_e d\mathbf{x} = \frac{1}{2}\epsilon_0 \sum_n^\infty \sum_m^\infty \mathbf{E}_n \cdot \mathbf{E}_m^*(\psi_n, \psi_m) = \frac{1}{2}\epsilon_0 \sum_n^\infty |\mathbf{E}|_n^2.$$

Due to the orthonormality of the eigenfunctions ψ_n, we could find that the total electric energy U_e is distributed among the energies residing in each[24] normal mode $\mathbf{E}_n$.

For instance, if the k^{th} normal mode is exited (due to the conditions imposed on the boundary), it will concentrate most of the electric energy. The shape in which the energy will distribute inside the cavity will be directly related to the shape of the respective eigenfunction ψ_k.[25]

As an example, Fig. 2.2 illustrates the first six eigenfunctions of the domain analyzed in the previous section.

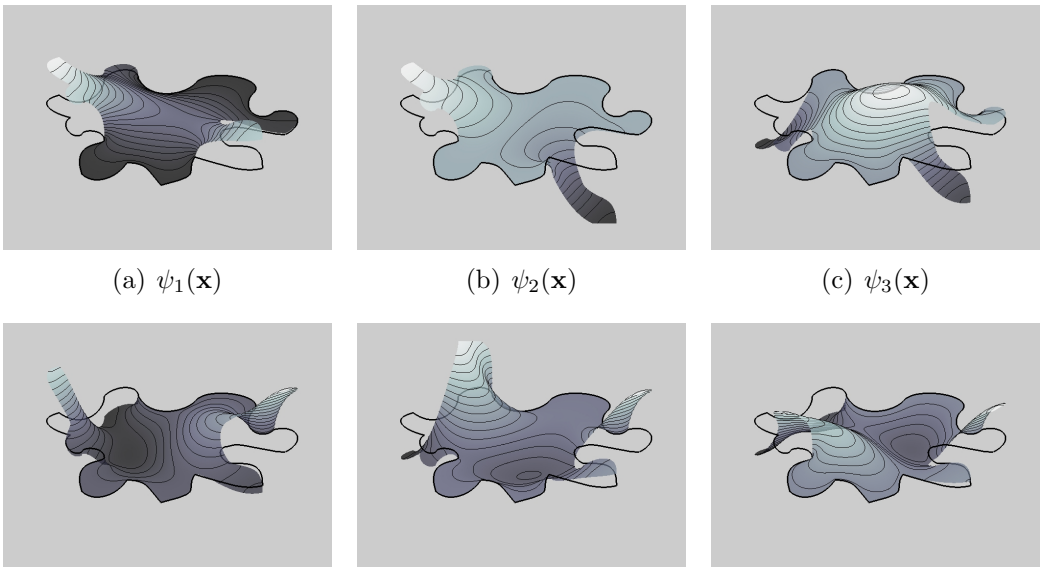

(a) $\psi_1(\mathbf{x})$ (b) $\psi_2(\mathbf{x})$ (c) $\psi_3(\mathbf{x})$

(d) $\psi_4(\mathbf{x})$ (e) $\psi_5(\mathbf{x})$ (f) $\psi_6(\mathbf{x})$

Figure 2.2: First six eigenfunctions of the domain Ω.

The most important question to answer is whether the boundary conditions will excite some of the normal modes or not. If the boundary conditions slowly change in time (i.e. the driving frequency is much lower than the

[24] This is an extension of Parseval's theorem.

[25] The same procedure can be used in order to obtain a representation for the magnetic energy U_m.

fundamental frequency of the cavity) we may use the "electrostatic" approximation, and we can neglect the contributions due to time derivatives in Eqs. (2.13), (2.14), (2.5), and (2.6). This assumption also changes the hyperbolic nature of the problem to an elliptic behavior.

On the other hand, if the external sources impose fast changes on the boundaries (comparable or higher than the fundamental frequency), there will be many modes which will be exited, the electromagnetic energy will distribute among them and the electromagnetic field pattern will completely diverge from the one founded in the electrostatic regime.

When both electrostatic and time-dependent regimes coexist, the most general expression for the electric energy will be

$$U_e = \int_\Omega u_e d\mathbf{x} = \frac{1}{2}\epsilon_0 \mathbf{E}_0^2 + \frac{1}{2}\epsilon_0 \sum_{n=1}^{\infty} \mathbf{E}_n^2$$

where $\mathbf{E}_0$ represents the electrostatic component, and $\mathbf{E}_n$ represents the energy distributed in the time-dependent modes.

2.6 Floating potential

Introducing a metallic probe inside a plasma chamber is a very common tool for plasma diagnostic. Langmuir and Mott-Smith developed a probe theory[26] which founded the research on low temperature plasmas. If we consider the probe as a perfect conductor, its surface will then be at a constant (but unknown) potential. This potential, also known as *floating potential*, can be measured by connecting the probe to an external circuit. Also, current-voltage characteristic curves can be found by setting this potential at a certain voltage and then measuring the current through the probe.

Yet, introducing a metallic probe inside a cavity changes its topology, therefore, we actually do not measure the properties of the chamber but rather of the modified chamber.[27]

Let us consider the original problem (2.16) of finding the electric potential ϕ inside a cavity Ω (containing media of permittivity ϵ and permeability μ)

[26] See Ref. 86.

[27] For instance, the introduction of a floating probe in a chamber containing complex plasma induces a secondary void. See Refs. 87-89.

subject to boundary conditions on $\Gamma = \Gamma_1 \cup \Gamma_2$

$$\begin{aligned} -\nabla^2\phi + \frac{1}{c^2}\frac{\partial^2\phi}{\partial t^2} &= \frac{\rho}{\epsilon} \qquad \text{in } \Omega \times (0,T) \\ \phi &= g \qquad \text{on } \Gamma_1 \times (0,T) \\ \nabla\phi \cdot \mathbf{n} &= h \qquad \text{on } \Gamma_2 \times (0,T). \end{aligned} \tag{2.30}$$

By introducing a metallic object of volume Ω' and surface Γ_3, the previous problem changes to

$$\begin{aligned} -\nabla^2\phi + \frac{1}{c^2}\frac{\partial^2\phi}{\partial t^2} &= \frac{\rho}{\epsilon} \qquad \text{in } \overline{\Omega} \times (0,T) \\ \phi &= g \qquad \text{on } \Gamma_1 \times (0,T) \\ \nabla\phi \cdot \mathbf{n} &= h \qquad \text{on } \Gamma_2 \times (0,T) \\ \phi &= \phi_f \qquad \text{on } \Gamma_3 \times (0,T), \end{aligned} \tag{2.31}$$

where the solution ϕ has to be found in the new domain $\overline{\Omega} = \Omega \cap \Omega'$. The boundary Γ_3 is at an unknown floating potential ϕ_f, and the boundary between the cavity and the probe (considering that the probe is made of a perfect conductor material) can be modeled as[28]

$$\epsilon\mathbf{E}\cdot\mathbf{n} = -\sigma_f \qquad \mathbf{E}\times\mathbf{n} = 0 \qquad \phi = \phi_f \qquad \mathbf{B}\times\mathbf{n} = \mu\mathbf{J}_f \qquad \mathbf{B}\cdot\mathbf{n} = \mathbf{0}$$

We can estimate the total current flowing to the floating probe as

$$I_f = \int_{\Gamma_3} \mathbf{J}_f \cdot \mathbf{n} ds$$

and since $\mathbf{J}_f \cdot \mathbf{n} = \frac{1}{\mu}(\mathbf{B}\times\mathbf{n})\cdot\mathbf{n} = 0$, the total current flowing to the probe is $I_f = 0$.

On the other hand, the total charge on the probe is defined as

$$Q_f = \int_{\Gamma_3} \sigma_f ds,$$

and since $I_f = \frac{d}{dt}Q_f = 0$, the total charge on the probe is kept constant.

Let us for instance introduce a small probe inside the same domain analyzed in Sec. 2.4. The new problem to solve is (2.32), where Γ_4 now represents the surface of the metallic probe.

The floating potential can be estimated by the alternative boundary condition

$$\epsilon_0\nabla\phi\cdot\mathbf{n} = \sigma_f \qquad \text{on } \Gamma_4$$

[28] The normal $\mathbf{n}$ points towards the probe.

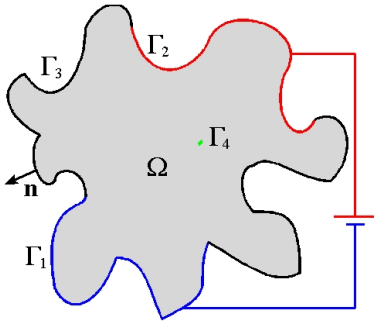

$$\begin{aligned} -\nabla^2\phi &= 0 \quad \text{in } \overline{\Omega} \\ \phi &= \phi_1 \quad \text{on } \Gamma_1 \\ \phi &= \phi_2 \quad \text{on } \Gamma_2 \\ \nabla\phi\cdot\mathbf{n} &= 0 \quad \text{on } \Gamma_3 \\ \phi &= \phi_f \quad \text{on } \Gamma_4 \end{aligned} \tag{2.32}$$

Schematic representation of a small probe inserted in the domain Ω

and the total charge is then a *constrain* for the potential on Γ_4

$$Q_f = \int_{\Gamma_4} \sigma_f ds = \int_{\Gamma_4} \epsilon_0 \nabla\phi\cdot\mathbf{n} ds$$

This "floating potential" boundary condition is implemented as a weak constrain by the finite element method (see Appendix A).[29]

Figure 2.3 shows the changes on the equipotential contours and electric field lines in the neighborhood of the probe, as well as the changes on the electric energy density u_e.

This example has shown how a metallic object inside a cavity changes the way in which the electric energy distributes around it. This can be the explanation of the "induced voids" in complex plasmas experiments. Chapter 6 will discuss this point.

2.7 Final remarks

The use of numerical methods gives an idea of how electromagnetic energy distributes inside complex geometries, where standard methods cannot be used for obtaining analytical expressions of the electric fields, potentials, etc.

When the problem under study does not depend on time (the electrostatic regime), the numerical method solves an elliptic problem.

When the problem is time-dependent, the Sturm-Liouville theory introduces the idea of expanding the time-dependent solution in terms of the eigenfunctions of the cavity. The electromagnetic energy will distribute among the

[29] By calculating the unknown floating potential ϕ_f, we introduced an extra degree of freedom in the problem. Thus, an extra equation must be added in order to obtain a well-posed problem. This also implies that the obtained numerical representation [see for instance Eq. (A.8)] is no longer symmetric.

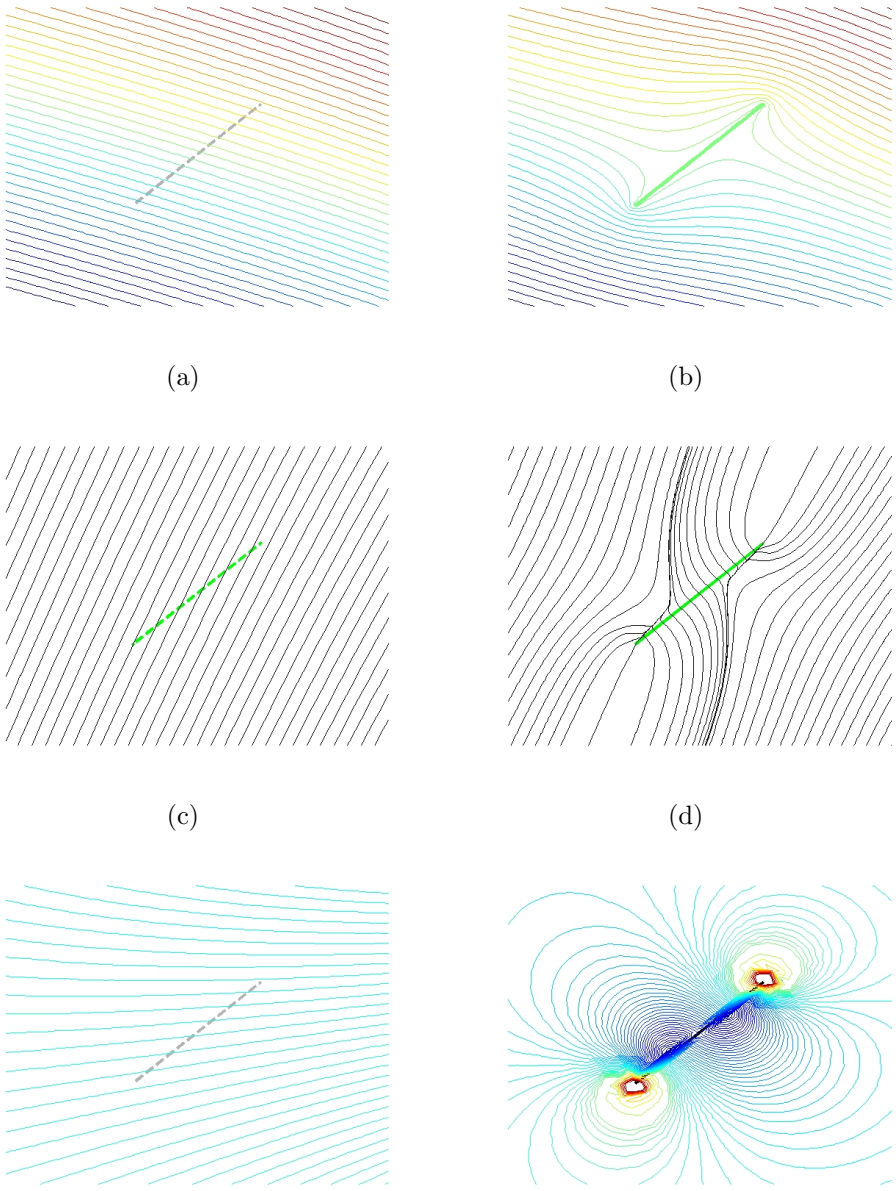

(a) (b)

(c) (d)

(e) (f)

Figure 2.3: (Zoom)(a) Contours of equipotential lines before and (b) after inserting the probe. (c) Electric field lines without and (d) with the probe. (e) Contours of electric energy density u_e before and (f) after introducing the floating probe.

exited modes, and the pattern of the electromagnetic fields will completely change from the one found in the electrostatic case.

A multi-mode cavity will have many resonant modes in the vicinity of the operating frequency. A single-mode cavity will create a single field pattern, and the wavelength of the resonant frequency is approximately twice of the typical cavity's dimension.

For instance, if we consider the distance between the electrodes L as the characteristic spatial scale of the PK-3 Plus chamber, we can estimate (by considering the wave-length $\lambda = 2L$) the first resonant frequency of the electromagnetic waves as

$$\text{freq}_1 = \frac{c}{\lambda} \approx \frac{3 \cdot 10^8}{2 \cdot 3} \frac{\text{m/s}}{\text{cm}} \approx 5 \text{ GHz}$$

The numerical estimation with the finite element method gives[30]

$$\text{freq}_1 = 4.24 \text{ GHz}$$

The radio-frequency used in the PK-3 Plus experiment (for obtaining the plasma discharge) is 13.67 MHz, which is two orders of magnitude below the natural frequency of the cavity. Yet, this driving frequency is seven orders of magnitude above the electrostatic regime (or zero frequency).

It is not clear whether the PK-3 Plus experiment is ruled by pure electrostatic effects or not. A full three-dimensional model has been implemented in order to analyze the distribution of the electric energy inside the plasma chamber. Chapter 6 shows how the electric energy distributes in both cases (electrostatic and first resonant mode).

This numerical implementation introduces us with the idea that the results observed in the PK-3 Plus experiment (more specifically, the observation of a dust-free region or "void") are not only due to electrostatic fields, but are also influenced by the first resonance mode of the cavity.

Also, a small metallic probe is introduced in the chamber in order to observe the changes on the energy distribution. This is used for showing how the probe could induce secondary voids.

[30] See Appendix A.

Electromagnetic forces on classical particles

3

This chapter will review the electromagnetic forces acting on point charges, point dipoles and polarized particles inside the cavity described in the previous chapter. The formalism of classical mechanics will be followed. Neither quantum nor relativistic effects will be addressed.[1]

3.1 The classical picture

Lagrangian mechanics defines $\boldsymbol{\xi}$ as the *generalized coordinates* of a system. The number of required coordinates is called the *degree of freedom*. At every time, the system will be defined by the vector of N coordinates $\boldsymbol{\xi}$. When the system is in motion, the time variation of the coordinates $\dot{\boldsymbol{\xi}}(t)$ must also be specified. This 2N dimensional space is called the *phase space*.

3.1.1 Euler-Lagrange equations

In classical mechanics, the trajectory of a system is derived by finding the path[2] for which the action integral S is stationary. Considering the general problem defined by the *Lagrangian* $L(\boldsymbol{\xi}, \dot{\boldsymbol{\xi}}, t)$, the action S is the integral (over the time variable) of this Lagrangian between given starting and end points in the phase space

$$S = \int_{t_1}^{t_2} L(\boldsymbol{\xi}, \dot{\boldsymbol{\xi}}, t) dt.$$

Finding the stationary point of the action along a path (or $\delta S = 0$) is equivalent to impose a set of N second order differential equations on the Lagrangian. This set is called the *Euler-Lagrange equations*[3]

$$\frac{d}{dt}\frac{\partial L}{\partial \dot{\boldsymbol{\xi}}} - \frac{\partial L}{\partial \boldsymbol{\xi}} = 0. \tag{3.1}$$

The choice of the appropriated Lagrangian gives the correct derivation of the forces acting on the system.

[1] See Ref. 94 Chap. 2.
[2] See Ref. 80 Chap. 19.
[3] See derivation in Refs. 94 Chap. 2, and 96 Chap. 15.

These equations will be used in the following chapter in order to derive the electromagnetic forces acting on point charges (Lorentz force), point dipoles, polarizable particles and dielectric fluids.

3.2 Forces on point charges

Let us analyze the classical motion of a charged particle in an external[4] electromagnetic field. Consider first a bounded vacuum region Ω, surrounded by a closed surface $\partial\Omega$. This boundary may be composed by different types of boundaries, such as conducting or insulating walls.

The boundary conditions imposed on $\partial\Omega$, the topology of Ω and the Maxwell equations in vacuum will define the behavior of the electromagnetic fields inside this cavity (see Chap. 2).

Let us now insert a small[5] charge q in Ω and suppose that the presence and motion of this particle will not affect the external source (or sources) of these fields.

If the particle is considered to be a point of mass and charge, three coordinates are enough to describe its position, and also three coordinates are enough to describe its velocity.

If we denote $\mathbf{x}(t)$ as the position of the particle, $\mathbf{v}(t) = \frac{d}{dt}\mathbf{x}(t) = \dot{\mathbf{x}}(t)$ its velocity and m its mass, the classical Lagrangian is given (in SI units) by[6]

$$L = T - U = \frac{1}{2}m\mathbf{v}^2 - q\phi + q\mathbf{v}\cdot\mathbf{A}. \tag{3.2}$$

In order to obtain an expression for the Lorentz force acting on this particle, we can apply the Euler-Lagrange equations (3.1) to this Lagrangian (considering the mass and charge as constants)

$$\frac{\partial L}{\partial \mathbf{v}} = m\mathbf{v} + q\mathbf{A}, \qquad \frac{d}{dt}\frac{\partial L}{\partial \mathbf{v}} = \frac{d}{dt}(m\mathbf{v} + q\mathbf{A}),$$
$$\frac{\partial L}{\partial \mathbf{x}} = -q\nabla\phi + q(\mathbf{v}\cdot\nabla)\mathbf{A} + q\mathbf{v}\times\nabla\times\mathbf{A},$$

where the notation $\nabla = \partial/\partial\mathbf{x}$ and the vector identity (B.4) have been used.

Now consider that the magnetic potential is a function of time and the position of the particle, i.e. $\mathbf{A} = \mathbf{A}(\mathbf{x}(t), t)$. By using $\dot{\mathbf{A}} = \frac{\partial}{\partial t}\mathbf{A} + (\mathbf{v}\cdot\nabla)\mathbf{A}$

[4] "External fields" are thought to be generated by external sources applied on the boundaries of the cavity.

[5] It dimension been much smaller than the size of the cavity, so one could treat it as a *point of charge*.

[6] See Refs. 95 p. 83, 94 p. 22, 96 p. 327, and 97 p. 192. For a relativistic approach, see Refs. 94 p. 313, 81 p. 582, 97 p. 534, and 80 Chap. 19.

together with the definitions of the electric and magnetic fields in Eqs. (2.7) and (2.8), one obtains the *Lorentz force*

$$\begin{aligned}\mathbf{F}_{Lorentz} &= \frac{d}{dt}(m\mathbf{v}) = -q(\nabla\phi + \frac{\partial}{\partial t}\mathbf{A}) + q\mathbf{v}\times\nabla\times\mathbf{A} \\ &= q(\mathbf{E} + \mathbf{v}\times\mathbf{B}).\end{aligned} \tag{3.3}$$

The presence and motion of the particle inside Ω will modify (or at least perturb) the electromagnetic field in the whole domain. In the classical approach, these modified fields should not exert work on the particle (because otherwise, the fields created by the particle would act on itself).

The presence and motion of the particle inside the cavity will also perturb the boundary conditions. If there is a Lorentz force acting on the particle, there will be work done by the electric field. The external sources, which create the electromagnetic fields, should provide the required energy through changes on the boundary conditions.

3.3 Forces on point dipoles

Lets us first consider the case when a small[7] dipole $\mathbf{p}$ moves with a velocity $\mathbf{v}(t)$ inside Ω. By neglecting angular rotations, six coordinates will also be enough to describe the position and velocity of this "point dipole".

Since we have not considered angular rotations, its kinetic energy will be

$$T = \frac{1}{2}m\mathbf{v}^2.$$

At the same time, the potential energy due to the electric field will be[8]

$$U_e = -\mathbf{p}\cdot\mathbf{E}.$$

Also, a moving electric dipole may be seen as a magnetic dipole[9] $\mathbf{m} = \mathbf{p}\times\mathbf{v}$. The potential energy due to the magnetic field will then be

$$U_m = -\mathbf{m}\cdot\mathbf{B} = -(\mathbf{p}\times\mathbf{v})\cdot\mathbf{B} = -\mathbf{p}\cdot(\mathbf{v}\times\mathbf{B}),$$

and the classical Lagrangian of this point dipole will be

$$L = T - (U_e + U_m) = \frac{1}{2}m\mathbf{v}^2 + \mathbf{p}\cdot(\mathbf{E} + \mathbf{v}\times\mathbf{B}). \tag{3.4}$$

[7] Smaller than the cavity's dimensions.
[8] See Ref. 80 Chap. 15.
[9] See Ref. 81 p. 292.

Now, by using the Euler-Lagrange equations (3.1) and the identity (B.5)

$$\begin{aligned} \frac{\partial L}{\partial \mathbf{v}} &= m\mathbf{v} - \mathbf{p} \times \mathbf{B}, & \frac{d}{dt}\frac{\partial L}{\partial \mathbf{v}} &= m\dot{\mathbf{v}} - \mathbf{p} \times \dot{\mathbf{B}}, \\ \frac{\partial L}{\partial \mathbf{x}} &= (\mathbf{p} \cdot \nabla)(\mathbf{E} + \mathbf{v} \times \mathbf{B}) + \mathbf{p} \times \nabla \times (\mathbf{E} + \mathbf{v} \times \mathbf{B}), \end{aligned} \tag{3.5}$$

we can obtain the force acting on this dipole

$$m\dot{\mathbf{v}} = (\mathbf{p} \cdot \nabla)(\mathbf{E} + \mathbf{v} \times \mathbf{B}) + \mathbf{p} \times (\nabla \times (\mathbf{E} + \mathbf{v} \times \mathbf{B}) + \dot{\mathbf{B}}).$$

We could simplify the *r.h.s.* by using the identities (B.6) and (B.7)

$$\mathbf{F}_{dip} = (\mathbf{p} \cdot \nabla)(\mathbf{E} + \mathbf{v} \times \mathbf{B}) + \mathbf{p} \times (\nabla \times \mathbf{E} + \mathbf{v}\nabla \cdot \mathbf{B} + \frac{\partial \mathbf{B}}{\partial t}).$$

Finally, by using the Maxwell equations (2.2) and (2.3), we obtain the force acting on the dipole

$$\mathbf{F}_{dip} = (\mathbf{p} \cdot \nabla)(\mathbf{E} + \mathbf{v} \times \mathbf{B}). \tag{3.6}$$

If the dipole has a time dependency, i.e. $\mathbf{p} = \mathbf{p}(t)$, there will be an extra term in Eq. (3.5)

$$\frac{d}{dt}\frac{\partial L}{\partial \mathbf{v}} = m\dot{\mathbf{v}} - \mathbf{p} \times \dot{\mathbf{B}} - \dot{\mathbf{p}} \times \mathbf{B},$$

and then the force defined in Eq. (3.6) will become

$$\mathbf{F}_{dip} = (\mathbf{p} \cdot \nabla)(\mathbf{E} + \mathbf{v} \times \mathbf{B}) + \dot{\mathbf{p}} \times \mathbf{B}. \tag{3.7}$$

This result is similar to the one obtained by other authors[10] for dipoles moving with non-relativistic velocities.

If the dipole moves "slowly", the electric field is much stronger than the magnetic, or equivalently $|\mathbf{v}||\mathbf{B}| << |\mathbf{E}|$, the force defined in Eq. (3.7) simplifies to[11]

$$\mathbf{F}_{dip} = (\mathbf{p} \cdot \nabla)\mathbf{E} + \dot{\mathbf{p}} \times \mathbf{B}. \tag{3.8}$$

[10] See for instance Ref. 98.

[11] See another approach in Ref. 81 p. 294.

3.4 Forces on two point charges

Let us now consider the most general case: a system of two point particles, each one of different mass and charge.

The classical Lagrangian of this system will be[12]

$$\begin{aligned} L &= T_1 - U_1 + T_2 - U_2 - \phi_{int} \\ &= \frac{1}{2}m_1\mathbf{v}_1^2 - q_1\phi(\mathbf{x}_1) + q_1\mathbf{v}_1 \cdot \mathbf{A}(\mathbf{x}_1) \\ &+ \frac{1}{2}m_2\mathbf{v}_2^2 - q_2\phi(\mathbf{x}_2) + q_2\mathbf{v}_2 \cdot \mathbf{A}(\mathbf{x}_2) - \phi_{int}(\mathbf{x}_1 - \mathbf{x}_2), \end{aligned} \tag{3.9}$$

where $\phi_{int}(\mathbf{x}_1 - \mathbf{x}_2)$ is the internal potential energy between the particles, which can be any function of the interparticle distance.[13]

3.4.1 Force on the center of mass

Consider the total mass M and the reduced mass μ

$$M = m_1 + m_2, \qquad \mu^{-1} = m_1^{-1} + m_2^{-1},$$

the position and velocity of the center of mass

$$\mathbf{x} = (m_1\mathbf{x}_1 + m_2\mathbf{x}_2)/M, \qquad \mathbf{v} = \dot{\mathbf{x}} = (m_1\mathbf{v}_1 + m_2\mathbf{v}_2)/M,$$

and the relative distance and velocity between the particles

$$\mathbf{d} = (\mathbf{x}_1 - \mathbf{x}_2), \qquad \mathbf{u} = \dot{\mathbf{d}} = (\mathbf{v}_1 - \mathbf{v}_2).$$

We could rewrite the Lagrangian defined in Eq. (3.9) in terms of the variables $\mathbf{x}$, $\mathbf{d}$, $\mathbf{v}$ and $\mathbf{u}$ (instead of $\mathbf{x}_1$, $\mathbf{x}_2$, $\mathbf{v}_1$ and $\mathbf{v}_2$), by using the following relations:

$$\begin{aligned} \mathbf{x}_1 &= \mathbf{x} + \frac{m_2}{M}\mathbf{d}, & \mathbf{x}_2 &= \mathbf{x} - \frac{m_1}{M}\mathbf{d}, \\ \mathbf{v}_1 &= \mathbf{v} + \frac{m_2}{M}\mathbf{u}, & \mathbf{v}_2 &= \mathbf{v} - \frac{m_1}{M}\mathbf{u}. \end{aligned} \tag{3.10}$$

The kinetic energy of the system then reaches[14]

$$T = \frac{1}{2}m_1\mathbf{v}_1^2 + \frac{1}{2}m_2\mathbf{v}_2^2 = \frac{1}{2}M\mathbf{v}^2 + \frac{1}{2}\mu\mathbf{u}^2, \tag{3.11}$$

[12] We now need six coordinates for describing the positions and six coordinates for the velocities, so there will be twelve degrees of freedom.

[13] In a quantum dynamic approach, one has to follow a *lagrangian density* formalism.

[14] See Refs. 94 p. 71, and 96 pp. 74-75.

which now considers both the translation of the center of mass and the angular rotation of the particles about it.

In terms of the new variables, the potential energy due to the electric and magnetic potentials can be written as

$$\begin{aligned} U = {} & q_1\phi(\mathbf{x}+\frac{m_2}{M}\mathbf{d}) - q_1(\mathbf{v}+\frac{m_2}{M}\mathbf{u})\cdot\mathbf{A}(\mathbf{x}+\frac{m_2}{M}\mathbf{d}) \\ & + q_2\phi(\mathbf{x}-\frac{m_1}{M}\mathbf{d}) - q_2(\mathbf{v}-\frac{m_1}{M}\mathbf{u})\cdot\mathbf{A}(\mathbf{x}-\frac{m_1}{M}\mathbf{d}) + \phi_{int}(\mathbf{d}). \end{aligned} \tag{3.12}$$

When the distance $\mathbf{d}$ is very small (with respect to the cavity's dimensions) one could perform a Taylor expansion of any function $f(\mathbf{x})$ around the center of mass, i.e.

$$f(\mathbf{x}+\mathbf{d}) = f(\mathbf{x}) + (\mathbf{d}\cdot\nabla)f(\mathbf{x}) + \frac{(\mathbf{d}\cdot\nabla)^2}{2!}f(\mathbf{x}) + \cdots + \frac{(\mathbf{d}\cdot\nabla)^n}{n!}f(\mathbf{x}) + R_n,$$

where the remainder[15] R_n is of the order $\mathrm{O}(d^{n+1})$.

By using the kinetic energy defined in Eq. (3.11) and this Taylor expansion in the expressions for the electric and magnetic potentials in Eq. (3.12), the Lagrangian defined in Eq. (3.9) becomes

$$\begin{aligned} L = {} & \frac{1}{2}M\mathbf{v}^2 + \frac{1}{2}\mu\mathbf{u}^2 \\ & - \Bigg((q_1+q_2) + \left(q_1\frac{m_2}{M} - q_2\frac{m_1}{M}\right)(\mathbf{d}\cdot\nabla) + \left(q_1\frac{m_2^2}{M^2} + q_2\frac{m_1^2}{M^2}\right)\frac{(\mathbf{d}\cdot\nabla)^2}{2!} \\ & \qquad + \left(q_1\frac{m_2^3}{M^3} - q_2\frac{m_1^3}{M^3}\right)\frac{(\mathbf{d}\cdot\nabla)^3}{3!} + \ldots\Bigg)\phi(\mathbf{x}) \\ & + \mathbf{v}\cdot\Bigg((q_1+q_2) + \left(q_1\frac{m_2}{M} - q_2\frac{m_1}{M}\right)(\mathbf{d}\cdot\nabla) + \left(q_1\frac{m_2^2}{M^2} + q_2\frac{m_1^2}{M^2}\right)\frac{(\mathbf{d}\cdot\nabla)^2}{2!} \\ & \qquad + \left(q_1\frac{m_2^3}{M^3} - q_2\frac{m_1^3}{M^3}\right)\frac{(\mathbf{d}\cdot\nabla)^3}{3!} + \ldots\Bigg)\mathbf{A}(\mathbf{x}) \\ & + \mathbf{u}\cdot\Bigg(\left(q_1\frac{m_2}{M} - q_2\frac{m_1}{M}\right) + \left(q_1\frac{m_2^2}{M^2} + q_2\frac{m_1^2}{M^2}\right)(\mathbf{d}\cdot\nabla) \\ & \qquad + \left(q_1\frac{m_2^3}{M^3} - q_2\frac{m_1^3}{M^3}\right)\frac{(\mathbf{d}\cdot\nabla)^2}{2!} + \ldots\Bigg)\mathbf{A}(\mathbf{x}) - \phi_{int}(\mathbf{d}). \end{aligned} \tag{3.13}$$

Let us now suppose that the particles have equal but opposite charges, i.e. $q_1 = -q_2 = q$. Rearranging and truncating terms of order $\mathrm{O}(d^2)$ and

[15] The reminder is $R_n = \frac{(\mathbf{d}\cdot\nabla)^{n+1}}{n+1!}f(\mathbf{x}+\boldsymbol{\xi})$, where $|\boldsymbol{\xi}| < |\mathbf{d}|$. See Ref. 93, pp. 64-70.

higher, the Lagrangian defined in Eq. (3.13) becomes[16]

$$L = \frac{M}{2}\mathbf{v}^2 + \frac{\mu}{2}\mathbf{u}^2 - q\mathbf{d}\cdot\nabla\phi + q\mathbf{v}\cdot(\mathbf{d}\cdot\nabla)\mathbf{A} + q\mathbf{u}\cdot\mathbf{A} - \phi_{int}(\mathbf{d}) + \mathrm{O}(d^2). \quad (3.14)$$

Now, if we use the Euler-Lagrange equations (3.1) for the coordinates $\mathbf{x}$ and $\mathbf{v}$, together with the identity (B.8)

$$\frac{\partial L}{\partial \mathbf{v}} = M\mathbf{v} + q(\mathbf{d}\cdot\nabla)\mathbf{A}, \qquad \frac{d}{dt}\frac{\partial L}{\partial \mathbf{v}} = M\dot{\mathbf{v}} + q(\mathbf{u}\cdot\nabla)\mathbf{A} + q(\mathbf{d}\cdot\nabla)\dot{\mathbf{A}},$$
$$\frac{\partial L}{\partial \mathbf{x}} = -q(\mathbf{d}\cdot\nabla)\nabla\phi + q(\mathbf{v}\cdot\nabla)(\mathbf{d}\cdot\nabla)\mathbf{A} + q\mathbf{v}\times\nabla\times(\mathbf{d}\cdot\nabla)\mathbf{A} + q(\mathbf{u}\cdot\nabla)\mathbf{A} + q\mathbf{u}\times\nabla\times\mathbf{A},$$

we obtain an expression for the force that the external electromagnetic fields exert on the system's center of mass

$$M\dot{\mathbf{v}} = q(\mathbf{d}\cdot\nabla)(-\nabla\phi + (\mathbf{v}\cdot\nabla)\mathbf{A} + \mathbf{v}\times\nabla\times\mathbf{A} - \dot{\mathbf{A}}) + q\mathbf{u}\times\nabla\times\mathbf{A}.$$

We can simplify the *r.h.s.* by using the identity (B.9) and the definitions of the electric and magnetic fields[17]

$$\mathbf{F}_{cm} = (q\mathbf{d}\cdot\nabla)(\mathbf{E} + \mathbf{v}\times\mathbf{B}) + q\mathbf{u}\times\mathbf{B} + \mathrm{O}(d^2). \quad (3.15)$$

Finally, by using the definition of the dipole $\mathbf{p} = q\mathbf{d}$ and $\dot{\mathbf{p}} = q\mathbf{u}$, we obtain the same expression previously found for the electromagnetic force acting on the dipole's center of mass (see Eq. (3.7), but we now know that this expression is accurate in $\mathrm{O}(d^2)$)

$$\mathbf{F}_{cm} = (\mathbf{p}\cdot\nabla)(\mathbf{E} + \mathbf{v}\times\mathbf{B}) + \dot{\mathbf{p}}\times\mathbf{B} + \mathrm{O}(d^2). \quad (3.16)$$

3.4.2 Torque about the center of mass

If we use the Euler-Lagrange equations (3.1) for the variables $\mathbf{d}$ and $\mathbf{u}$ on the Lagrangian defined in Eq. (3.13) (also truncating terms of order $\mathrm{O}(d^2)$ and higher)

$$\frac{\partial L}{\partial \mathbf{u}} = \mu\mathbf{u} + q\mathbf{A}, \qquad \frac{d}{dt}\frac{\partial L}{\partial \mathbf{u}} = \mu\dot{\mathbf{u}} + q\dot{\mathbf{A}},$$
$$\frac{\partial L}{\partial \mathbf{d}} = -q\nabla\phi + q((\mathbf{v}\cdot\nabla)\mathbf{A} + \mathbf{v}\times\nabla\times\mathbf{A}) - \frac{\partial \phi_{int}}{\partial \mathbf{d}},$$

[16] Organizing a bit more, it reaches
$L = \frac{1}{2}M\mathbf{v}^2 + \frac{1}{2}\mu\mathbf{u}^2 + (\mathbf{d}\cdot\nabla)(-q\phi + q\mathbf{v}\cdot\mathbf{A}) + q\mathbf{u}\cdot\mathbf{A} - \phi_{int}(\mathbf{d}) + \mathrm{O}(d^2)$.

[17] If we use a more accurate expression, this force becomes ($\gamma = (m_2 - m_1)/M$)
$\mathbf{F}_{cm} = (q\mathbf{d}\cdot\nabla)(\mathbf{E} + \mathbf{v}\times\mathbf{B}) + q\mathbf{u}\times\mathbf{B} + \gamma q\left(\frac{(\mathbf{d}\cdot\nabla)^2}{2!}(\mathbf{E} + \mathbf{v}\times\mathbf{B}) + (\mathbf{d}\cdot\nabla)\mathbf{u}\times\mathbf{B}\right) + \mathrm{O}(d^3)$.

together with the identity (B.9), we obtain the internal force of the system[18]

$$\begin{aligned}\mathbf{F}_{int} = \mu\dot{\mathbf{u}} &= q(-\nabla\phi + (\mathbf{v}\cdot\nabla)\mathbf{A} + \mathbf{v}\times\mathbf{B} - \dot{\mathbf{A}}) - \frac{\partial\phi_{int}}{\partial\mathbf{d}} \\ &= q(\mathbf{E} + \mathbf{v}\times\mathbf{B}) - \frac{\partial\phi_{int}}{\partial\mathbf{d}} + \mathrm{O}(d). \end{aligned} \tag{3.17}$$

By using the previously derived expressions in Eq. (3.10) for the relative distances of the particles with respect to the center of mass $\big(\mathbf{d}_1 = \frac{m_2}{M}\mathbf{d}$ and $\mathbf{d}_2 = -\frac{m_1}{M}\mathbf{d}\big)$, we can define the *moment of inertia* of the system (with respect to the center of mass) as

$$I = m_1 d_1^2 + m_2 d_2^2 = \frac{m_1 m_2}{M} d^2 = \mu d^2.$$

We can also define the *angular velocity*

$$\boldsymbol{\omega} = \frac{1}{d^2}\mathbf{d}\times\mathbf{u},$$

and by combining both expressions, we obtain the *angular momentum* with respect the center of mass

$$\mathbf{L} = I\boldsymbol{\omega} = \mu\mathbf{d}\times\mathbf{u}.$$

By using the internal force defined in Eq. (3.17), we can derive an expression for the torque acting on the system

$$\begin{aligned}\mathbf{N} = \frac{d}{dt}\mathbf{L} &= \mu\mathbf{d}\times\dot{\mathbf{u}} = \mathbf{d}\times\mathbf{F}_{int} \\ &= \mathbf{d}\times\left(q(\mathbf{E} + \mathbf{v}\times\mathbf{B}) - \frac{\partial\phi_{int}}{\partial\mathbf{d}}\right) + \mathrm{O}(d^2). \end{aligned} \tag{3.18}$$

Any dependence of the internal potential $\phi_{int}(\mathbf{d})$ in terms of the interparticle distance will give rise to a radial force, i.e. the internal force will be parallel[19] to the vector $\mathbf{d}$. This implies $\partial\phi_{int}/\partial\mathbf{d} = f(d)\mathbf{d}$ and $\mathbf{d}\times\partial\phi_{int}/\partial\mathbf{d} = 0$.

Thus, the internal potential does not exert any torque on the system, and the torque is solely due to the external fields[20]

$$\mathbf{N} = q\mathbf{d}\times(\mathbf{E} + \mathbf{v}\times\mathbf{B}) = \mathbf{p}\times(\mathbf{E} + \mathbf{v}\times\mathbf{B}) + \mathrm{O}(d^2). \tag{3.19}$$

[18] If we use a more accurate expression, this force becomes ($\gamma = (m_2 - m_1)/M$)
$\mathbf{F}_{int} = q(\mathbf{E} + \mathbf{v}\times\mathbf{B}) + \gamma q\big((\mathbf{d}\cdot\nabla)(\mathbf{E} + \mathbf{v}\times\mathbf{B}) + \mathbf{u}\times\mathbf{B}\big) - \frac{\partial}{\partial\mathbf{d}}\phi_{int} + \mathrm{O}(d^2)$.

[19] See Ref. 94 p. 7.

[20] If we use a more accurate expression, the torque becomes ($\gamma = (m_2 - m_1)/M$)
$\mathbf{N} = \mathbf{p}\times(\mathbf{E} + \mathbf{v}\times\mathbf{B}) + \gamma\mathbf{p}\times\big((\mathbf{d}\cdot\nabla)(\mathbf{E} + \mathbf{v}\times\mathbf{B}) + \mathbf{u}\times\mathbf{B}\big) + \mathrm{O}(d^3)$.

Both the force and the torque acting on the center of mass (of this two-particle system) are exclusively due to the external fields. Although each particle will feel both the external fields and the fields generated by the other particle, the internal potential between them does not influence the dynamic of the center of mass.

The same procedure (although a bit more cumbersome) can be applied to a system of N charged particles. They will interact with each other in many different ways, but the motion of the center of mass of this N-body system will be solely dictated by the external fields, which will depend on the boundary conditions and on the topology of the cavity. This issue will be addressed in the next chapter, while analyzing the macroscopic behavior of gases and plasmas.

3.5 Forces on polarizable particles

Let us now consider the case when the external fields induce the electric dipole on an, otherwise, non-polar particle. The total charge of this particle is zero, i.e. it contains the same amount of positive and negative charges.[21]

Let us assume that the particle does not have a permanent dipole arising from its internal configuration.[22]

Let us also suppose that the total angular momentum, of the positive and negative charges with respect to the center of mass, is kept constant during the polarization process.[23] If this is the case, the torque exert by the external fields will be zero.[24]

Considering the previously derived expression (see Eq. (3.19)) for the torque

$$\mathbf{N} = \mathbf{p} \times (\mathbf{E} + \mathbf{v} \times \mathbf{B}) + \mathrm{O}(d^2).$$

It implies that in order to have zero net torque, the induced dipole must be parallel to $(\mathbf{E} + \mathbf{v} \times \mathbf{B})$. It means that

$$\mathbf{p} = \alpha(\mathbf{E} + \mathbf{v} \times \mathbf{B}) + \mathrm{O}(d^2),$$

with α the *linear polarizability* of the particle. In general, the polarizability can be a second order tensor, and when the fields are time-dependent, it

[21] This is the case of neutral atoms or molecules, composed by an equal amount of positive and negative charges. This approach does not consider quantum-dynamic effects.

[22] For polar molecules, see Refs. 81 p. 164, and 80 Chap. 11.

[23] For an alternative derivation of the molecular polarizability, see Refs. 80 Chap. 11, and 81 p. 162.

[24] It makes sense to assume that external fields do not exert any torque in induced dipoles, since these dipoles will immediately align with the fields.

might also be a function of the alternating frequency. In this case, the induced dipole can be defined as

$$\mathbf{p} = \frac{1}{2}\alpha(\mathbf{E} + \mathbf{v} \times \mathbf{B}).$$

Yet, one has to keep in mind that this linear expression is valid as long as the wavelength of the external fields is much larger than the dimension of the particle. Otherwise, the external fields (for molecules it would be light on the nanometer wavelength) will excite atomic resonances and in order to give a more accurate description of these phenomena, a quantum-mechanic derivation would be necessary.[25]

The electric potential energy of the induced dipole will then be

$$U_e = -\mathbf{p} \cdot \mathbf{E}^*, \tag{3.20}$$

where $\mathbf{E}^*$ denotes the *complex-conjugate* of the field. The magnetic potential energy then becomes

$$U_m = -\mathbf{m} \cdot \mathbf{B}^* = -(\mathbf{p} \times \mathbf{v}) \cdot \mathbf{B}^* = -\mathbf{p} \cdot (\mathbf{v} \times \mathbf{B}^*), \tag{3.21}$$

which gives the total potential energy[26]

$$U = U_e + U_m = -\mathbf{p} \cdot (\mathbf{E}^* + \mathbf{v} \times \mathbf{B}^*) = -\frac{1}{2}\alpha|\mathbf{E} + \mathbf{v} \times \mathbf{B}|^2. \tag{3.22}$$

The classical Lagrangian of the dielectric particle will then be

$$L = T - U = \frac{1}{2}m\mathbf{v}^2 + \frac{1}{2}\alpha|\mathbf{E} + \mathbf{v} \times \mathbf{B}|^2. \tag{3.23}$$

Finally, when the particle moves "slowly", the magnetic field is much weaker than the electric one, or correspondingly $|\mathbf{v}||\mathbf{B}| << |\mathbf{E}|$, then the potential energy defined in Eq. (3.22) approximates

$$U \approx -\frac{1}{2}\alpha|\mathbf{E}|^2, \tag{3.24}$$

and the Lagrangian of the polarizable particle defined in Eq. (3.23) becomes

$$L = T - U = \frac{1}{2}m\mathbf{v}^2 + \frac{1}{2}\alpha|\mathbf{E}|^2. \tag{3.25}$$

In order to calculate the force acting on the particle, we can apply the Euler-Lagrange equations (3.1) to this Lagrangian, obtaining[27]

$$\mathbf{F}_{DEP} = m\dot{\mathbf{v}} = \frac{1}{2}\alpha\nabla|\mathbf{E}|^2. \tag{3.26}$$

Note that in the "electrostatic" regime[28] $\mathbf{F}_{DEP} = \alpha(\mathbf{E} \cdot \nabla)\mathbf{E} = (\mathbf{p} \cdot \nabla)\mathbf{E}$.

[25] See Refs. 113-118.
[26] Note that this expression is accurate in $O(d^2)$.
[27] Note that this expression is accurate in $O(d^2)$.
[28] $\mathbf{E} = -\nabla\phi$ and $\nabla\mathbf{E}^2 = 2(\mathbf{E} \cdot \nabla)\mathbf{E}$. Also $\mathbf{p} = \alpha\mathbf{E}$.

If we use the full expression of the Lagrangian (3.23), we reach the same force acting on the dipole previously found (see Eqs. (3.7) and (3.16))

$$\mathbf{F}_{DEP} = (\mathbf{p} \cdot \nabla)(\mathbf{E} + \mathbf{v} \times \mathbf{B}) + \dot{\mathbf{p}} \times \mathbf{B}.$$

For a macroscopic particle (composed by a material of dielectric permittivity ϵ_r) floating in vacuum, the polarizability will be $\alpha = \text{vol}(\epsilon_r - 1)\epsilon_0$.[29]

3.5.1 Dielectrophoresis

The force $\mathbf{F}_{DEP} \propto \nabla|\mathbf{E}|^2$ acting on polarizable particles was named dielectrophoresis by H. A. Pohl[30] during the 1950s. Since then, it has been intensively studied,[31] finding (today) many applications in fields like nanotechnology, microfluidic control, colloidal interactions, virus separation, lab-on-chip systems, etc.[32]

It is worth noting that, although this force have been studied since the 1950s, the author was not able to find its classical mechanics derivation in any of the quoted references.

One of the most interesting properties of the dielectrophoretic force, is that the motion of the particle is independent of the direction of the electric field $\mathbf{E}$ (unlike the *Lorentz* force). The force on the particle is proportional to the gradient of the electric energy density ∇u_e.

When the polarizability of the particle is positive (actually, when it is more polarizable than the surrounding environment), this force will attract it towards regions of high electric energy density. When the particle is less polarizable than the surrounding media, dielectrophoresis will push the particle towards low energy regions, and in mixtures of particles of different polarizability, dielectrophoretic forces will separate the blend, arranging high polarizability particle closer to high energy regions, and low polarizability particles in regions of low energy.

If the electric field is uniform, the electric energy density u_e will also be homogeneous (and its gradient will be zero). In order to observe dielectrophoretic forces one needs non-uniform, highly divergent or fringing electric fields.

Finally, in order to estimate the direction and magnitude of dielectrophoretic forces, one must know the way in which the electric energy density

[29] See Ref. 99.
[30] See Refs. 100-101.
[31] See Refs. 102-104.
[32] See Refs. 105-112.

$u_e = \frac{\epsilon}{2}|\mathbf{E}|^2$ distributes in the region of interest (note that this energy is frequency dependent, and the shape in which it will distribute inside the cavity will depend on the boundary conditions, see Chap. 2).

3.6 Polarizability of gases

The molecular polarizability α is measured in units of volume×permittivity, but it is usually expressed in volume units $\overline{\alpha} = \alpha/\epsilon_0$. For instance, the atomic polarizability of argon in volume units[33] is $\overline{\alpha} = 1.586$ Å^3.

For rarefied gases in thermal equilibrium, the electric susceptibility χ_e and the dielectric constant ϵ_r (or relative permittivity) depend linearly on the atomic polarizability and the density of the gas[34]

$$\chi_e = n\overline{\alpha} \qquad \epsilon_r = 1 + \chi_e = 1 + n\overline{\alpha}. \tag{3.27}$$

In the case of gases composed by polar molecules, the macroscopic polarizability also depends inversely on the temperature of the gas.[35]

If we consider the dielectrophoretic force defined in Eq. (3.26) as the only force acting on the molecules of the gas, we could calculate the external force (per unit volume) on the dielectric (monoatomic) gas as

$$n\mathbf{F}_{DEP} = n\overline{\alpha}\frac{\epsilon_0}{2}\nabla|\mathbf{E}|^2 = \chi_e\frac{\epsilon_0}{2}\nabla|\mathbf{E}|^2 = \chi_e\nabla u_e. \tag{3.28}$$

In dielectric fluids, and in order for the dielectrophoretic force to overcome the Brownian motion, one has to verify whether the potential energy is higher than the kinetic energy of the random motion of the molecules. This case will be addressed in the following chapter, by means of a dimensional analysis (see Sec. 4.6.2).

3.7 Final remarks

Lagrangian mechanics assumes that one can measure (at every instant of time) each variable representing a degree of freedom of the system under study. This classical viewpoint crashes at the limit of the uncertainty principle, where the more certainly the position of a particle is determined, the less accurately its momentum can be known, and vice versa.

[33] http://www.chemicool.com/elements/argon.html.
[34] See Refs. 80 Chap. 11, 90 p. 200, and 91 p. 38.
[35] See Ref. 81 p. 165.

In low-temperature low-pressure plasma discharges, like the PK-3 Plus experiment, there are about 10^{16} neutral particles and 10^{10} ions and electrons per cubic-centimeter. This amount of particles will give rise to a Brownian motion. Since it would be impossible to follow the trajectory of each of them, the dynamics of this bunch of particles will be analyzed, in the next chapter, by means of the kinetic theory of rarefied gases and plasmas.

It is important to notice that (at slow velocities and/or under weak magnetic fields), charged particles follow the streamlines of electric field $\nabla\phi$ while dielectric particles follow streamlines of the gradient of the electric energy density ∇u_e. These different forces, acting on a blend of charged and dielectric particles, lead to a separation of the mixture. Next chapter will develop this idea, and a dimensional analysis will be used in order to weigh the importance of dielectric to Lorentz forces in complex plasmas.[36]

[36] Dipole effects in complex plasmas have been analyzed in Refs. 196-199.

Kinetic theory of rarefied gases and plasmas

4

The kinetic theory of gases bridges the gap between microscopic and macroscopic descriptions. It explains how macroscopic properties of dilute gases (like temperature, pressure, mass flux, etc.) can be obtained starting from the microscopic interaction of its constituents.[1]

Following the previous chapter, we have seen that the greater the amount of particles, the more complicated it becomes to describe the motion of all of them. For instance, in order to compute the trajectory of N point-mass particles moving in a three-dimensional space, it would be necessary to solve 3N second-order ordinary differential equations (ODEs), or equivalently, 6N first-order ODEs. Furthermore, when the particles interact with each other through long-distance forces (for example, gravitational or electromagnetic forces), it would be necessary to compute N(N-1)/2 forces[2] and the 6N ODEs will be coupled. Also the time-step of the numerical algorithm has to be at least as small as the smallest time-scale of the phenomena under study.

In order to overcome the problems arising from the numerical implementation, one could use parallel algorithms or specific hardware.[3] Yet, when one is interested in the macroscopic properties of an ensemble of particles, such a detailed description is unnecessary.

This introduces us to the idea of taking averages over a large number of particles, by means of a statistical description or any other coarse graining method.[4]

In the kinetic theory of gases, the statistical description of the gas will be given by a distribution function $f(\mathbf{x}, \mathbf{v}, t)$ in the *phase space*. The phase space is a six dimensional space consisting on six independent variables (three cartesian coordinates for both the position and the velocity). This distribution function, in principle, may have any dependence upon the variables $\mathbf{x}, \mathbf{v}$ and t (it does not have to be a Maxwell distribution).

This chapter will describe the mathematical formulation of the kinetic

[1] See Refs. 119-132. For a review on the Kinetic theory of complex plasmas, see Refs. 161-172.

[2] The calculation of N(N-1)/2 distances implies the intensive use of root-square algorithms and the allocation of N(N-1)/2 *doubles* in memory.

[3] `http://www.astrograpе.org`.

[4] See for instance P. Español, *Statistical mechanics of coarse-graining*, in Ref. 140.

theory of ideal gases, and then these concepts will be extended to weakly ionized plasmas and complex plasmas.

4.1 The moments of a distribution function

Let us first consider a distribution function f which only depends on a single variable ξ. The n^{th} *moment* about the origin is defined as

$$\mu_n = \int \xi^n f(\xi) d\xi. \tag{4.1}$$

The mean value (or $zero^{th}$ moment) is defined as $\mu = \int f(\xi) d\xi$. When this mean value is different from zero, it also makes sense to calculate the k^{th} moments about it (also called *central moments*).[5] The k^{th} central moment is defined as

$$\mu_k = \int (\xi - \mu)^k f(\xi) d\xi. \tag{4.2}$$

By definition, the first central moment is equal to zero. The *variance, skewness* and *kurtosis* are the second, third and fourth moments about the mean value, respectively. These central moments share properties of homogeneity and translational invariance.

4.2 Moments of a distribution function in the velocity space

Let us now analyze the case when the distribution function f depends on more than one variable.[6] In order to obtain macroscopic quantities in the physical space of coordinates $\mathbf{x}$, one has to take averages of $f(\mathbf{x}, \mathbf{v}, t)$ with respect to all possible velocities in the *velocity space*.[7]

In general, it is possible to define any macroscopic quantity of the gas $\langle\psi\rangle$ by averaging the microscopic variable $\psi(\mathbf{x}, \mathbf{v}, t)$ in the velocity space

$$\langle\psi\rangle(\mathbf{x}, t) = \frac{\int \psi(\mathbf{x}, \mathbf{v}, t) f(\mathbf{x}, \mathbf{v}, t) d\mathbf{v}}{\int f(\mathbf{x}, \mathbf{v}, t) d\mathbf{v}} = \frac{1}{n} \int \psi f d\mathbf{v},$$

[5] One could normalize the distribution function, so $\overline{f} = f/\mu$ and $\int \overline{f} d\xi = 1$.

[6] This section follows Refs. 123 pp. 79-83, and 124 pp. 123-125.

[7] The kinetic theory of gases was developed before the theory of relativity. Therefore, the velocity space was considered to be $\mathbb{R}^3$ and the integrals were evaluated between $-\infty$ and ∞. Defining c as the speed of light, a relativistic approach should consider the velocity space as the bounded domain $(-\mathrm{c},\mathrm{c})^3 \subset \mathbb{R}^3$.

where the *number density* is defined as

$$n(\mathbf{x}, t) = \int f(\mathbf{x}, \mathbf{v}, t) d\mathbf{v}.$$

4.2.1 Mass density

Let us consider a gas inside a vessel, and suppose that all of the molecules have the same mass m. The *mass density* is defined as

$$\rho(\mathbf{x}, t) = \int m f(\mathbf{x}, \mathbf{v}, t) d\mathbf{v} = m n(\mathbf{x}, t), \tag{4.3}$$

which corresponds to the $zero^{th}$ moment of $f(\mathbf{x}, \mathbf{v}, t)$ in the velocity space. The total mass of the gas is then $M = \int_\Omega \rho d\mathbf{x}$, where Ω represents the volume of the cavity containing the gas.

4.2.2 Momentum density

One could calculate higher moments. For instance, the first moment of f is called the *momentum density*

$$\rho(\mathbf{x}, t)\mathbf{u}(\mathbf{x}, t) = \int m \mathbf{v} f(\mathbf{x}, \mathbf{v}, t) d\mathbf{v}. \tag{4.4}$$

The *macroscopic velocity* (or mass velocity) $\mathbf{u}(\mathbf{x}, t) = \frac{1}{n} \int \mathbf{v} f d\mathbf{v}$ is the drift velocity of the gas, and it is equal to zero for a gas in equilibrium inside a vessel.[8]

Yet, when the mean velocity is zero, this does not imply that each single molecule is at rest. The random deviation of the molecular velocity with respect to the mean velocity is called the *peculiar* or *random velocity* $\mathbf{c} = \mathbf{v} - \mathbf{u}$.

Analogously to the mono-variable case, in the velocity space the first central moment of f is zero

$$\int \mathbf{c} f d\mathbf{v} = \int (\mathbf{v} - \mathbf{u}) f d\mathbf{v} = \mathbf{0}. \tag{4.5}$$

[8] From here we will use the short notation $f = f(\mathbf{x}, \mathbf{v}, t)$, $\rho = \rho(\mathbf{x}, t)$, $\mathbf{u} = \mathbf{u}(\mathbf{x}, t)$, etc.

4.2.3 Momentum flow

The random motion of the molecules also gives rise to the *stress tensor*. The second moment of f about the mean velocity $\mathbf{u}$ is the tensor[9]

$$\begin{aligned}\boldsymbol{\sigma}(\mathbf{x},t) &= \int m\mathbf{c}\mathbf{c}f d\mathbf{v} = \int m(\mathbf{v}-\mathbf{u})(\mathbf{v}-\mathbf{u})f d\mathbf{v} \\ &= \int m\mathbf{v}\mathbf{v}f d\mathbf{v} - \rho\mathbf{u}\mathbf{u}. \end{aligned} \tag{4.6}$$

The tensor $\boldsymbol{\Pi}(\mathbf{x},t)$, which represents the *total momentum flow*, decomposes into two parts: one is the *macroscopic momentum flow* (momentum density $\times$ velocity) and the other part is the contribution due to the molecular random motion (represented by the stress tensor)

$$\boldsymbol{\Pi} = \int m\mathbf{v}\mathbf{v}f d\mathbf{v} = \rho\mathbf{u}\mathbf{u} + \boldsymbol{\sigma}. \tag{4.7}$$

4.2.4 Energy density

The random motion of the molecules would also suggest the idea of calculating the internal energy of the gas. By defining $\varepsilon(\mathbf{x},t)$ as the *internal energy per unit mass*, it leads to a representation of the *internal energy density*

$$\begin{aligned}\rho\varepsilon &= \frac{1}{2}\int mc^2 f d\mathbf{v} = \frac{1}{2}\int m(v-u)^2 f d\mathbf{v} \\ &= \frac{1}{2}\int mv^2 f d\mathbf{v} - \frac{1}{2}\rho u^2. \end{aligned} \tag{4.8}$$

The *total energy density* $e(\mathbf{x},t)$ can be split into the *macroscopic kinetic energy density* and the internal energy density

$$e = \frac{1}{2}\int mv^2 f d\mathbf{v} = \frac{1}{2}\rho u^2 + \rho\varepsilon. \tag{4.9}$$

Isotropy of the random motion

Let us assume that the random motion of the particles does not have a preferred direction. This assumption relates the internal energy density (defined in Eq. (4.8)) to the temperature of the monoatomic gas consisting of point-mass molecules. If we define the average energy per translational degree of freedom as $\frac{1}{2}kT$ (where k is the Boltzmann constant), we can find a relation

[9] Note that the stress tensor $\boldsymbol{\sigma}$ is symmetric.

between the internal energy density and the temperature of the monoatomic gas (only three degrees of freedom)

$$\rho\varepsilon = \frac{3}{2}nkT.$$

It is worth noting that the trace of the stress tensor in Eq. (4.6) is twice the internal energy density defined in Eq. (4.8)

$$tr(\boldsymbol{\sigma}) = tr(\int m\mathbf{cc}f d\mathbf{v}) = \int m\mathbf{c}\cdot\mathbf{c}f d\mathbf{v} = 2\rho\varepsilon.$$

Also, the isotropic assumption relates the trace of the stress tensor $\boldsymbol{\sigma}$ to the gas pressure as $p = tr(\boldsymbol{\sigma})/3$. By combining these expressions, one gets the *equation of state* for the ideal (monoatomic) gas[10]

$$p = \frac{2}{3}\rho\varepsilon = nkT. \tag{4.10}$$

Viscid fluids

When the fluid is at rest (the macroscopic velocity $\mathbf{u}$ is zero), the *hydrostatic* pressure is related to the stress tensor defined in Eq. (4.6) as $\sigma_{ij} = p\delta_{ij}$.[11]

When the fluid is in motion, the stress tensor can be split into two parts: the contribution due to the hydrostatic part plus the contribution due to the *viscous tensor*[12]

$$\sigma_{ij} = p\delta_{ij} - \pi_{ij}. \tag{4.11}$$

For Newtonian fluids, the viscous tensor $\boldsymbol{\pi}$ depends linearly on the gradients of the macroscopic velocity $\mathbf{u}$. In tensor notation this means

$$\pi_{ij} = A_{ijkl}\frac{\partial u_k}{\partial x_l},$$

where A_{ijkl} is a fourth order cartesian tensor.[13]

It can be shown[14] that the most general representation of an isotropic tensor of the fourth order is given by three coefficients

$$A_{ijkl} = \lambda\delta_{ij}\delta_{kl} + \mu\delta_{ik}\delta_{jl} + \nu\delta_{il}\delta_{jk}.$$

[10] See Ref. 124 p. 233.
[11] The symbol δ_{ij} represents the Kronecker delta.
[12] Sometimes also called the *deviatoric stress*.
[13] This tensor has $3^4 = 81$ coeffs. independent of $\mathbf{u}$ (they may depend on ρ, T, etc.).
[14] See Ref. 141 pp. 96-98.

If this tensor is also symmetric, i.e. $\boldsymbol{\pi} = \boldsymbol{\pi}^{\mathrm{T}}$, it implies that $\nu = \mu$ and A_{ijkl} is expressed in terms of only two coefficients λ and μ

$$A_{ijkl} = \lambda\delta_{ij}\delta_{kl} + \mu(\delta_{ik}\delta_{jl} + \delta_{il}\delta_{jk}).$$

Then, the representation of the (isotropic symmetric) viscous tensor becomes[15]

$$\pi_{ij} = \lambda\delta_{ij}\frac{\partial u_k}{\partial x_k} + \mu\left(\frac{\partial u_i}{\partial x_j} + \frac{\partial u_j}{\partial x_i}\right).$$

Note that the trace of the viscous tensor equals

$$tr(\boldsymbol{\pi}) = (3\lambda + 2\mu)\nabla\cdot\mathbf{u}.$$

The *Stokes assumption* implies zero trace for the viscous tensor. This means $3\lambda + 2\mu = 0$ and $\lambda = -\frac{2}{3}\mu$. The stress tensor in Eq. (4.11) then becomes

$$\sigma_{ij} = p\delta_{ij} - \pi_{ij} = p\delta_{ij} - \mu\left(-\frac{2}{3}\frac{\partial u_k}{\partial x_k}\delta_{ij} + \frac{\partial u_i}{\partial x_j} + \frac{\partial u_j}{\partial x_i}\right).$$

Note that the Stokes assumption implies $tr(\boldsymbol{\sigma})/3 = p$ and

$$\nabla\cdot\boldsymbol{\sigma} = \nabla p - \mu\left(\frac{1}{3}\nabla\nabla\cdot\mathbf{u} + \nabla^2\mathbf{u}\right).$$

The coefficient μ is called the *shear* or *dynamic viscosity*, λ is named *second coefficient of viscosity*, and $\mu_B = \lambda + \frac{2}{3}\mu$ is called the *bulk viscosity*.

Neglecting the Stokes assumption, the stress tensor in Eq. (4.11) reads[16]

$$\sigma_{ij} = \left(p - \lambda\frac{\partial u_k}{\partial x_k}\right)\delta_{ij} - \mu\left(\frac{\partial u_i}{\partial x_j} + \frac{\partial u_j}{\partial x_i}\right),$$

and its trace reaches $tr(\boldsymbol{\sigma})/3 = p - \mu_B\nabla\cdot\mathbf{u}$.

[15] We can write it in the compact form $\boldsymbol{\pi} = \lambda\nabla\cdot\mathbf{u}\mathbf{I} + 2\mu\boldsymbol{\varepsilon}(\mathbf{u})$, where

$$\varepsilon_{ij}(\mathbf{u}) = \frac{1}{2}\left(\frac{\partial u_i}{\partial x_j} + \frac{\partial u_j}{\partial x_i}\right) \qquad \text{is the } \textit{rate of strain} \text{ tensor.}$$

[16] Some times also defined with opposite sign. See http://www.navier-stokes.net.

Temperature and rms velocity

The temperature of the gas is a macroscopic measure of the agitation of the molecules. Since the random velocity does not have a preferred direction of motion, the *peculiar velocity* can be decomposed in the sum of its cartesian components

$$c^2 = c_x^2 + c_y^2 + c_z^2 = 3c_x^2 = 3c_y^2 = 3c_z^2,$$

and then one could define its *root-mean-square* value as

$$c_{\text{rms}} = \sqrt{\frac{1}{n}\int c^2 f d\mathbf{v}} = \sqrt{\frac{1}{n}\int 3c_x^2 f d\mathbf{v}}. \tag{4.12}$$

Since the random energy of the molecules (in each cartesian direction) is proportional to the temperature, we can use the definition of the average energy per translational degree of freedom in order to obtain a relation between the temperature of the gas and the random velocity in each cartesian direction

$$\frac{1}{2}kT = \frac{1}{2}mc_{x\,\text{rms}}^2 = \frac{1}{2}m\frac{1}{n}\int c_x^2 f d\mathbf{v},$$

and the total internal kinetic energy of the gas will be then defined as

$$\frac{3}{2}kT = \frac{3}{2}mc_{x\,\text{rms}}^2 = \frac{1}{2}mc_{\text{rms}}^2.$$

We can obtain a relationship between the temperature and the root-mean-square velocity[17]

$$c_{\text{rms}} = \sqrt{3c_{x\,\text{rms}}^2} = \sqrt{\frac{3kT}{m}}, \tag{4.13}$$

so we could express the total energy density defined in Eq. (4.9) in terms of

[17] For argon molecules at room temperature, this velocity is approximately 430 m/s.

the variables T, p or c_{rms}[18]

$$e = \frac{1}{2}\int v^2 f d\mathbf{v} = \frac{1}{2}\rho u^2 + \rho\varepsilon = \frac{1}{2}\rho u^2 + \frac{1}{2}\rho c_{\text{rms}}^2$$
$$= \frac{1}{2}\rho u^2 + \frac{3}{2}p = \frac{1}{2}\rho u^2 + \frac{3}{2}nkT. \tag{4.14}$$

4.2.5 Heat flow

The random motion of the particles also gives rise to the *heat flow* vector

$$\mathbf{q} = \frac{1}{2}\int m\mathbf{c}c^2 f d\mathbf{v} = \frac{1}{2}\int m\mathbf{v}c^2 f d\mathbf{v} - \frac{1}{2}\int m\mathbf{u}c^2 f d\mathbf{v}$$
$$= \frac{1}{2}\left(\int m\mathbf{v}v^2 f d\mathbf{v} - \int 2m\mathbf{u}\cdot\mathbf{v}\mathbf{v} f d\mathbf{v} + \int m\mathbf{v}u^2 f d\mathbf{v}\right) - \frac{1}{2}\int m\mathbf{u}c^2 f d\mathbf{v}. \tag{4.15}$$

Since the macroscopic velocity $\mathbf{u}$ can be taken out of the integrals, and using the definitions given in Eqs. (4.4), (4.7), and (4.8), we obtain an expression for the heat flow

$$\mathbf{q}(\mathbf{x},t) = \frac{1}{2}\int m\mathbf{v}v^2 f d\mathbf{v} - \mathbf{u}\cdot\boldsymbol{\Pi} + \frac{1}{2}\rho\mathbf{u}u^2 - \mathbf{u}\rho\varepsilon$$
$$= \frac{1}{2}\int m\mathbf{v}v^2 f d\mathbf{v} - \mathbf{u}(\frac{1}{2}\rho u^2 + \rho\varepsilon) - \mathbf{u}\cdot\boldsymbol{\sigma}. \tag{4.16}$$

By using the definition given in Eq. (4.14), the *total energy flow* $\mathbf{Q}$ (velocity $\times$ energy density) is defined as[19]

$$\mathbf{Q}(\mathbf{x},t) = \frac{1}{2}\int m\mathbf{v}v^2 f d\mathbf{v} = \mathbf{u}e + \mathbf{u}\cdot\boldsymbol{\sigma} + \mathbf{q}. \tag{4.17}$$

[18] Following Eq. (4.14) $p = \frac{2}{3}(e - \frac{1}{2}\rho u^2) = \frac{2}{3}\rho\varepsilon$. Defining $\gamma = \frac{5}{3}$ as the ratio of specific heat of the monoatomic gas, we find that $p = (\gamma - 1)\rho\varepsilon$. Also, we could define the *speed of sound* in the ideal gas as

$$s = \sqrt{\gamma\frac{p}{\rho}} = \sqrt{\gamma\frac{kT}{m}} = \sqrt{\gamma c_{\text{x rms}}^2} = 320 \text{ m/s for argon at room temperature.}$$

The Mach number $M = |\mathbf{u}|/s$ gives an estimation of the macroscopic kinetic energy respect to the internal energy. For $M << 1$ the flow is sub-sonic and $\frac{1}{2}\rho u^2 << \rho\varepsilon$.

[19] See Ref. 124 p. 232.

Fourier law of heat conduction

The Fourier law assumes that the heat flow $\mathbf{q}$ linearly depends on the gradient of the temperature

$$\mathbf{q} = -\kappa \nabla T,$$

where the proportionality constant κ is the thermal conductivity.

4.3 Conservation of mass, momentum and energy

The previous sections have described how the distribution function $f(\mathbf{x}, \mathbf{v}, t)$ is linked to macroscopic quantities such as density, momentum, pressure, etc. In order to get the conservation equations of these quantities (also called *continuity equations*), one could use the Boltzmann equation.[20] This equation[21] is derived from the Liouville theorem[22]

$$\frac{\partial f}{\partial t} + \mathbf{v} \cdot \frac{\partial f}{\partial \mathbf{x}} + \mathbf{a} \cdot \frac{\partial f}{\partial \mathbf{v}} = 0. \tag{4.18}$$

By dividing the forces acting on the particles into external and internal forces (due to molecular interactions), one obtains the Boltzmann equation[23]

$$\frac{\partial f}{\partial t} + \mathbf{v} \cdot \frac{\partial f}{\partial \mathbf{x}} + \mathbf{a}_{\text{ext}} \cdot \frac{\partial f}{\partial \mathbf{v}} = C(f), \tag{4.19}$$

where the *collision integral* $C(f)$ represents the internal interaction of the molecules through collisions,[24] and the term $\mathbf{a}_{\text{ext}}$ represents the acceleration of the particles due to external forces.

---

[20] L. Boltzmann, *Further studies on the thermal equilibrium of gas molecules*. See Ref. 119 pp. 88-175.

[21] See Refs. 97 pp. 184-189, 94 pp. 418-421, 96 pp. 364-368, 123 Chap. 2, 124 Chap. 4, and 128 Chap. 7.

[22] The distribution function which exactly fulfills the Liouville equation is
$f(\mathbf{x}, \mathbf{v}, t) = \sum_i \delta(\mathbf{x} - \boldsymbol{\xi}_i(t))\delta(\mathbf{v} - \dot{\boldsymbol{\xi}}_i(t))$
where $\boldsymbol{\xi}_i(t)$ and $\dot{\boldsymbol{\xi}}_i(t)$ are the position and velocity of each particle (Refs. 126 p. 49, 127 p. 17, and 125 p. 210).

[23] See Refs. 120 p. 133, 121 p. 46, 125 pp. 7-10, 128 p. 449, and 129.

[24] It does not have to be hard spheres collisions, as a matter of fact, one could use any kind of interacting potential among the particles.

4.3.1 Collision invariants

Although the collision integral $C(f)$ may have a very complicate dependence on the distribution function f, some of its properties can be inferred even without knowing its exact form.

The interaction among particles does not change the velocity of the center of mass, neither the total mass nor the total kinetic energy, this introduces us with the concept of *collision invariants*.[25]

The collision invariants are such that the macroscopic behavior of the gas is independent of the type of collision among it constituent molecules, this can be written as

$$\int \psi_\alpha C(f) d\mathbf{v} = 0,$$

where the collision invariants ψ_α are m, $m\mathbf{v}$ and $\frac{1}{2}m\mathbf{v}^2$ (or any linear combination of them).

In order to obtain the conservation equations[26] of macroscopic quantities, we can multiply Eq. (4.19) by any of these collision invariants, and then integrate it over the velocity space

$$\int \psi_\alpha \left(\frac{\partial f}{\partial t} + \mathbf{v} \cdot \frac{\partial f}{\partial \mathbf{x}} + \mathbf{a}_{\text{ext}} \cdot \frac{\partial f}{\partial \mathbf{v}} \right) d\mathbf{v} = \int \psi_\alpha C(f) d\mathbf{v}.$$

Since these invariants are independent on the variables t and $\mathbf{x}$, and since $\int C(f)\psi_\alpha d\mathbf{v} = 0$, this equation becomes

$$\int \left(\frac{\partial}{\partial t}(\psi_\alpha f) + \frac{\partial}{\partial \mathbf{x}} \cdot (\psi_\alpha \mathbf{v} f) + \frac{\partial}{\partial \mathbf{v}} \cdot (\mathbf{a}_{\text{ext}} \psi_\alpha f) - \frac{\partial}{\partial \mathbf{v}} \cdot (\mathbf{a}_{\text{ext}} \psi_\alpha) f \right) d\mathbf{v} = 0.$$

Also, assuming that the distribution function f tends to zero on the boundary of the velocity space,[27] it implies $\int \frac{\partial}{\partial \mathbf{v}} \cdot (\mathbf{a}_{\text{ext}} \psi_\alpha f) d\mathbf{v} = 0$, and we finally obtain

$$\frac{\partial}{\partial t} \int \psi_\alpha f d\mathbf{v} + \nabla \cdot \int \psi_\alpha \mathbf{v} f d\mathbf{v} - \int \frac{\partial}{\partial \mathbf{v}} \cdot (\mathbf{a}_{\text{ext}} \psi_\alpha) f d\mathbf{v} = 0. \tag{4.20}$$

[25] See Refs. 124 pp. 228-230, 123 pp. 67-77, 122 pp. 40-44, 121 pp. 49-50, 125 pp. 14-15, 128 pp. 455-459, and 131 pp. 123-124.

[26] See Refs. 124 pp. 231-234, 131 Chap. 6, 125 pp. 14-15, and 128 pp. 459-462.

[27] The classical kinetic approach assumes that none molecule has infinite velocity, i.e. $f \xrightarrow{\mathbf{v} \to \pm\infty} 0$, (this is due to D. Hilbert, see *Foundations of the kinetic theory of gases* in Ref. 120 pp. 89-101).

By choosing the first collision invariant $\psi_0 = m$, and the definitions given in Eqs. (4.3) and (4.4); Eq. (4.20) becomes the continuity equation for the mass density[28]

$$\frac{\partial \rho}{\partial t} + \nabla \cdot \rho \mathbf{u} = 0. \tag{4.21}$$

By using the collision invariants $\psi_{1,2,3} = m\mathbf{v}$ and the definitions given in Eqs. (4.4) and (4.7); Eq. (4.20) becomes the equation for the continuity of momentum density[29]

$$\frac{\partial \rho \mathbf{u}}{\partial t} + \nabla \cdot \mathbf{\Pi} - \rho \mathbf{a}_{\text{ext}} = 0. \tag{4.22}$$

By using the collision invariant $\psi_4 = \frac{1}{2} m\mathbf{v}^2$ in Eq. (4.20), together with the definitions given in Eqs. (4.9) and (4.17), we achieve the equation for the continuity of energy density

$$\frac{\partial e}{\partial t} + \nabla \cdot \mathbf{Q} - \rho \mathbf{u} \cdot \mathbf{a}_{\text{ext}} = 0 \tag{4.23}$$

The equations for the conservation of mass, momentum and energy densities are

$$\frac{\partial \rho}{\partial t} + \nabla \cdot \rho \mathbf{u} = 0 \tag{4.24}$$

$$\frac{\partial \rho \mathbf{u}}{\partial t} + \nabla \cdot \mathbf{\Pi} = \rho \mathbf{a}_{\text{ext}} \tag{4.25}$$

$$\frac{\partial e}{\partial t} + \nabla \cdot \mathbf{Q} = \rho \mathbf{u} \cdot \mathbf{a}_{\text{ext}}, \tag{4.26}$$

where $\rho \mathbf{a}_{\text{ext}}$ represents the external forces (per unit volume) acting on the gas, and $\rho \mathbf{u} \cdot \mathbf{a}_{\text{ext}}$ is the power (per unit volume) supplied by the external sources.

[28] This is valid for external forces such as $\frac{\partial}{\partial \mathbf{v}} \cdot \mathbf{F}_{\text{ext}} = 0$, which is the case of gravity, Lorentz and dielectrophoretic forces.

[29] It is possible to verify that $\frac{\partial}{\partial \mathbf{v}} \cdot (\mathbf{F_{ext}} \mathbf{v}) = (\frac{\partial}{\partial \mathbf{v}} \cdot \mathbf{F_{ext}})\mathbf{v} + (\mathbf{F_{ext}} \cdot \frac{\partial}{\partial \mathbf{v}})\mathbf{v} = \mathbf{F_{ext}}$ (when $\frac{\partial}{\partial \mathbf{v}} \cdot \mathbf{F}_{\text{ext}} = 0$), so the macroscopic Lorentz force in (4.20) becomes (Ref. 131 p. 159)

$$\int \frac{\partial}{\partial \mathbf{v}} \cdot (\mathbf{F_{Lorentz}} \mathbf{v}) f d\mathbf{v} = \int q(\mathbf{E} + \mathbf{v} \times \mathbf{B}) f d\mathbf{v} = qn\mathbf{E} + qn\mathbf{u} \times \mathbf{B}.$$

4.3.2 Fluid dynamic equations

Further simplifications are needed in order to obtain the classical equations of fluid dynamics.

By using the gradient of the total momentum flow in Eq. (4.7)

$$\nabla \cdot \mathbf{\Pi} = \nabla \cdot (\rho \mathbf{u}\mathbf{u} + \boldsymbol{\sigma}) = \nabla \cdot (\rho \mathbf{u})\mathbf{u} + \rho(\mathbf{u} \cdot \nabla)\mathbf{u} + \nabla \cdot \boldsymbol{\sigma},$$

together with the equality $\frac{\partial \rho \mathbf{u}}{\partial t} = \frac{\partial \rho}{\partial t}\mathbf{u} + \rho \frac{\partial \mathbf{u}}{\partial t}$, and the continuity equation (4.24), it is possible to write Eq. (4.25) as the *Cauchy's equation of motion*

$$\rho \left(\frac{\partial \mathbf{u}}{\partial t} + (\mathbf{u} \cdot \nabla)\mathbf{u} \right) + \nabla \cdot \boldsymbol{\sigma} = \rho \mathbf{a}_{\text{ext}}. \tag{4.27}$$

We could also write Eq. (4.26) in terms of the variables ε, p or T. For instance, by performing (4.26)$-$($\mathbf{u}\cdot$(4.25)$/2+\mathbf{u}\cdot$(4.27)$/2$), it gives the continuity equation for the internal energy $\rho\varepsilon$

$$\frac{\partial \rho \varepsilon}{\partial t} + \nabla \cdot \rho \varepsilon \mathbf{u} + \nabla \mathbf{u} : \boldsymbol{\sigma} + \nabla \cdot \mathbf{q} = 0.$$

With the help of Eq. (4.24), it becomes

$$\rho \left(\frac{\partial \varepsilon}{\partial t} + (\mathbf{u} \cdot \nabla)\varepsilon \right) + \nabla \mathbf{u} : \boldsymbol{\sigma} + \nabla \cdot \mathbf{q} = 0,$$

where $\nabla \mathbf{u} = \frac{\partial u_i}{\partial x_j}$ is the velocity gradient tensor and $\nabla \mathbf{u} : \boldsymbol{\sigma}$ denotes[30] the contraction $\sum_{ij} \frac{\partial u_i}{\partial x_j} \sigma_{ij}$.

Following Eq. (4.14), it is clear that we could write the equation of conservation of energy density (4.26) in terms of the variables p, T, c_{rms} or ε. The choice of variables $(\rho, \rho\mathbf{u}, e)$, $(\rho, \mathbf{u}, p)$, etc. will depend on the nature of the problem under study.

Euler equations

The Euler equations describe the dynamic of compressible inviscid isothermal flows. The inviscid assumption relates the stress tensor in Eq. (4.11) to the isotropic pressure $\boldsymbol{\sigma} = \mathbf{I}p$. Also, the isothermal assumption (together with

[30] Since $\boldsymbol{\sigma}$ is symmetric

$$\nabla \mathbf{u} : \boldsymbol{\sigma} = \sum_{ij} \frac{\partial u_i}{\partial x_j} \sigma_{ij} = \sum_{ij} \frac{\partial u_j}{\partial x_i} \sigma_{ji} = \boldsymbol{\sigma}^{\mathrm{T}} : \nabla \mathbf{u}^{\mathrm{T}} = \boldsymbol{\sigma} : \nabla \mathbf{u}^{\mathrm{T}}.$$

the Fourier law of heat conduction) implies $\mathbf{q} = -\kappa\nabla T = 0$. Therefore, the total energy flow in Eq. (4.17) becomes $\mathbf{Q} = \mathbf{u}e + \mathbf{u}\cdot\boldsymbol{\sigma} = \mathbf{u}(e+p)$.

By using the previously described approximations, the continuity equations (4.24), (4.27), and (4.26) become the Euler equations

$$\begin{aligned}
\frac{\partial \rho}{\partial t} + \nabla\cdot\rho\mathbf{u} &= 0 \\
\rho\left(\frac{\partial \mathbf{u}}{\partial t} + (\mathbf{u}\cdot\nabla)\mathbf{u}\right) + \nabla p &= \rho\mathbf{a}_{\text{ext}} \\
\frac{\partial e}{\partial t} + \nabla\cdot((e+p)\mathbf{u}) &= \rho\mathbf{u}\cdot\mathbf{a}_{\text{ext}}.
\end{aligned}$$

Finally, we can close this system (in order to have five unknowns and five PDEs) by using the relationship found in (4.14): $p = (\gamma-1)(e - \frac{1}{2}\rho\mathbf{u}^2)$.

Navier-Stokes equations

The Navier-Stokes equations describe the motion of incompressible viscid flows; i.e. ρ is constant, the stress tensor is composed by the hydrostatic and viscous parts $\boldsymbol{\sigma} = \mathbf{I}p - \boldsymbol{\pi}$, and $\nabla\cdot\boldsymbol{\sigma} = \nabla p - \nabla\cdot\boldsymbol{\pi}$.

For Newtonian fluids $\nabla\cdot\boldsymbol{\pi} = \mu\nabla^2\mathbf{u}$, where μ is the *dynamic viscosity*. All of these assumptions define the incompressible Navier-Stokes equations

$$\nabla\cdot\mathbf{u} = 0 \tag{4.28a}$$

$$\rho\left(\frac{\partial \mathbf{u}}{\partial t} + (\mathbf{u}\cdot\nabla)\mathbf{u}\right) + \nabla p - \mu\nabla^2\mathbf{u} = \rho\mathbf{a}_{\text{ext}}. \tag{4.28b}$$

The partial differential equations describing the motion of fluids have been one of the major topics of study in physics and mathematics during the last century, and yet, there are still unsolved problems.[31]

For steady compressible flows, the speed of the flow characterizes the partial differential equations which describe its motion. If the speed is supersonic (waves, shocks, etc.) the PDEs are hyperbolic, while for the subsonic case, laminar and incompressible flows, the PDEs are basically elliptic. Unsteady incompressible flows have a mixture of parabolic-elliptic behavior. Before implementing an appropriate numerical method of the mathematical model, one has to study the character of the flow by means of a dimensional analysis.

[31] In year 2000, the Clay Mathematics Institute set up seven *Prize Problems* in modern mathematics. One of the problems is to make substantial progress toward a mathematical theory for the Navier-Stokes equations (and the prize is $1 million).
See http://www.claymath.org/millennium.

4.3.3 Dimensional analysis

The partial differential equations which describe the dynamic of fluids present different scales (of time, length, etc.). This different scales make it difficult to analyze the original PDE formulation.

One way to overcome this problem is to normalize the variables under study (pressure, velocity, density, etc.), in order to obtain dimensionless equations. For instance, if l denotes the characteristic length of the phenomenon under study, u_0 the characteristic velocity, $t_0 = l/u_0$ the time-scale associated to u_0, and p_0 the characteristic pressure, we can obtain the dimensionless variables (the bar denotes dimensionless units)

$$\nabla = \frac{1}{l}\overline{\nabla} \qquad \frac{\partial}{\partial t} = \frac{u_0}{l}\frac{\partial}{\partial \overline{t}} \qquad \mathbf{u} = u_0\overline{\mathbf{u}} \qquad p = p_0\overline{p}.$$

As an example, by using the previously defined variables, the Navier-Stokes equations (4.28) can be written as

$$\overline{\nabla}\cdot\overline{\mathbf{u}} = 0$$
$$\rho\frac{u_0^2}{l}\left(\frac{\partial\overline{\mathbf{u}}}{\partial\overline{t}} + (\overline{\mathbf{u}}\cdot\overline{\nabla})\overline{\mathbf{u}}\right) + \frac{p_0}{l}\overline{\nabla}\overline{p} - \mu\frac{u_0}{l^2}\overline{\nabla}^2\overline{\mathbf{u}} = \rho\mathbf{a}_{\text{ext}},$$

if we normalize the pressure, so $p_0 = \rho u_0^2$; we obtain the classical Navier-Stokes equations in the dimensionless form

$$\overline{\nabla}\cdot\overline{\mathbf{u}} = 0 \tag{4.30a}$$
$$\frac{\partial\overline{\mathbf{u}}}{\partial\overline{t}} + (\overline{\mathbf{u}}\cdot\overline{\nabla})\overline{\mathbf{u}} + \overline{\nabla}\overline{p} - \frac{1}{Re}\overline{\nabla}^2\overline{\mathbf{u}} = \frac{l}{\rho u_0^2}\rho\mathbf{a}_{\text{ext}}, \tag{4.30b}$$

where $Re = \rho u_0 l/\mu$ is the *Reynolds number*.

For instance, if the external force is due to gravity (in the y direction), the acceleration due to this force will be $\mathbf{a}_{\text{ext}} = g\hat{\mathbf{y}}$ and the *r.h.s.* becomes $1/Fr^2\ \hat{\mathbf{y}}$, where $Fr = u_0/\sqrt{lg}$ is the *Froude number*.

The dimensionless equations are useful for analytical purposes. In this example, a small Reynolds number[32] indicates that the flow is laminar, on the other hand, high Reynolds numbers characterize turbulent flows.

Also, the dimensionless form is useful for determining the relative importance of various terms in the PDEs and it is the starting point for numerical schemes.

A similar dimensional analysis have been used in section 4.6.2 in order to estimate the relative importance of the forces acting on dielectric fluids.

[32] $Re < 10^3$. For an historical review see Ref. 142.

Boundary conditions

The fluid dynamic equations (as well as the electrodynamic equations) are not well-posed if they are not provided with appropriate boundary conditions.

For instance, if we define the cavity containing the fluid as the bounded domain Ω, surrounded by a surface Γ and unit outward normal $\mathbf{n}$, we could define the different variables on the boundary Γ as: $\rho = \rho_0$, $\mathbf{n} \cdot \mathbf{u} = u_0$, $p = p_0$, $\mathbf{\Pi} \cdot \mathbf{n} = 0$, $T = T_0$, etc.

4.4 Mixture of gases and plasmas

This section will describe how macroscopic quantities can be obtained from the microscopic description of each constituent within a mixture of gases and plasmas. Defining statistical expressions of the different components of the mixture, it is possible to find a description for the total mass, momentum and energy densities.[33]

Let m_s and $f_s(\mathbf{x}, \mathbf{v}, t)$ be the mass and the distribution function of each species within the mixture.

4.4.1 Density

The mass density of each species is defined as

$$\rho_s(\mathbf{x}, t) = \int f_s(\mathbf{x}, \mathbf{v}, t) d\mathbf{v}, \tag{4.31}$$

and the total density of the mixture as

$$\rho(\mathbf{x}, t) = \sum_s \rho_s. \tag{4.32}$$

The *number density* for each species is defined as $n_s = \rho_s / m_s = \int f_s d\mathbf{v}$.[34]

4.4.2 Momentum density

The momentum density of each species is defined as

$$\rho_s(\mathbf{x}, t)\mathbf{u}_s(\mathbf{x}, t) = \int m_s \mathbf{v} f_s(\mathbf{x}, \mathbf{v}, t) d\mathbf{v}, \tag{4.33}$$

[33] This section is based on Ref. 132.
[34] See Ref. 132 p. 168.

and the total momentum density of the mixture as[35]

$$\rho(\mathbf{x},t)\mathbf{u}(\mathbf{x},t) = \sum_s \rho_s \mathbf{u}_s. \tag{4.34}$$

The macroscopic velocity (or *barycentric velocity*) of the mixture is defined as $\mathbf{u}(\mathbf{x},t) = \sum \rho_s \mathbf{u}_s/\rho$.

The *peculiar velocity* is calculated with respect to the barycentric velocity $\mathbf{c} = \mathbf{v} - \mathbf{u}$. Contrary to the mono-species case, the first central moment of f_s with respect to the macroscopic velocity $\mathbf{u}$ is not zero

$$\int m_s \mathbf{c} f_s d\mathbf{v} = \int m_s(\mathbf{v}-\mathbf{u}) f_s d\mathbf{v} = \rho_s \mathbf{u}_s - \rho_s \mathbf{u}, \tag{4.35}$$

but the sum among all the species is zero

$$\sum_s \int m_s \mathbf{c} f_s d\mathbf{v} = \sum_s (\rho_s \mathbf{u}_s - \rho_s \mathbf{u}) = \rho\mathbf{u} - \rho\mathbf{u} = 0. \tag{4.36}$$

4.4.3 Momentum flow

The random motion of the particles gives rise to the stress tensor for each species

$$\begin{aligned} \boldsymbol{\sigma}_s(\mathbf{x},t) &= \int m_s \mathbf{c}\mathbf{c} f_s d\mathbf{v} = \int m_s (\mathbf{v}-\mathbf{u})(\mathbf{v}-\mathbf{u}) f_s d\mathbf{v} \\ &= \int m_s \mathbf{v}\mathbf{v} f_s d\mathbf{v} - \rho_s \mathbf{u}_s \mathbf{u} - \rho_s \mathbf{u}\mathbf{u}_s + \rho_s \mathbf{u}\mathbf{u}, \end{aligned} \tag{4.37}$$

and the momentum flow of each species is the tensor

$$\boldsymbol{\Pi}_s = \int m_s \mathbf{v}\mathbf{v} f_s d\mathbf{v} = \rho_s \mathbf{u}_s \mathbf{u} + \rho_s \mathbf{u}\mathbf{u}_s - \rho_s \mathbf{u}\mathbf{u} + \boldsymbol{\sigma}_s. \tag{4.38}$$

The total momentum flow of the mixture decomposes in two parts, one of which is the macroscopic momentum flow tensor and the other part is the contribution due to the molecular random motion

$$\boldsymbol{\Pi} = \sum_s \boldsymbol{\Pi}_s = \rho\mathbf{u}\mathbf{u} + \boldsymbol{\sigma}, \tag{4.39}$$

where the sum among all the species in the mixture gives the total stress tensor[36]

$$\boldsymbol{\sigma} = \sum_s \boldsymbol{\sigma}_s. \tag{4.40}$$

[35] See Ref. 132 p. 168.

[36] Note that the tensors $\boldsymbol{\sigma}_s$ and $\boldsymbol{\Pi}_s$ are symmetric.

4.4.4 Energy density

Defining $\varepsilon_s(\mathbf{x}, t)$ as the internal energy per unit mass (of each species), the internal energy density per species gets

$$\begin{aligned}\rho_s\varepsilon_s &= \frac{1}{2}\int m_s c^2 f_s d\mathbf{v} = \frac{1}{2}\int m_s(v-u)^2 f_s d\mathbf{v} \\ &= \frac{1}{2}\int m_s v^2 f_s d\mathbf{v} - \rho_s \mathbf{u}_s\cdot\mathbf{u} + \frac{1}{2}\rho_s u^2,\end{aligned} \tag{4.41}$$

and the total energy density per species becomes

$$e_s = \frac{1}{2}\int m_s v^2 f_s d\mathbf{v} = \rho_s \mathbf{u}_s\cdot\mathbf{u} - \frac{1}{2}\rho_s u^2 + \rho_s\varepsilon_s. \tag{4.42}$$

The total energy density e of the mixture is the sum of total energy density per species e_s

$$e = \sum_s e_s = \frac{1}{2}\rho u^2 + \rho\varepsilon, \tag{4.43}$$

where summing among all species gives the total internal energy of the mixture

$$\rho\varepsilon = \sum_s \rho_s\varepsilon_s. \tag{4.44}$$

4.4.5 Temperature, pressure and rms velocity

Let us assume that the random motion of each species is isotropic. Then we could define the temperature and pressure of the mixture as the sum of the internal energy densities of all the species

$$\rho\varepsilon = \sum_s \frac{3}{2} n_s k T_s = \sum_s \frac{3}{2} p_s = \sum_s \frac{1}{2}\rho_s c_{s\,\mathrm{rms}}^2. \tag{4.45}$$

The mixture's temperature then becomes

$$T = \frac{1}{n}\sum_s n_s T_s,$$

where $n = \sum_s n_s$ is the total number density of the mixture,[37] and the total pressure becomes

$$p = \sum_s p_s.$$

[37] See Refs. 128 p. 455, and 132 p. 169.

4.4.6 Heat flow

The heat flow vector for each species is defined as[38]

$$\begin{aligned}\mathbf{q}_s = \frac{1}{2}\int m_s \mathbf{c} c^2 f_s d\mathbf{v} &= \frac{1}{2}\int m_s \mathbf{v} c^2 f_s d\mathbf{v} - \frac{1}{2}\int m_s \mathbf{u} c^2 f_s d\mathbf{v} \\ &= \frac{1}{2}\Big(\int m_s \mathbf{v} v^2 f_s d\mathbf{v} - \int 2 m_s \mathbf{u}\cdot\mathbf{v}\mathbf{v} f_s d\mathbf{v} \\ &\quad + \int m_s \mathbf{v} u^2 f_s d\mathbf{v}\Big) - \frac{1}{2}\int m_s \mathbf{u} c^2 f_s d\mathbf{v}. \quad (4.46)\end{aligned}$$

Since the macroscopic velocity $\mathbf{u}$ can be taken out of the integrals, and by using the definitions in Eqs. (4.33), (4.38) and (4.41); we obtain the heat flow per species

$$\mathbf{q}_s = \frac{1}{2}\int m_s \mathbf{v} v^2 f_s d\mathbf{v} - \mathbf{u}\cdot\boldsymbol{\Pi}_s + \frac{1}{2}\rho_s \mathbf{u}_s u^2 - \mathbf{u}\rho_s \varepsilon_s. \quad (4.47)$$

The total energy flow $\mathbf{Q}_s$ (velocity $\times$ energy density) per species is defined as

$$\mathbf{Q}_s = \frac{1}{2}\int m_s \mathbf{v} v^2 f_s d\mathbf{v} = \mathbf{u}\cdot\boldsymbol{\Pi}_s - \frac{1}{2}\rho_s \mathbf{u}_s u^2 + \mathbf{u}\rho_s \varepsilon_s + \mathbf{q}_s. \quad (4.48)$$

Summing among all the species, and using the expressions given in Eqs. (4.34), (4.39) and (4.44); this expression becomes the total energy flow of the mixture

$$\begin{aligned}\mathbf{Q} = \sum_s \mathbf{Q}_s &= \mathbf{u}\cdot\boldsymbol{\Pi} - \frac{1}{2}\rho \mathbf{u} u^2 + \mathbf{u}\rho\varepsilon + \mathbf{q} \\ &= \mathbf{u}(\frac{1}{2}\rho u^2 + \rho\varepsilon) + \mathbf{u}\cdot\boldsymbol{\sigma} + \mathbf{q} = \mathbf{u}e + \mathbf{u}\cdot\boldsymbol{\sigma} + \mathbf{q}, \quad (4.49)\end{aligned}$$

where $\mathbf{q} = \sum_s \mathbf{q}_s$ is the heat flow of the mixture.

4.5 Conservation equations of mixtures and plasmas

In the case of multicomponent plasmas, the collision term $C(f_s) = \sum_l C(f_s, f_l)$ in the Boltzmann equation[39] represents the rate of change of

[38] See Ref. 132 p. 169.
[39] See Refs. 132 pp. 163-167, 123 pp. 77-78, and 133 pp. 97-98.

f_s resulting from the interaction with particles of the same and of all other species l

$$\frac{\partial f_s}{\partial t} + \mathbf{v} \cdot \frac{\partial f_s}{\partial \mathbf{x}} + \mathbf{a}_s \cdot \frac{\partial f_s}{\partial \mathbf{v}} = C(f_s), \tag{4.50}$$

where $\mathbf{a}_s$ represents the acceleration of the "s" particles due to external forces.

Following section 4.3, we obtain the continuity equations (4.24), (4.25) (4.26) for each species[40] by multiplying the Boltzmann equation by each collision invariant, and then integrating over velocity space (the collision invariants ψ_α are m_s, $m_s\mathbf{v}$ and $\frac{1}{2}m_s\mathbf{v}^2$, different for each species)

$$\frac{\partial \rho_s}{\partial t} + \nabla \cdot \rho_s \mathbf{u}_s = r_s \tag{4.51}$$

$$\frac{\partial \rho \mathbf{u}}{\partial t} + \nabla \cdot \mathbf{\Pi} = \rho_s \mathbf{a}_s + \mathbf{p}_s \tag{4.52}$$

$$\frac{\partial e_s}{\partial t} + \nabla \cdot \mathbf{Q}_s = \rho_s \mathbf{u}_s \cdot \mathbf{a}_s + w_s, \tag{4.53}$$

where $r_s = \int m_s C(f_s) d\mathbf{v}$ represents the gain or loss of species s due to interaction with other species.[41] Also, $\mathbf{p}_s = \int m_s \mathbf{v} C(f_s) d\mathbf{v}$ is the transfer of momentum from or towards other species, and $w_s = \int \frac{1}{2} m_s \mathbf{v}^2 C(f_s) d\mathbf{v}$ is the gain or loss of kinetic energy due to interaction with particles of other species.

Note that, different than in the mono-species case, the integral of the collision term $\int \psi_\alpha C(f_s) d\mathbf{v}$ is not zero, but rather it denotes the transfer of mass, momentum and kinetic energy among species. But the sum of this integral among all the species is zero

$$\sum_s \int \psi_\alpha C(f_s) d\mathbf{v} = 0.$$

It is important to notice that, although collisions may lead to transfer of mass, momentum and kinetic energy among species; the total mass, momentum and kinetic energy of the mixture is kept constant by those collisions.

Summing equations (4.51), (4.52) and (4.53) among all the species gives

[40] See Ref. 128 pp. 461-463.

[41] For instance, the basic ionization process in plasmas create one electron and one ion, but "destroy" one neutral.

the continuity equations for the mixture

$$\frac{\partial \rho}{\partial t} + \nabla \cdot \rho \mathbf{u} = 0 \tag{4.54}$$

$$\frac{\partial \rho \mathbf{u}}{\partial t} + \nabla \cdot \mathbf{\Pi} = \sum_s \rho_s \mathbf{a}_s \tag{4.55}$$

$$\frac{\partial e}{\partial t} + \nabla \cdot \mathbf{Q} = \sum_s \rho_s \mathbf{u}_s \cdot \mathbf{a}_s. \tag{4.56}$$

Note that, if the components of the mixture feel different external forces $\mathbf{F}_s = m_s \mathbf{a}_s$ (for instance, Lorentz forces, dielectrophoresis, etc.) pointing in different directions, there will be a de-mixing process, and the mixture will not be homogeneous. This happens, for instance, during the sedimentation of colloids, and in the de-mixing of complex plasmas. The following section will give an estimation of these phenomena.

4.6 Complex fluids

The complexity of complex fluids may basically arise from two mechanisms: On the one hand, fluids made of non-spherical particles give rise to liquid-crystalline phases. As the particles are anisotropic, the binary collision between two particles do not follow the hard-sphere approach and in the long run they may align along one preferred direction, yielding nematic phases or even more complex phases.

On the other hand, mixtures can be made of particles of different sizes and shapes. They present different phase transitions than mono-component fluids: they may phase separate or split into two or more different phases, each rich in one component. One of the open problems in mixtures is to determine the phenomenology arising from this mechanism. The nature of the separated phases (whether they are fluids, or one is a crystal, for instance) is not yet well understood.[42]

Next section will derive the conservation equations for hot plasmas, dielectric gases and low-temperature plasmas. These derivations will then be used in order to determine the main forces acting on complex plasmas.

4.6.1 Magnetohydrodynamics

When a plasma is fully ionized, it becomes a very good conductor. The ideal MHD model describes the non-relativistic motion of a perfect conducting

[42] http://valbuena.fis.ucm.es/gisc/content/view/18/46.

fluid.[43]

Let us consider a fully-ionized plasma, consisting of electrons and ions. The external force acting on each species s will be $\mathbf{F}_s = q_s(\mathbf{E} + \mathbf{u}_s \times \mathbf{B})$, where q_s and $\mathbf{u}_s$ represent the charge and mean velocity of each species.

The total force (per unit volume) on the fluid will become

$$n\mathbf{F}_{\text{ext}} = \sum_s n_s \mathbf{F}_s = \sum_s n_s q_s(\mathbf{E} + \mathbf{u}_s \times \mathbf{B}) = \rho_e \mathbf{E} + \mathbf{J} \times \mathbf{B},$$

where $\rho_e = \sum_s n_s q_s$ is the total charge density and $\mathbf{J} = \sum_s q_s n_s \mathbf{u}_s$ is the total current density.

The perfect conducting approach assumes that the electric field $\mathbf{E}'$ expressed in the co-moving frame should vanish, i.e.

$$\mathbf{E}' \equiv \mathbf{E} + \mathbf{u} \times \mathbf{B} = 0.$$

This is equivalent to apply the Ohm's law $\mathbf{E}' = \mathbf{J}/\sigma_e$ with infinite conductivity σ_e.

This assumption also implies that the electric field becomes a secondary variable (determined by $\mathbf{E} = -\mathbf{u} \times \mathbf{B}$), which simplifies Faraday law in Maxwell equation (2.3)

$$-\nabla \times (\mathbf{u} \times \mathbf{B}) + \frac{\partial \mathbf{B}}{\partial t} = 0.$$

Furthermore, the non-relativistic approach (the speed of the fluid is much slower than the speed of light) neglects the displacement current in the Maxwell equation (2.4), recovering the original Ampère's law

$$\nabla \times \mathbf{B} = \mu_0 \mathbf{J}.$$

The non-relativistic assumption also simplifies the Lorentz force since

$$|\rho_e \mathbf{E}| << |\mathbf{J} \times \mathbf{B}|,$$

and the force (per unit volume) on the fluid becomes

$$n\mathbf{F}_{\text{ext}} = \mathbf{J} \times \mathbf{B} = \frac{1}{\mu_0}(\nabla \times \mathbf{B}) \times \mathbf{B} = -\frac{1}{2\mu_0}\nabla \mathbf{B}^2 + \frac{1}{\mu_0}(\mathbf{B} \cdot \nabla)\mathbf{B}.$$

The ideal MHD model also considers the fluid as inviscid and isothermal, so the continuity equations (4.54) and (4.55) become

$$\frac{\partial \rho}{\partial t} + \nabla \cdot \rho \mathbf{u} = 0 \tag{4.57}$$

$$\rho\left(\frac{\partial \mathbf{u}}{\partial t} + (\mathbf{u} \cdot \nabla)\mathbf{u}\right) + \nabla p = -\frac{1}{2\mu_0}\nabla \mathbf{B}^2 + \frac{1}{\mu_0}(\mathbf{B} \cdot \nabla)\mathbf{B}. \tag{4.58}$$

[43] See Refs. 133 and 134 Chap. 4.

This equations are then coupled to the modified Maxwell equations

$$\nabla \cdot \mathbf{B} = 0 \tag{4.59}$$

$$\frac{\partial \mathbf{B}}{\partial t} - \nabla \times (\mathbf{u} \times \mathbf{B}) = 0. \tag{4.60}$$

For an incompressible isotropic plasma undergoing an adiabatic process, this model describes which nowadays are called *Alfvén waves*.[44]

Note that the gradient of the magnetic energy density $u_b = \frac{1}{2\mu_0}\mathbf{B}^2$ acts like a gradient of pressure on the perfect conducting plasma.

4.6.2 Electrohydrodynamics

The Electrohydrodynamic regimen represents the limit of a perfect dielectric fluid (or low degree of ionization), in opposite to the MHD regimen which represents the perfect conducting fluid (or high degree of ionization).

Following Eq. (3.26), the external force acting on each molecule of a dielectric gas composed of particles of polarizability $\overline{\alpha}$ will be

$$\mathbf{F}_{\text{ext}} = \mathbf{F}_{DEP} = \overline{\alpha}\frac{\epsilon_0}{2}\nabla|\mathbf{E}|^2 = \overline{\alpha}\nabla u_e,$$

and the equation for the continuity of momentum (4.25) will become

$$\frac{\partial \rho \mathbf{u}}{\partial t} + \nabla \cdot \mathbf{\Pi} = n\mathbf{F}_{\text{ext}} = n\overline{\alpha}\nabla u_e. \tag{4.61}$$

Dielectrophoresis occurs when there are induced (polarization) charges and results in motion only in the presence of non-uniform electric fields. The starting point for the theory of fluid DEP is based on the Maxwell stress tensor formulation.[45] It gives a force per unit volume acting on the dielectric fluid as

$$n\mathbf{F} = -\frac{1}{2}|\mathbf{E}|^2\nabla\epsilon + \frac{1}{2}\nabla\left(\rho\frac{\partial\epsilon}{\partial\rho}|\mathbf{E}|^2\right), \tag{4.62}$$

where term involving $\frac{\partial\epsilon}{\partial\rho}$ represents the elastic deformation of the fluid under the forces exerted by the electric fields (also called *electrostriction*).

For rarefied gases, the electric permittivity ϵ linearly depends on the density (see Eq. (3.27))

$$\epsilon = \epsilon_0\epsilon_r = \epsilon_0(1 + \chi_e) \qquad\qquad \chi_e = n\overline{\alpha}$$

[44] See Refs. 135 and 136 Chap. 3.

[45] See Refs. 91 pp. 65-68, 85 pp. 137-139, and 92 p. 784. See discussion in Ref. 99.

where χ_e denotes the electric susceptibility. Therefore, the electrostriction term in Eq. (4.62) equals

$$\rho\frac{\partial\epsilon}{\partial\rho} = n\frac{\partial\epsilon}{\partial n} = \epsilon_0\chi_e,$$

and the force per unit volume [defined in Eq. (4.62)] acting on the dielectric fluid becomes

$$n\mathbf{F} = -\frac{1}{2}|\mathbf{E}|^2\nabla\epsilon + \frac{1}{2}\nabla(\epsilon_0\chi_e|\mathbf{E}|^2) = \frac{1}{2}\epsilon_0\chi_e\nabla|\mathbf{E}|^2 = \chi_e\nabla u_e,$$

which is the same result previously found in Eq. (4.61).

In order to estimate the importance of dielectrophoretic forces acting on a viscous isotropic fluid, we can use a dimensional analysis similar to the one previously done for the Navier-Stokes equations (see Eq. (4.28)). The dielectrophoretic force in the dimensionless form reaches

$$n\mathbf{F}_{\text{ext}} = \chi_e\nabla u_e = \chi_e\frac{u_{eo}}{l}\overline{\nabla}\overline{u}_e,$$

where u_{eo} is the characteristic electric energy density and l is the characteristic length associated to the phenomenon under study. Under these considerations, we can write the equation for the continuity of momentum density (4.61) as

$$\rho\frac{u_0^2}{l}\left(\frac{\partial\overline{\mathbf{u}}}{\partial\overline{t}} + (\overline{\mathbf{u}}\cdot\overline{\nabla})\overline{\mathbf{u}}\right) + \frac{p_0}{l}\overline{\nabla}\overline{p} - \mu\frac{u_0}{l^2}\overline{\nabla}^2\overline{\mathbf{u}} = \chi_e\frac{u_{eo}}{l}\overline{\nabla}\overline{u}_e.$$

If we normalize the pressure, so $p_0 = \rho u_0^2$, we obtain the dimensionless form

$$\frac{\partial\overline{\mathbf{u}}}{\partial\overline{t}} + (\overline{\mathbf{u}}\cdot\overline{\nabla})\overline{\mathbf{u}} + \overline{\nabla}\overline{p} - \frac{1}{Re}\overline{\nabla}^2\overline{\mathbf{u}} = \chi_e\frac{u_{eo}}{\rho u_0^2}\overline{\nabla}\overline{u}_e. \tag{4.63}$$

The term on the *r.h.s.* represents the importance of electric energy density relative to the kinetic energy of the fluid. For very low-pressure gases (or high electric energy densities), the gradient of the electric energy density acts like a gradient of pressure. The question to answer is not whether the electric energy density is higher or smaller than the pressure, but rather if the gradient $\chi_e\nabla u_e$ is comparable with the gradient ∇p.

Figure 4.1 shows a lateral view of the PK-3 Plus chamber filled with a dielectric gas. The gas is considered incompressible, and the conservation of momentum is due to equation (4.63). The electrostatic fields have been used,

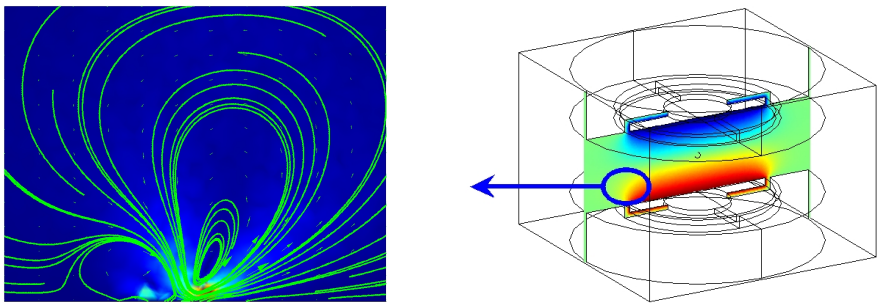

(a) (b)

Figure 4.1: (a) Eddies created by the electrostatic pressure $\chi_e \nabla u_e$. The background image shows the *cell Reynolds number* in color code ($Re \in [0.05,5]$). (b) Electrostatic potential. The color code represents the dimensionless electric potential. The top electrode is forced at $\phi = -1$, the lower electrode at $\phi = +1$, and the grounded shield is at $\phi = 0$.

the dynamics of the fluid is laminar (Reynolds number close to unity) and the dimensionless number $\chi_e \frac{u_{eo}}{\rho u_0^2}$ is 10^{-7}.

It is possible to observe that high gradients of electric energy density produce the effect of "electric pumping", stirring the fluid in regions of high electric energy density variations.[46]

It is worth noting that two fluids at the same pressure and with the same Reynolds numbers, will behave in a different way while exposed to the same high electric energy gradients. The fluid with the higher electric susceptibility χ_e will feel a higher gradient of pressure, and therefore will experience an stronger "electric drift".

4.6.3 Low-temperature plasmas

In cold plasmas, there will be present both magnetohydrodynamics and electrohydrodynamics effects, the former due to Lorentz forces acting on electrons and ions, and the latter due to dielectrophoretic forces acting on the neutral atoms and/or molecules.

Let us consider the general force (per unit volume) acting on an isotropic

[46] This phenomenon has been observed in nanofluids pumped by microelectrodes driven by AC electric fields, although the whirlpools were explained in terms of the electrical double layer on the electrode's surfaces. See Refs. 137-139.

mixture composed by charged and dielectric particles

$$n\mathbf{F} = \sum_s \rho_s \mathbf{a}_s = \sum_i n_i q_i (\mathbf{E} + \mathbf{u}_i \times \mathbf{B}) + \sum_j n_j \overline{\alpha}_j \nabla u_e + \rho \mathbf{g}$$
$$= \rho_e \mathbf{E} + \mathbf{J} \times \mathbf{B} + \chi_e \nabla u_e + \rho \mathbf{g},$$

where the subindex i denotes charged particles of charge q_i, and the subindex j denotes dielectric particles of polarizability $\overline{\alpha}_j$, $\rho_e = \sum_i n_i q_i$ is the total charge density and $\mathbf{J} = \sum_i n_i q_i \mathbf{u}_i$ the total current density, $\chi_e = \sum_j n_j \overline{\alpha}_j$ the total electric susceptibility, $\rho = \sum_s \rho_s$ the total mass density and $\mathbf{g}$ the gravity acceleration.

Using this expression for the external force, the continuity equations (4.54) and (4.55) of an isotropic viscid mixture (composed by charged and dielectric particles) under electromagnetic and gravitational forces will be

$$\frac{\partial \rho}{\partial t} + \nabla \cdot \rho \mathbf{u} = 0 \tag{4.64}$$

$$\rho \left(\frac{\partial \mathbf{u}}{\partial t} + (\mathbf{u} \cdot \nabla)\mathbf{u} \right) + \nabla p - \mu \nabla^2 \mathbf{u} = \rho_e \mathbf{E} + \mathbf{J} \times \mathbf{B} + \chi_e \nabla u_e + \rho \mathbf{g}, \tag{4.65}$$

where $\mathbf{u} = \sum \rho_s \mathbf{u}_s / \rho$ the barycentric velocity of the mixture, $p = \sum p_s$ the total pressure and μ the total viscosity.

At high degrees of ionization (hot plasma regime), the MHD model will describe the motion of the perfect conducting plasma (see Sec. 4.6.1). On the other hand, at very low (or zero) degree of ionization, the EHD model will rule the dynamics of the dielectric gas (see Sec. 4.6.2).

Complex plasmas in the laboratory are formed by adding dust particles into a low-temperature plasma. Most of the time, silica or melamine microdispersive particles are used. These particles may collect electric charges through collision with the electrons and ions. Also, the permittivity of their constitutive material makes them excellent induced dipoles (both silica and melamine have high dielectric constants $\epsilon_r \sim 5$).

Which effect is the most important? Electric charge or induced polarization? If we neglect gravitational forces, the external force acting on the mixture will be

$$n\mathbf{F} = \rho_e \mathbf{E} + \mathbf{J} \times \mathbf{B} + \chi_e \nabla u_e.$$

The crucial question to answer is whether the dust should be considered as a charged or polarized particle.

On the one had, if dust particles are considered to be point charges, this force simplifies to (neglecting dielectrophoretic effects)

$$n\mathbf{F} = \rho_e \mathbf{E} + \mathbf{J} \times \mathbf{B},$$

where $\rho_e = \sum_i n_i q_i$ is the charge density, $\mathbf{J} = \sum_i n_s q_i \mathbf{u}_i$ is the total current density, and q_i represents the charge of electrons, ions and dust particles.

On the other hand, if the main source of the dust dynamics is polarization effects, this force simplifies to (neglecting Lorentz force)

$$n\mathbf{F} = \chi_e \nabla u_e,$$

where $\chi_e = \sum_s n_s \overline{\alpha}_s$ is the electric susceptibility of the mixture.

In order to compare the importance of these forces, a computational model has been implemented. Chapter 6 shows the results obtained by the finite element method.[47]

It is important to notice that the shape of the cavity containing the plasma (either for the conducting or dielectric approximations) will define the way in which the electromagnetic energy distributes inside it (see Chap. 2) and the module and direction of the applied fields. External sources, which impose certain boundary conditions on the electromagnetic fields, will play an important role, because fast time variations may led to the excitation of resonant modes of the cavity.

4.7 Final remarks

This chapter has reviewed the procedure necessary to obtain the conservation equations of complex plasmas, based on the Kinetic theory of gases.[48]

We have defined the macroscopic velocity of the complex plasma as the weighted sum of its components' velocities, i.e. $\mathbf{u} = \frac{1}{\rho} \sum \rho_s \mathbf{u}_s$, where ρ_s and $\mathbf{u}_s$ are the mass densities and velocities of electrons, ions, neutrals and dust particles, and ρ is the total mass density of the complex plasma.

Complex plasmas are thermodynamically open systems: electron and ions are constantly produced, transported and lost by recombination in the plasma bulk and in the surfaces of walls and dust particles. In the same way, neutral molecules are lost by ionization, and are produced by recombination processes. Dust particles are created by the sputtering of surfaces or arbitrarily introduced in the plasma chamber.

[47] See also Appendix A.
[48] See Refs. 161-172.

Although there are losses and gains of each species, the total mass of the complex plasma (inside a closed cavity) ca be assumed to be constant (after the insertion of the dust particles).

In the same way, electrons, ions, neutral and dust particles transfer momentum to each other via collisions, but the total momentum of the complex fluid will just be increased by the work exert by the external sources, in this case, the radio-frequency discharge.

Other remarkable feature of complex plasmas is that charges on the grains are not constant, but stochastically fluctuate around some equilibrium value (which also depends on the spatial coordinates). Complex plasmas are a novel type of non-Hamiltonian systems where the energy of the particle ensemble is not conserved due to the charge variations. This energy varies not only in the presence of the external electric fields, but also due to mutual particle collisions.[49]

The dynamics of complex plasmas, just as the dynamics of complex fluids, is characterized by the interplay of different components at microscopic and mesoscopic levels. These interactions result in a mixture of electrodynamics and fluid dynamics effects.

The key question to answer is whether complex plasmas are dominated by Lorentz forces ($\sim Q\mathbf{E}$ at low velocities and/or low magnetic fields) or by dielectrophoretic effects.

Different theories on the charge of the dust particles immersed in plasma have been proposed (for instance the OML theory), all of them based on the assumption that dust particles are so small that they can be treated as "point charges". Assuming that the dust particle is a point of charge implies that the dust surface is at a *floating potential*, which also implies that this particle may collect electric charges through collision with electrons and ions[50] (Langmuir used the word *collector* when he referred to floating probes).

The assumption that the surface of the dust particle is at equipotential, necessarily implies that the dust is made of a perfect conductor (as assumed by Langmuir) and when it is immersed in an ionized gas *it becomes surrounded by a symmetrical space-charge region or "sheath" of positive or of negative ions (or electrons).*[51]

In complex plasma experiments, like the PK-3 plus experiment, the plasma chamber is filled with dust particles made of silica and/or melamine. Both materials are good dielectrics (at the operative radio-frequency) and therefore we cannot expect their surface to be at a certain equipotential volt-

[49] See Refs. 73 and 173-177.

[50] This is the starting point for the theory of floating potential in spherical probes and dust particles. See Refs. 86, 143-160.

[51] See Ref. 86.

age. This introduces us with the idea of considering dielectrophoretic effects in the dynamics of complex plasmas (Dipole effects have been analyzed in [196-199]).

In order to analyze the importance of the forces $Q\mathbf{E}$ versus $\chi_e \nabla u_e$ in the dynamics of complex plasmas,[52] Chapter 6 will illustrate how the electric fields and the electric energy density distribute inside the PK-3 Plus chamber.

Other forces that might play a role in the dynamics of complex plasmas, such as thermophoresis, radiation pressure, etc. are not addressed by our model.[53]

[52] Where Q is the electric charge of the dust particles and χ_e their electric susceptibility, $\mathbf{E}$ is the electric field and u_e the electric energy density.

[53] For an exhaustive study of those forces, see Refs. in 64-75 and 113-118.

Complex plasmas under microgravity

5

Complex plasmas formed under microgravity conditions have been intensively investigated in radio-frequency discharges during the last ten years. The results of the first microgravity experiments (parabolic flights and Texus rockets) were reported by G. E. Morfill *et al.* in 1999.[1]
PKE-Nefedov, a complex plasma laboratory installed on the International Space Station, was operative between 2001 and 2005. It carried out 13 experimental missions, resulting in more than 50 hours of separate experimental runs. It was the first long term experiment on complex plasmas in space, and so far, it has been the most actively used scientific experiment on the ISS, with a scientific outcome of more than 30 refereed publications (April 2005).[2]

Only small complex plasma crystals (of few lattice layers) can be investigated under normal gravity conditions (in regions where gravity is compensated by strong electric fields). Large complex plasma systems extended in the whole plasma chamber were observed in this weightlessness setup.

This experiment showed that under microgravity conditions much broader and different regions of parameters were accessible, providing means for researching new physics not attainable under standard gravity conditions.

Figure 5.1 illustrates the typical static and dynamic behavior of complex plasmas in the space laboratory. This figure shows three seconds of the dust particles trajectory (color coded from red to blue).

The main features which have been investigated in the PKE-Nefedov experiment are:

- A dust-free "void" in the center of the system, present for most experimental parameters. The void can be closed under special experimental conditions (neutral gas pressures below 50 Pa and the lowest possible rf-voltage, close to the plasma-off condition).
- A sharp boundary between the void and the complex plasma.
- Demixing of complex plasma clouds formed by particles of different sizes. Smaller particles became situated closer to the center, and bigger particles are located closer to the electrodes.

[1] See Ref. 24.
[2] http://www.mpe.mpg.de/theory/plasma-crystal.

- Crystalline structures along the central axis fill the whole area between the void and sheath, and between the vortices at the borders. In contrast to crystalline structures formed under normal gravity (with similar types of particles), it was found that in space the crystal planes where not oriented parallel to the electrodes.

- In the boundary regions the trajectories of the particles show eddies of motion. This is caused by strong electric field inhomogeneities, which occur at the edge of the electrodes and at the interface between the electrodes and the particle dispensers, impelling the particle cloud to perform a whirlpool-like motion.

All of the above mentioned features have been investigated in detail over the last years.[3]

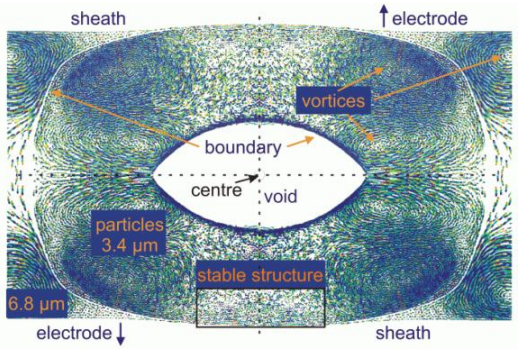

Figure 5.1: Main features observed in the PKE-Nefedov experiment: A central void (of around 20 mm in length), separation of dust particles of different sizes (6.8 and 3.4 μm in diameter), crystalline structures along the central axis and vortices close to the electrodes' edges.

5.1 PK-3 Plus experiment

PK-3 Plus[4], as its precursor PKE-Nefedov[5], is a joint Russian/German scientific project onboard the International Space Station (ISS). The cooperating teams, from the Institute for High Energy Densities (Russian Academy of Sciences, Moscow) and from the Max-Planck Institute for Extraterrestrial

[3] See Refs. 9, 24-31, 64-75.
[4] http://www.mpe.mpg.de/theory/plasma-crystal.
[5] http://www.dlr.de/rd/fachprog/fuw/projects/pke.

Physics (Garching), have been working since 2002 on the realization of this second generation microgravity experiment.

On the 21^{st} of December 2005, the Russian rocket "Progress M55" was launched to the ISS from the cosmodrome in Baikonur, Kasakhstan, and the first round of experiments was carried out between 12-16 January 2006.[6]

The PK-3 Plus experiment is a symmetrical radio-frequency plasma discharge chamber. Due to many design improvements, it provides new possibilities for the investigation of complex plasmas under microgravity condition.

The experiment is divided into two units: the *Experimental Block* and the *Telescience System* (TS) (in the same fashion as in the PKE-Nefedov experiment).

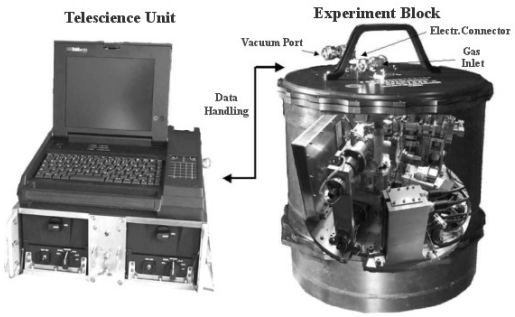

Figure 5.2: Telescience and Experiment Units (PKE-Nefedov).

The Experimental Block is housed in a closed container with electrical and vacuum connections to the outside. It includes the experiment itself, a computer and additional electronic components. An internal turbo-molecular pump has also been added in order to reach high-vacuum regimes ($<$ mPa). A valve to space is utilized to reach the necessary pre-vacuum conditions. This is needed for cleaning the chamber and for obtaining high repeatability of the experiments.

The Telescience Unit is the control console for the cosmonauts. It enables the storage of digital data and videos. The digital data is available on ground one day after the performance of the experiment. The analogue videos are stored on hard-drives and have to be transported back via a Sojus capsule, or when the crew is exchanged (via a space shuttle). Quicklook videos are also available right after the experimental run and are transported via the ROKVISS S-band antenna to the DLR center in Weilheim, Germany. In order to define a sequential measurement, an autonomous software procedure

[6] http://www.dlr.de/rd/news/PK3Plus.htm.

is written and uploaded onto the ISS computer. If necessary, the cosmonauts can also control the experiment via the Telescience Unit.

Before performing microgravity experiments, the different experimental parameters are checked on the *Science Model* in Garching, and on the equivalent *Training Model* in Moscow. The Science Model (which is fully functional and was tested on two parabolic flight campaigns) contains additional diagnostic tools, which allow further laboratory investigations for the planning and testing of experiments on the ISS.

Figure 5.3: Cosmonaut Valery Tokarev, flight engineer of the 12th ISS crew, holding the PK-3 Plus Experimental Block (12 January 2006).

5.2 Technical information

The PK-3 Plus experiment allows investigations at neutral gas pressures (neon or argon) between 5 and 250 Pa and radio-frequency power between 0.01 and 1 Watts.

Up to six types of mono-disperse particles (with sizes ranging from 1 to 20 μm in diameter) can be introduced into the plasma chamber. During one experiment, it is possible to change the number and composition of the injected particles, the plasma conditions and the neutral gas pressure.

The particle cloud can also be excited by applying an electrical low frequency signal on the electrodes (0.1 - 100 Hz at a maximum amplitude of 50 V), or by modulating the rf amplitude with different wave forms (sinusoidal, square, pulse, etc.).

The major improvements on the PK-3 Plus experiment (compared to the predecessor PKE-Nefedov) are:

- Larger electrodes and a wider ground shield produce an enhanced homogeneity and symmetry in the plasma.
- The new chamber produces a more homogenous and symmetric complex plasma, avoiding temperature gradients across the chamber.
- The continuous gas flow, added for procuring stable high-purity gas conditions, allows high repeatability of the experiments.
- Up to six different particle sizes can be injected in a single experiment (previously 2).
- A new radio-frequency control allows investigations at very low power levels (10 mW).
- There is a new function generator with enhanced performances (larger amplitude, different wave forms, etc).
- Two additional cameras were added in order to supervise the glow and the whole chamber.
- An enhanced gas regulation allows fine tuning of the gas pressure.
- The gas reservoirs for Argon and Neon are bigger.
- A more sophisticated house keeping system.
- A turbomolecular pump inside the container provides high vacuum conditions in the mPa range.
- Progressive scan cameras avoid interleaved images.
- Digital storage of analog video signals on hard disks.
- Modular concept for the electronics.

All of these improvements have not only enhanced the homogeneity of the complex plasma, but also have made the process of making three-dimensional computational simulations a much easier task.

Next chapter illustrates the main outcomes of this three-dimensional model.

Results

6

The previous chapters have shown the different steps in order to get a macroscopic description of low-temperature plasmas. Sections 4.6.1, 4.6.2, and 4.6.3 have derived the macroscopic forces (per unit volume) acting on hot plasmas, dielectric gases and complex plasmas.

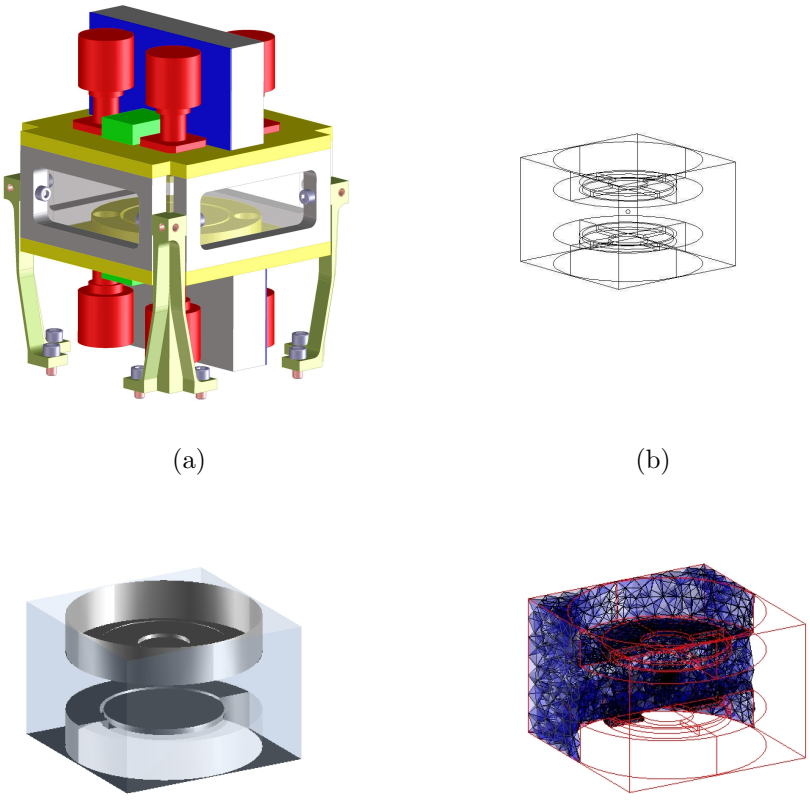

(a) (b)

(c) (d)

Figure 6.1: Different stages of the process of getting a computational model. Starting from the drawing, one gets the three-dimensional domain needed for the numerical method.

In order to compare the importance of the different forces acting in a low-temperature plasma chamber, we have implemented a three dimensional model of the PK-3 Plus experiment. Figure 6.1 shows the main steps in order to implement numerical simulations by means of the finite element method (see appendix A). Starting from a drawing, a computational domain consisting of 108171 tetrahedral elements (320628 degrees of freedom) is obtained.

6.1 Electrostatic regime

As a first step, we have calculated the electric fields, electric potential and the electric energy density inside the plasma chamber, for the electrostatic regime. This is the case when the electrodes are in a push-pull configuration (+1 and -1 dimensionless voltage) but there are no time-variation (DC mode). Figure 6.2 shows the main features[1] of this electrostatic regime. Note that, as expected, the electric field is homogeneous in the center of the chamber, but it curves close to the electrodes' edges. It is shown that the strength of the fields also increases close to these borders.

6.2 Time-dependent regime

We have shown in section 2.5, that the electric energy distributes among the the electrostatic and the time-dependent components

$$U_e = \int_\Omega u_e d\mathbf{x} = \frac{1}{2}\epsilon_0 \mathbf{E}_0^2 + \frac{1}{2}\epsilon_0 \sum_{n=1}^{\infty} \mathbf{E}_n^2.$$

With the finite element method, we have calculated the first resonant frequency of the PK-3 Plus chamber ($f_1 = 4.24$ GHz).

In the PK-3 Plus experiment, the radio-frequency used for obtaining the plasma discharge is $f_{RF} = 13.67$ MHz, which is two orders of magnitude below the natural frequency of the cavity. Yet, this driving frequency is seven orders of magnitude above the electrostatic regime (or zero frequency)

$$f_0 < f_{RF} < f_1.$$

If we assume that the electric energy mainly resides in the electrostatic field and in the first resonant mode (since the driving frequency is between

[1] We have used a *dimensionless color code scale* for representing the obtained results. Since the dimensionless equations do not include physical quantities, the dimensionless variables are represented in a RGB scale, where red represents the maximum value and blue the minimum.

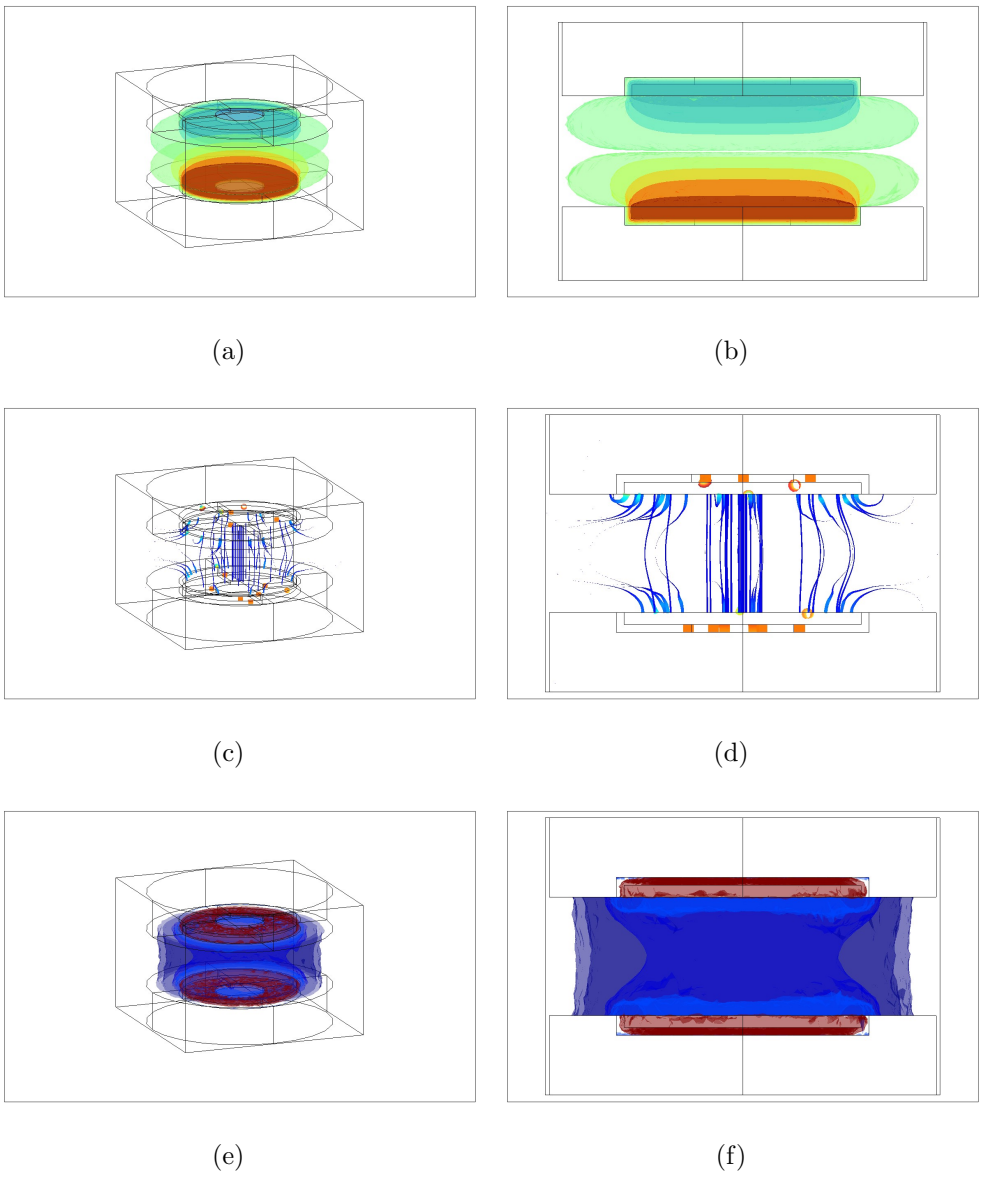

Figure 6.2: Isosurfaces of electrostatic potential ϕ (dimensionless color code) (a) three dimensional view (b) lateral view. Streamlines of electrostatic fields $\mathbf{E}$ (c) three dimensional view (d) lateral view. Isosurfaces of electrostatic energy density u_e (e) three dimensional view (f) lateral view.

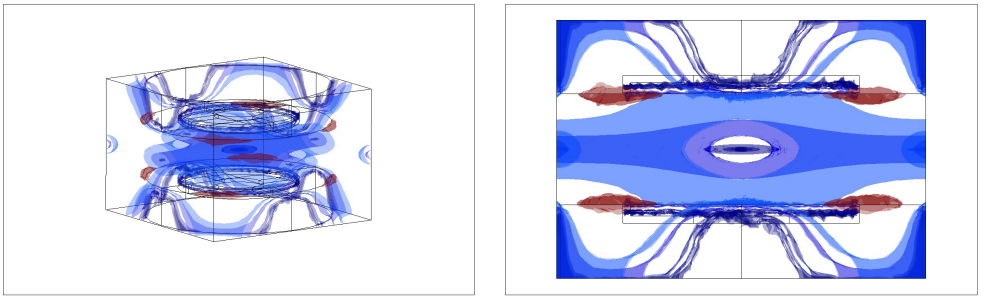

(a) (b)

Figure 6.3: Isosurfaces of electric energy density for the first resonant mode (a) three dimensional view (b) lateral view (dimensionless color code).

them), we can express this energy in terms of these two components

$$U_e \approx \frac{1}{2}\epsilon_0 \left(\mathbf{E}_0^2 + \mathbf{E}_1^2\right).$$

This is equivalent to considering

$$\mathbf{E}(\mathbf{x}, t) \approx \mathbf{E}_0(\mathbf{x}) + \mathbf{E}_1(t)\psi_1(\mathbf{x}).$$

Figure 6.5 shows the distribution of electric energy density for both the electrostatic and the first resonant mode. Note that for the first mode, high energy regions have moved towards the electrodes' edges.

6.2.1 Vortices

Let us consider a mixture composed of charged and dielectric particles. The macroscopic force (per unit volume) acting on this isotropic viscid complex plasma (see Eq. (4.65)) under the action of electromagnetic and gravitational forces is (see derivation in Sec. 4.6.3)

$$\rho\left(\frac{\partial \mathbf{u}}{\partial t} + (\mathbf{u}\cdot\nabla)\mathbf{u}\right) + \nabla p - \mu\nabla^2\mathbf{u} = \rho_e\mathbf{E} + \mathbf{J}\times\mathbf{B} + \chi_e\nabla u_e + \rho\mathbf{g}$$

If the dielectric effects are more important than gravitational and Lorentz forces, this equation simplifies to (see Sec. 4.6.2)

$$\rho\left(\frac{\partial \mathbf{u}}{\partial t} + (\mathbf{u}\cdot\nabla)\mathbf{u}\right) + \nabla p - \mu\nabla^2\mathbf{u} = \chi_e\nabla u_e.$$

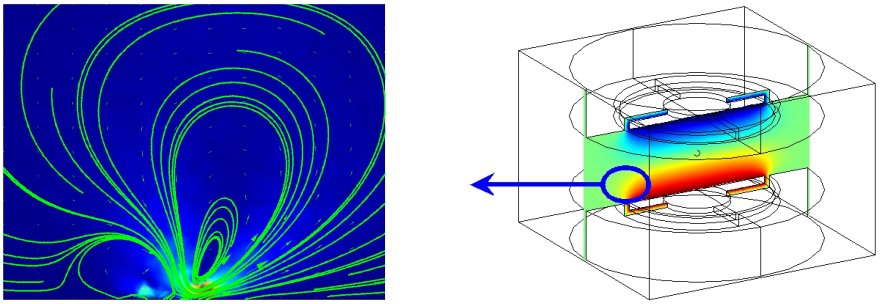

(a) (b)

Figure 6.4: (a) Convection created by the electrostatic pressure $\chi_e \nabla u_e$. The background image shows the *cell Reynolds number* in color code ($Re \in [0.05,5]$). (b) Electrostatic potential. The color code represents the dimensionless electric potential. The top electrode is forced at $\phi = -1$, the lower electrode at $\phi = +1$, and the grounded shield is at $\phi = 0$.

This equation have been implemented in dimensionless form in a 2D computational domain. The term u_e corresponds to the electrostatic energy density. Figure 6.4 illustrates the induced convection-like motion due to this "electric pressure".

Note that high electric energy density gradients, close to the electrodes' edges, act like gradients of pressure.

6.2.2 Sharp boundaries

The observed sharp boundaries between regions containing particles of different sizes can also be attributed to the distribution of the electric energy density inside the plasma chamber. These peculiar boundaries can be explained by looking at the isosurfaces of electric energy density (see figure 6.5) for both the electrostatic case and for the first resonant mode.

If dielectrophoretic forces are more important than gravitational and Lorentz forces, i.e. if the polarizability of a dust particle is more important than its charge, Eq. (4.65) simplifies to

$$\rho \left(\frac{\partial \mathbf{u}}{\partial t} + (\mathbf{u} \cdot \nabla)\mathbf{u} \right) + \nabla p - \mu \nabla^2 \mathbf{u} = \chi_e \nabla u_e.$$

For steady-state problems, we can neglect the terms due to the macroscopic velocity (i.e. $\mathbf{u} = 0$), obtaining the simplified expression

$$\nabla p = \chi_e \nabla u_e.$$

This equation relates the hydrostatic pressure to the electric energy density. For steady-state problems, this equation explains why bigger particles (higher polarizability, if all particles are made of the same material) move towards the electrodes' edges (regions of high electric energy density), and why smaller particles move towards the center of the chamber (region of low electric energy density, see Fig. 6.5).

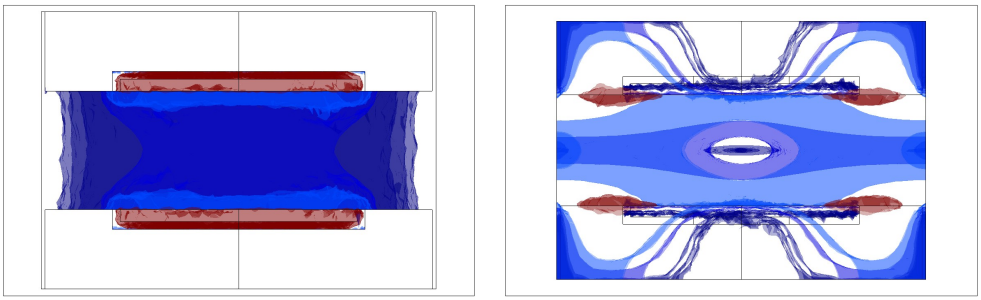

(a) (b)

Figure 6.5: Lateral view of the isosurfaces of electric energy density u_e (a) electrostatic regime (b) first resonant mode (dimensionless color code).

We have shown in section 3.5.1 that dielectrophoretic forces push particles of high polarizability towards high energy regions. Under normal laboratory conditions, these forces compete against gravity, which makes it very hard to observe them. Under microgravity conditions, it may be possible to observe complex structures due to this effect.

6.2.3 Void

The central void observed in complex plasmas under microgravity conditions[2] can also be explained (at least qualitatively) in terms of the electric energy distribution.

We can see in Fig. 6.3 that the first eigenfunction of the chamber (denoted $\psi_1(\mathbf{x})$ in chapter 2) presents a void in the center, this might be the source of the observed void in the PK-3 Plus experiment.

If we consider the expression obtained in the previous section for the steady-state regime

$$\nabla p = \chi_e \nabla u_e,$$

[2] See Refs. 24-31.

the void can be explained by the equilibrium isosurface between the gradients of the neutral gas pressure and potential electric energy of the dust particles (due to polarization).[3]

This is in agrement with the experimental results, which have shown that the void can be closed by decreasing the gas pressure (this is, moving the equilibrium boundary towards an inner isosurface) or by decreasing the supplied electric power (which also implies moving the equilibrium boundary towards the center of the chamber).

These experiments have also shown that under the same experimental setup (gas pressure, supplied electric power, etc.), bigger particles[4] form bigger voids. This can be explained because a higher polarizability in the particles would make them align on an isosurface of higher electric energy (which are located close the electrodes).

6.2.4 Probe induced void

In Sec. 2.6 we have discussed how a floating probe, wire or any other metallic object, can change the way in which the electric energy distributes inside a plasma chamber.

The introduction of a metallic object also changes the eigenfunctions and resonant frequencies of the chamber. Figure 6.6 shows how a small probe (of 3 mm in length and .1 mm in diameter, located 10 mm below the upper electrode) modified the first mode of the energy density inside the PK-3 Plus chamber.

It is observed that the first resonant frequency has a small shift of +0.3% with respect to the resonant frequency calculated without the probe.

Figure 6.7 shows a zoom to the neighborhood of this floating probe. Note how the electric energy density might also be correlated to the shape of the secondary voids observed in complex plasmas experiments.[5]

[3] Note the equilibrium isosurface is not when $p = \chi_e u_e$, but rather when the gradient of the pressure equals the gradient of the electric energy density, or equivalently $\nabla p = \chi_e \nabla u_e$.

[4] When big and small particles are made of the same material.

[5] See Refs. 87-89.

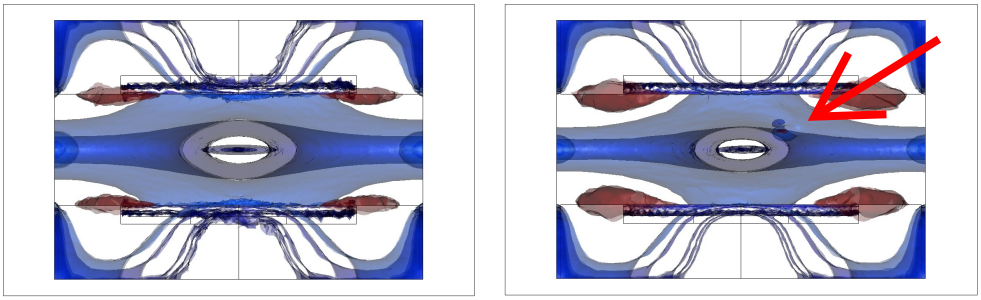

(a) (b)

Figure 6.6: Lateral view of the isosurfaces of electric energy density u_e for the first resonant mode (a) without the probe (b) with the probe (dimensionless color code).

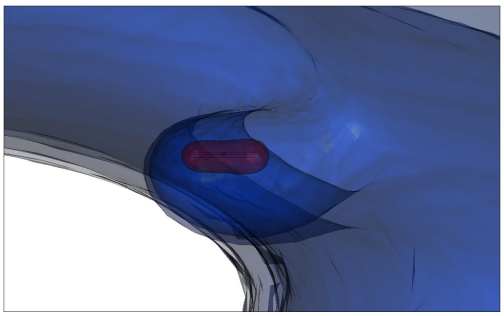

Figure 6.7: Zoom of figure 6.6(b). Isosurfaces of electric energy density u_e for the first resonant mode, modified by inserting a metallic probe (dimensionless color code).

Conclusions 7

The dynamics of complex plasmas, just as the dynamics of complex fluids, is characterized by the interplay of different components at microscopic and mesoscopic levels. These interactions result in a mixture of electrodynamics and fluid dynamics effects.

This thesis has reviewed the process of implementing numerical simulations of a complex plasma chamber, based on a set of coupled partial differential equations (PDEs). This coupled set of PDEs is proposed to be solved by the finite element method (FEM), which allows to couple different physical phenomena in bounded three-dimensional domains.

First, the profiles of the electric energy density inside the cavity have been calculated, both for the electrostatic case, and for the first six resonance modes of the electromagnetic waves. It has been found that the applied radio-frequency voltage has a driving frequency (13.67 MHz) which is below the first resonant frequency of the cavity (4.24 GHz).

The Sturm-Liouville theory has been used for obtaining a mathematical description of the Maxwell equations in a bounded cavity with inhomogeneous boundary conditions, and the finite element method has numerically implemented this representation.

It has been shown that the electromagnetic energy inside the plasma chamber splits among the natural modes of resonance, and that the boundary conditions dictate which modes are excited. The electromagnetic energy will apportion among the exited modes, and the shape in which this energy distributes is correlated to the eigenfunctions of the respective excited modes.

In order to obtain a macroscopic description of the complex plasma dynamics, the modeling of the fluid dynamic equations has followed the kinetic theory of rarefied gases, where the coupling to the external electromagnetic fields has been done at the kinetic level. This approach overcomes the jump from the microscopic description of the Boltzmann equation to the macroscopic (or continuum) description. This approach is different than the one followed by other authors, where the electromagnetic forces acting on the fluid are derived from macroscopic considerations.[1]

We have shown that both dielectric particles and gases feel a kind of

[1] See Refs. 91 pp. 65-68, 85 pp. 137-139, and 92 p. 784.

"electric pressure". High gradients of this pressure may result on the formation of eddies of neutral gas in low-temperature low-pressure plasmas. This approach is new, since the current theory considers the neutral gas at rest, exerting a viscous (Epstein) drag on the other complex plasmas constitutes. The observed vortices (close to the electrodes' borders) in the PK-3 Plus experiment are explained by the streamlines caused by these electric energy density gradients. The higher the permittivity of the particles, the bigger the eddies.

We have found that the existence and shape of the void in the PK-3 Plus experiment could be explained by considering both the electrostatic and the first resonance mode of the plasma chamber. This could not have been possible to visualize without a three-dimensional model. An experimental proof of this alternative approach would be to excite higher resonant modes of the cavity, leading to the observation of different void patterns. This model also explains the formation of secondary voids, induced by the introduction of metallic probes inside the chamber.

The hypothesis of the electric energy density as the source of the central and induced voids, also explains the demixing process in complex plasmas (compounded by dust particles of different sizes or different polarizability). Dielectrophoretic forces will push particles of higher permittivity (bigger particles, if all are made of the same material) towards regions of high electric energy densities, and the frontiers between particles of different size (or permittivity) will be dictated by isosurfaces of electric energy density.

The explanation of these phenomena, based on the distribution of the electric energy density, offers a new point of view to the current state of the theory, which attributes the void formation to the ion-drag force. The ion-drag theory is based on the assumption that the force is proportional to the cross section of the collision between ions and dust particles. Therefore, particles of the same radii should experience a similar drag, independently of its constitutive material. On the other hand, dielectrophoretic forces are proportional to the permittivity of the particle, therefore, particles of the same radii but of different material (different permittivity) should experience different accelerations. This would be another way of proving this hypothesis.

Also, to perform complex plasma experiments under the same parameters (pressure, peak-to-peak voltage, etc.) with dust particles of the same size but of different permittivity, could help to collate the importance of dielectrophoretic forces to Lorentz forces on the dynamics of complex plasmas.

7.1 Future work

From the numerical point of view, this set of coupled PDEs challenges the state of the art of the numerical algorithms, making the numerical implementation a very interesting problem by itself.

The virtual prototype of a complex plasma chamber makes it possible to try different sets of parameters, before launching experiments like the International Microgravity Plasma Facility (IMPF). One could thereby check whether changes in the chamber (by inserting probes, rings, wires, etc. or by changing its geometry) would lead to different void topologies or not.

The use of virtual prototypes could lead to an optimal use of resources in future experiments. It would be possible, for example, to design dust-traps by trying different probe shapes. The use of numerical models would turn the design of future plasma chambers a faster and cheaper task.

Finite element method

A.1 PDEs and mathematical modeling

The study of partial differential equations (PDEs) started in the 18th century as a modeling tool of physical problems. The Euler-Lagrange principle (which gave rise to PDEs and the calculus of variations) and later the Hamilton-Jacobi theory stimulated the analysis of first-order PDEs.

At the beginning of the 19th century, the three major examples of second-order PDEs (hyperbolic, elliptic and parabolic) were already introduced: in 1752 d'Alembert applied the one-dimensional wave equation for modeling vibrating strings (it was extended by Euler and D. Bernoulli into two and three dimensions); during the years 1784-1787 Laplace introduced in his *Méchanique Céleste* the equation which bears his name; and the heat equation was developed (1810-1822) by Fourier in his *Théorie analytique de la chaleur*.[1]

Besides these three classical examples, other PDEs associated with major physical phenomena appeared during the 18th and 19th centuries:

- The Euler equations of incompressible fluid flows (1755).
- The Laplace and Poisson equations for electric and magnetic problems, by Poisson (1813), Green (1828) and Gauss (1839).
- The theory of linear elasticity by Navier (1821) and Cauchy (1822).
- The Navier-Stokes equations by Navier (1822-1827) and Stokes (1845).
- The Helmholtz equation and the eigenvalue problem (1860).
- The Maxwell equations for electromagnetism (1864).
- The Boltzmann equation in the kinetic theory of gases (1872).
- The telegraph equation by O. Heaviside (1876).
- The Korteweg-De Vries equation for solitons (1896).

[1] See Ref. 178.

A.1.1 Well-posed problems

During the 19th century, a number of important methods were introduced in order to find solutions of PDEs satisfying boundary conditions, such as the method of separation of variables, Green's functions, the expansion in power series, etc. Nevertheless, these methods could only find explicit solutions for particular problems, and moreover, they were not well suitable for all kind of domains. Also, there were proposed without rigorous proofs of basic existence results.

Since the beginning of the 20th century, the need for a rigorous treatment of PDEs and their boundary value problems (BVPs) has been a strong motivation in the development of basic tools in real analysis and functional analysis.

In general, PDEs without boundary or initial conditions will either have infinite solutions, or no solution. Therefore, the problem to solve not only consists in the PDE by itself, but it also includes the domain in which the PDE is required to hold, and its initial and boundary conditions. This is called the *data* of the problem.

Whether boundary conditions are appropriate for a given data or not was clarified by (what is nowadays a fundamental mathematical insight) Hadamard in 1902.[2]

Hadamard stated that a *well-posed* mathematical model of a physical problem (*un problème bien posé*) has to fulfill three fundamental requirements:

- Existence: there is a solution of the problem.
- Uniqueness: there is at most one solution of the problem.
- Stability: the solution depends continuously on the data (in terms of suitable norms).

Problems which do not fulfill all of these properties are called *ill-posed*. The classical example (also given by Hadamard) of an ill-posed problem is the Cauchy (or initial value) problem for the Laplace equation.

From a numerical point of view, it is crucial to verify beforehand whether the problem is well-posed or not. Existence and uniqueness will guaranty that the numerical scheme reaches the sought solution, and the stability will assure that the numerical errors do not spread out.

[2] See Ref. 180 lecture 1. In the same lecture, Hadamard explained the way of elucidating whether a PDE is hyperbolic, elliptic or parabolic.

A.2 Finite element method

The finite element method is a general technique for implementing numerical solutions of partial differential equations. The method has its roots in developments by Rayleigh, Ritz and Galerkin. The first application as a numerical method, however, was given by Courant in 1943 in his solution of the St. Venant torsion problem.[3]

During the 1950s, Argyris and collaborators wrote a series of papers in which they applied the finite element method to structural analysis. The name "finite element method" appeared in 1960 in a paper by Clough devoted to plane stress analysis.[4] The mechanical structures (bars, plates, beams, etc.) were divided into small pieces, so-called *finite elements*. Soon it became clear that the method was a general technique for solving PDEs.

The first textbook on the mathematical theory of the finite element method was published in 1973.[5]

Nowadays, there are many commercial and open-source software which use this method for solving linear and nonlinear problems of acoustics, fluid dynamics, electromagnetism, structural mechanics, heat transfer, etc.[6]

A.2.1 Preliminaries

Let $\Omega \subset \mathbb{R}^n$ $(n = 1, 2, 3)$ be a simple bounded domain with boundary Γ and unit outward normal $\mathbf{n}$.

Let us introduce the concept of *inner product* between two real-valued functions $f, g : \Omega \to \mathbb{R}$

$$(f, g) \doteq \int_\Omega f(\mathbf{x}) g(\mathbf{x}) d\mathbf{x}. \tag{A.1}$$

This inner product defines the L^2-norm in Ω

$$\|f\|_{L^2} \doteq \sqrt{\int_\Omega f^2 d\mathbf{x}} = (f, f)^{1/2},$$

and functions with finite L^2-norm define an *infinite-dimensional* function

[3] See Ref. 179.
[4] See Ref. 185 pp. 4-5. For an historical introduction, see also Ref. 186.
[5] See Ref. 187.
[6] See Refs. 181-191.

space (so-called *Lebesgue* space)[7]

$$L^2(\Omega) = \left\{ f : \int_\Omega f^2 d\mathbf{x} < \infty \right\}.$$

We can generalize the L^2 norm and space in order to include derivatives. Let us define the *Sobolev space* $H^1(\Omega)$ as[8]

$$H^1(\Omega) = \left\{ f : \int_\Omega (|\nabla f|^2 + f^2) d\mathbf{x} < \infty \right\}.$$

This space is very useful when working with second-order PDEs.[9]

Let $\mathbf{u}, \mathbf{v}$ be real-valued vectors $\mathbf{u}, \mathbf{v} : \Omega \to \mathbb{R}^n$, with inner product between them defined as

$$(\mathbf{u}, \mathbf{v}) = \int_\Omega \mathbf{u}(\mathbf{x}) \cdot \mathbf{v}(\mathbf{x}) d\mathbf{x}.$$

Other useful spaces of functions with applications to problems of fluid dynamics and electrodynamics[10] are: the space $H(div; \Omega)$ defined[11] as

$$H(div; \Omega) = \left\{ \mathbf{u} \in L^2(\Omega)^n : \nabla \cdot \mathbf{u} \in L^2(\Omega) \right\},$$

and the space $H(curl; \Omega)$ defined[12] as

$$H(curl; \Omega) = \left\{ \mathbf{u} \in L^2(\Omega)^3 : \nabla \times \mathbf{u} \in L^2(\Omega)^3 \right\}.$$

Other spaces of functions $f : \Omega \to \mathbb{R}$ are

$$C^0(\Omega) = \{ f : f \text{ is continuous on } \Omega \},$$

$$C^k(\Omega) = \{ f : f \text{ is } k\text{-times continuously differentiable on } \Omega \},$$

$$C^\infty(\Omega) = \{ f : f \text{ is smooth on } \Omega \}.$$

---

[7] L^2 is a *Hilbert space*, which holds the Cauchy-Schwarz inequality $|(f, g)| \leq \|f\|_{L^2} \|g\|_{L^2}$.

[8] It is also a Hilbert space with scalar product $(f, g)_{H^1} \doteq \int_\Omega (\nabla f \cdot \nabla g + fg) d\mathbf{x}$ and norm $\|f\|_{H^1} \doteq \sqrt{(f, f)_{H^1}}$.

[9] For a formal definition of Sobolev spaces, see Refs. 192 and 189 Chap. 1.

[10] See Refs. 181,184.

[11] It is also a Hilbert space with inner product $(\mathbf{u}, \mathbf{v})_{H^{div}} = (\mathbf{u}, \mathbf{v}) + (\nabla \cdot \mathbf{u}, \nabla \cdot \mathbf{v})$ and norm $\|\mathbf{u}\|_{H^{div}} = \sqrt{(\mathbf{u}, \mathbf{u})_{H^{div}}}$.

[12] It is also a Hilbert space with inner product $(\mathbf{u}, \mathbf{v})_{H^{curl}} = (\mathbf{u}, \mathbf{v}) + (\nabla \times \mathbf{u}, \nabla \times \mathbf{v})$ and norm $\|\mathbf{u}\|_{H^{curl}} = \sqrt{(\mathbf{u}, \mathbf{u})_{H^{curl}}}$.

A.2.2 Weak formulation

Until the 1920's, the solutions of PDEs were generally understood to be "classical solutions", i.e., functions belonging[13] to C^k for PDEs containing differential operators of order $\leq k+1$. Also, until the 1960s, the classical way of numerically solve partial (ordinary) differential equations was the *finite difference method.*

As an example, consider the Poisson equation in Ω with inhomogeneous (Dirichlet and Neumann) boundary conditions on $\Gamma = \Gamma_1 \cup \Gamma_2$

$$\begin{aligned} -\nabla^2 u &= f \quad \text{in } \Omega \\ u &= g \quad \text{on } \Gamma_1 \\ \nabla u \cdot \mathbf{n} &= h \quad \text{on } \Gamma_2. \end{aligned} \tag{A.2}$$

For one-dimensional geometries, the finite difference method will approximate this problem with the numerical scheme

$$\frac{u_{i+1} - 2u_i + u_{i-1}}{h^2} = f_i,$$

where $u_i = u(x_i)$, $f_i = f(x_i)$, and $h = x_i - x_{i-1}$ (this approximation is $\mathrm{O}(h^2)$ accurate).

For a two-dimensional domain (on a square grid), the finite difference method will use the scheme

$$\frac{u_{i+1,j} + u_{i-1,j} + u_{i,j+1} + u_{i,j-1} - 4u_{i,j}}{h^2} = f_{i,j}.$$

It can be very difficult to prove existence, uniqueness, stability, and convergence of the finite difference scheme when dealing with arbitrary geometries, unstructured grids, general boundary conditions and nonlinear operators.

The finite element method does not approximate the differential form of the problem (A.2) as the finite difference approach, but it rather finds a projection of the solution u into a given finite-dimensional space of functions. Also, one of the most appreciated properties of the method is the simplicity to give *a priori* and *a posteriori* error estimates in terms of suitable norms, which leads to prove its well-posedness.

Let us introduce the idea of finding *weak solutions* of the original PDE. If u is the solution of the problem (A.2) and v is any (regular) *test function*

[13] Here C^k denotes the space of k-times continuously differentiable functions.

such that $v = 0$ on Γ_1, we can multiply the PDE by v and then integrate it over the whole domain, in order to obtain

$$\int_\Omega -\nabla^2 u v d\mathbf{x} = \int_\Omega f v d\mathbf{x}.$$

Integrating by parts, using the fact that $v = 0$ on Γ_1 and $\nabla u \cdot \mathbf{n} = h$ on Γ_2, together with the inner product defined in Eq. (A.1), we obtain

$$\int_\Omega \nabla u \cdot \nabla v d\mathbf{x} - \int_{\Gamma_2} h v ds = (f, v).$$

Defining the space of possible *test functions* as

$$V = \left\{ v \in H^1(\Omega) : v = 0 \text{ on } \Gamma_1 \right\},$$

and the *bilinear form*[14] $a(\cdot, \cdot) : V \times V \to \mathbb{R}$

$$a(u, v) = \int_\Omega \nabla u \cdot \nabla v d\mathbf{x},$$

the *weak formulation* of the original problem (A.2) becomes

$$\text{Find } u \in V \text{ such that } a(u, v) = F(v) \qquad \forall v \in V, \tag{A.3}$$

where the *linear form* $F : V \to \mathbb{R}$ is defined as $F(v) = (f, v) + \int_{\Gamma_2} h v ds$.

This is called the *weak formulation* of the original PDE (A.2), and u is called its *weak solution*,[15] since (A.3) is valid with less restrictive assumptions on f. It is also sometimes called the *abstract variational formulation* of (A.2) since the function v is allowed to vary arbitrarily.[16]

Note that the bilinear form $a(\cdot, \cdot)$ in (A.3) contains weaker derivatives than the original problem (A.2). In general, and depending on the PDE, the bilinear form is not necessary symmetric.

The weak formulation assumes that V is a closed subspace of a *Hilbert space* H, and that the bilinear form is *continuous, symmetric* and *coercive* on V. This is the starting point of the finite element method.

[14] In this example, $a(\cdot, \cdot)$ is bilinear, but the formulation can also be extended to other types of problems. Note that the spaces of trial functions ($u \in \hat{V}$) and test functions ($v \in V$) are not necessary equivalent, for simplicity we will assume so, but the weak formulation is not restricted to that assumption.

[15] Note that a *classical solution* of the PDE is always its *weak solution*, but the contrary is not necessarily true.

[16] See Ref. 189.

A.2.3 Ritz method

This variational method was introduced by W. Ritz[17] as a generalization of a technique described by Rayleigh.[18] Sometimes is also called the Rayleigh-Ritz method.

The Ritz method is based on the minimization of the functional

$$Q(v) = \frac{1}{2}a(v,v) - F(v)$$

and it is valid when the bilinear form $a(\cdot,\cdot)$ is *symmetric*. The minimization yields to the equivalent *symmetric variational problem*

$$\text{Find } u \in V \text{ such that } a(u,v) = F(v) \qquad \forall v \in V, \tag{A.4}$$

where existence and uniqueness of the solution u is demonstrated by the *Riesz representation theorem*.

The Ritz method is optimal in the sense that it minimizes the functional $Q(v)$, but it cannot be applied when there is not a corresponding minimum principle, or in other words, when the bilinear form $a(\cdot,\cdot)$ is not symmetric.

A.2.4 Galerkin method

Galerkin's method[19] was originally formulated with global polynomial subspaces and goes back to the variational principles of Leibniz, Euler, Lagrange, Dirichlet, Hamilton, Rayleigh, and Ritz.

Given a *finite-dimensional* subspace $V_h \subset V$, the variational problem (A.3) is approximated by

$$\text{Find } u_h \in V_h \text{ such that } a(u_h,v) = F(v) \qquad \forall v \in V_h. \tag{A.5}$$

The existence and uniqueness of the solution u_h come from the fact that $(V_h, a(\cdot,\cdot))$ is a proper *Hilbert space*.[20] The Galerkin method is much more general and can be used even if no minimum principle exists. For symmetric problems, the existence and uniqueness of the approximate solution u_h also follow the *Riesz representation theorem*. For nonsymmetric problems (i.e. the bilinear form $a(\cdot,\cdot)$ is not symmetric), the *Lax-Milgram theorem* guarantees both existence and uniqueness.

[17] See Ref. 193.
[18] See Ref. 194.
[19] See Ref. 195.
[20] This variational formulation is sometimes also called the Ritz-Galerkin approximation.

Galerkin orthogonality

Let us define the *energy norm*[21] as

$$\|v\|_E = \sqrt{a(v,v)} \qquad \forall v \in V.$$

The error of the Galerkin approximation is $e = u - u_h$, where $u \in V$ is the (weak) solution of the original variational problem (A.3), and $u_h \in V_h$ is the solution of the Galerkin approximation (A.5). Since $a(\cdot,\cdot)$ is bilinear and V_h is a finite-dimensional subset of V, we can subtract (A.5) from (A.3) in order to obtain

$$a(u - u_h, v) = 0 \qquad \forall v \in V_h. \tag{A.6}$$

The basic error estimation of the Galerkin method is given by the definition of the energy norm and the Cauchy-Schwarz inequality[22]

$$\|e\|_E = \|u - u_h\|_E = \min_{v \in V_h} \|u - v\|_E.$$

One of the most important corollary is that the error of the finite element approximation is optimal in the energy norm. For nonsymmetric problems, the *Céa's theorem* shows that, given a subspace V_h, the approximation u_h is *quasi-optimal* in the sense that the error's norm $\|u - u_h\|_V$ is proportional to the best it can be (given the subspace V_h)

$$\|e\|_V = \|u - u_h\|_V \leq C \min_{v \in V_h} \|u - v\|_V.$$

The finite element solution u_h is the closest projection of the weak solution $u \in V$ on the finite-dimensional subspace $V_h \subset V$, i.e. u_h is the best approximation of the weak solution u in the sense that it minimizes the error $e = u - u_h$ for a given finite-dimensional space V_h.

Galerkin approximation

In the previous sections we have shown that, given the weak formulation of a PDE, we can demonstrate that the Galerkin approximation is well-posed.

Given a finite-dimensional space V_h of test functions, the existence and uniqueness of the Galerkin approximation is proved by the Lax-Milgram theorem, and its (quasi) optimality by the Céa theorem.

[21] Also fulfills the Cauchy-Schwarz inequality $|a(v,w)| \leq \|v\|_E \|w\|_E \qquad \forall v, w \in V.$

[22] See proof in Ref. 189 Chaps. 2 and 5.

Let us suppose that the finite-dimensional space V_h is formed by a basis $\phi_i(\mathbf{x})$, $i = 1, .., N$, $\mathbf{x} \in \Omega$ (and therefore, any $v \in V_h$ can be written as a linear combination of this basis).

The Galerkin method approximates the solution u_h of the weak formulation

$$\text{Find } u_h \in V_h \text{ such that } a(u_h, v) = F(v) \qquad \forall v \in V_h, \tag{A.7}$$

in terms of the basis ϕ_i, i.e.

$$u_h(\mathbf{x}) = \sum_{i=1}^{N} u_i \phi_i(\mathbf{x}).$$

Since $a(u_h, v) = a(\sum u_i \phi_i, v) = \sum u_i a(\phi_i, v)$, this is equivalent to find the coefficients u_i such that

$$\sum_{i=1}^{N} u_i a(\phi_i, v) = F(v) \qquad \forall v \in V_h.$$

The weak formulation (A.7) has to be valid for all functions $v \in V_h$, therefore and without loss of generality, this is equivalent to solve the system

$$\sum_{i=1}^{N} u_i a(\phi_i, \phi_j) = F(\phi_j) \qquad \forall \phi_j \in V_h.$$

We can write this system in a matrix form

$$A\mathbf{u} = \mathbf{f}, \tag{A.8}$$

where $A_{ij} = a(\phi_i, \phi_j)$ is the $N \times N$ *stiffness matrix*, $\mathbf{f}_i = F(\phi_i)$ is the $N \times 1$ *load vector*,[23] and the vector $\mathbf{u} = (u_1, ..., u_N)^{\mathrm{T}}$ contains the N unknowns u_i.

Note that the stiffness matrix is *positive definite*

$$\mathbf{u} \cdot A\mathbf{u} = \sum_{j=1}^{N} u_j \sum_{i=1}^{N} u_i a(\phi_i, \phi_j) = a(u_h, u_h) = \|u_h\|_E^2 > 0 \qquad \forall u_h \neq 0,$$

and it is also symmetric when the bilinear form $a(\cdot, \cdot)$ is symmetric, since $A_{ij} = a(\phi_i, \phi_j)$.

Since A is positive definite, it is therefore non-singular, which guaranties the existence and uniqueness of the solution $\mathbf{u}$ of the discrete system (A.8).

[23] The names *stiffness matrix* and *load vector* have their origin in the first applications of the finite element method for structural analysis.

The idea behind the finite element method is that the basis ϕ_i is formed by smooth piecewise polynomials with a small compact support in Ω, so the matrix A will be *sparse*.[24] The drawback of this is that the size of the matrix A depends on the number of elements in this basis, therefore, for three-dimensional and/or coupled problems the system (A.8) can be "huge" for a given error tolerance.[25]

The use of piecewise polynomials also simplifies the computation of the stiffness and mass matrices, and the load vector $\mathbf{f}$, this task is called the *assembly process*.

Galerkin's method with piecewise polynomial subspaces with compact support in Ω is known as the finite element method.

Note that the system (A.8) is the finite element representation of the Poisson equation (A.2) used as an example. In general, and depending on the PDE under study, we will have other kinds of systems (eventually nonlinear or unsymmetric).[26]

Eigenvalue problems

For instance, the eigenvalue problem (or Helmholtz equation) in Ω with homogeneous boundary conditions on $\Gamma = \Gamma_1 \cup \Gamma_2$

$$\begin{aligned} -\nabla^2 u &= \lambda u \qquad \text{in } \Omega \\ u &= 0 \qquad \text{on } \Gamma_1 \\ \nabla u \cdot \mathbf{n} &= 0 \qquad \text{on } \Gamma_2, \end{aligned}$$

results in the (symmetric) weak formulation:

$$\text{Find } u \in V \text{ and } \lambda \in \mathbb{R}^+ \text{ such that } a(u,v) = \lambda(u,v) \qquad \forall v \in V.$$

By using the Galerkin approximation[27] $u_h(\mathbf{x}) = \sum u_i \phi_i(\mathbf{x})$, the discrete variational problem results in the (symmetric) system

$$A\mathbf{u} = \lambda M \mathbf{u},$$

where $A_{ij} = (\nabla\phi_i, \nabla\phi_j)$ is the stiffness matrix, and $M_{ij} = (\phi_i, \phi_j)$ is the *mass matrix*.[28]

[24] The elements of the matrix $A_{ij} = a(\phi_i, \phi_j)$ will therefore be non-zero for just few ϕ_i and ϕ_j.

[25] In terms of the computational cost to solve it.

[26] Symmetric problems are computationally easier to solve than unsymmetric problems. Nonlinear PDEs, such as fluid dynamics problems including the convection term $(\mathbf{u}\cdot\nabla)\mathbf{u}$, require special algorithms.

[27] The basis ϕ_i spans the finite-dimensional space $V_h \subset H^1(\Omega)$.

[28] The mass matrix is also positive definite.

Navier-Stokes formulation

Let us suppose that we try to solve the dimensionless Navier-Stokes equations (4.30) in a three-dimensional domain $\Omega \subset \mathbb{R}^3$

$$\nabla \cdot \mathbf{u} = 0$$
$$\frac{\partial \mathbf{u}}{\partial t} + (\mathbf{u} \cdot \nabla)\mathbf{u} + \nabla p - \frac{1}{Re}\nabla^2 \mathbf{u} = \mathbf{f},$$

where $\mathbf{u} = (u, v, w)^{\mathrm{T}}$ is the velocity field, p is the pressure, R_e is the Reynolds number and $\mathbf{f}$ represents the dimensionless acceleration due to external forces.

The (unsymmetric) weak formulation of the Navier-Stokes equations reads[29]

Find $\mathbf{u} \in \mathbf{V}$ and $p \in P$ such that

$$(\nabla \cdot \mathbf{u}, q) = 0 \qquad \forall q \in P$$
$$\left(\frac{\partial \mathbf{u}}{\partial t} + (\mathbf{u} \cdot \nabla)\mathbf{u} + \nabla p - \frac{1}{Re}\nabla^2 \mathbf{u}, \mathbf{v}\right) = (\mathbf{f}, \mathbf{v}) \qquad \forall \mathbf{v} \in \mathbf{V}$$

The velocity $\mathbf{u}$ is then approximated in the finite-dimensional space of functions $\mathbf{V}_h \subset \mathbf{H}(div; \Omega)$, so[30]

$$\mathbf{u}_h = \sum_{i=1}^{N_u} \mathbf{u}_i \phi_i(\mathbf{x}) = \sum_{i=1}^{N_u} \begin{pmatrix} u \\ v \\ w \end{pmatrix}_i \phi_i(\mathbf{x}),$$

and the pressure p is approximated by

$$p_h = \sum_{j=1}^{N_p} p_j \varphi_j(\mathbf{x}),$$

where the basis φ_j defines the finite-dimensional space $P_h \subset L^2(\Omega)$.

If we put the $3N_u$ unknowns of the velocity approximation $\mathbf{u}_h$ in a $3N_u \times 1$ vector, i.e. $\mathbf{U} = (u_1, ..., u_{N_u}, v_1, ..., v_{N_u}, w_1, ..., w_{N_u})^{\mathrm{T}}$, and the N_p unknowns of the pressure p_h in the $N_p \times 1$ vector $\mathbf{p} = (p_1, ..., p_{N_p})^{\mathrm{T}}$, this finite element approximation leads to the (unsymmetric) nonlinear system of equations

$$\mathbf{G}^{\mathrm{T}}\mathbf{U} = \mathbf{0}$$
$$\mathbf{M}\dot{\mathbf{U}} + \mathbf{C}(\mathbf{U})\mathbf{U} - \mathbf{G}\mathbf{p} + \frac{1}{R_e}\mathbf{A}\mathbf{U} = \mathbf{F}.$$

[29] Note that $(\mathbf{u}, \mathbf{v})$ represents the inner product of vectors in $\mathbb{R}^3$. See also Ref. 184.

[30] The basis ϕ_i spans the finite-dimensional space $V_h \subset H^1(\Omega)$.

The block matrices $\mathbf{M}$, $\mathbf{C}$, $\mathbf{G}$, and $\mathbf{A}$ are

$$\mathbf{M} = \begin{bmatrix} M & 0 & 0 \\ 0 & M & 0 \\ 0 & 0 & M \end{bmatrix} \quad \mathbf{A} = \begin{bmatrix} A & 0 & 0 \\ 0 & A & 0 \\ 0 & 0 & A \end{bmatrix} \quad \mathbf{C}(\mathbf{U}) = \begin{bmatrix} C & 0 & 0 \\ 0 & C & 0 \\ 0 & 0 & C \end{bmatrix} \quad \mathbf{G} = \begin{bmatrix} G_x \\ G_y \\ G_z \end{bmatrix},$$

where the $M_{ij} = (\phi_i, \phi_j)$ and $A_{ij} = (\nabla\phi_i, \nabla\phi_j)$ are the standard $N_u \times N_u$ mass and stiffness matrices, $C_{ij}(\mathbf{U}) = (\phi_i, (\mathbf{u}_h \cdot \nabla)\phi_j)$ is the (unsymmetric) $N_u \times N_u$ *convection matrix*[31] and $Gx_{ij} = (\partial_x\phi_i, \varphi_j)$ is the $N_u \times N_p$ projection matrix.[32]

For steady-state problems,[33] this system reduces to the nonlinear system

$$\begin{bmatrix} \mathbf{G}^{\mathrm{T}} & \mathbf{0} \\ \mathbf{C}(\mathbf{U}) + \frac{1}{Re}\mathbf{A} & -\mathbf{G} \end{bmatrix} \begin{bmatrix} \mathbf{U} \\ \mathbf{p} \end{bmatrix} = \begin{bmatrix} \mathbf{0} \\ \mathbf{F} \end{bmatrix}.$$

Note that in the finite element representation of the Navier-Stokes equations, the spaces of test functions for the velocity $\mathbf{V}_h$ and for the pressure P_h are different. This is called a *mixed problem*.

The finite element approximations for the Poisson equation, Helmholtz equation and Navier-Stokes equations have been used for the numerical examples given in Chaps. 2, 4, and 6.

A.2.5 The finite element space

Let us introduce the finite element implementation of the space V_h. This space consist of piecewise polynomial functions with local support on a *triangulation*[34] $T_h = \{K\}$. This triangulation is a subdivision of the bounded domain $\Omega \subset \mathbb{R}^n$ into a non-overlapping set of elements K.

The domain $K \subset \mathbb{R}^n$ is called the *element domain*, which can be a line interval, a triangle or a tetrahedron (when n represents one, two or three dimensions).

The Ciarlet's definition of a finite element is[35]

- Let $K \subseteq \mathbb{R}^n$ be a domain whit piecewise smooth boundary,
- $\mathcal{P}$ be a finite-dimensional space of functions defined on K, and

[31] The matrix C is *skew-symmetric*, i.e. $C^{\mathrm{T}} = -C$.

[32] Also $Gy_{ij} = (\partial_y\phi_i, \varphi_j)$ and $Gz_{ij} = (\partial_z\phi_i, \varphi_j)$.

[33] Defined by zero macroscopic acceleration, or $\dot{\mathbf{U}} = \mathbf{0}$.

[34] We will not discuss how to generate unstructured grids, as a reference, one of the most popular triangulation methods is the *Delaunay algorithm*.

[35] See Refs. 191, 189 Chap. 3 and 190 Chap. 3.

- $\mathcal{N} = N_1, N_2, ..., N_k$ be a basis for $\mathcal{P}'$,

Then $(K, \mathcal{P}, \mathcal{N})$ is a *finite element*.

The space of *shape functions* $\mathcal{P}$ includes the piecewise polynomials used for the approximation, and $\mathcal{N}$ are the nodal basis for $\mathcal{P}$.

As an example, let us consider the one-dimensional *Lagrange element*. Let $\Omega \subset \mathbb{R}^1$, $K = [0, 1]$, $\mathcal{P}_1$ the set of linear polynomials, and $\mathcal{N} = \{N_1, N_2\}$ the nodal variables where $N_1(v) = v(0)$ and $N_2(v) = v(1)$ $\forall v \in \mathcal{P}$.

Then $(K, \mathcal{P}, \mathcal{N})$ is a linear *Lagrange finite element*, and the nodal basis ϕ_i is defined as $\phi_1(x) = 1 - x$ and $\phi_2(x) = x$.

In general, the element domain K ia a subset of $\mathbb{R}^n$, and the finite-dimensional space of functions $\mathcal{P}_p$ includes all piecewise polynomials of degree $\leq p$ defined in $K \subset \mathbb{R}^n$. Also, the choice for $\mathcal{N}$ is not unique.

The choice of nodal variables $\mathcal{N}$ give rise to different families of elements, such as the *Lagrange*, *Hermite* and *Argirys* elements. Other special families are the *Serendipity*, *Nédélec* and *bubble* elements.

The choice of the space $\mathcal{P}_p(K)$ defines the order of the piecewise polynomials, i.e. $\mathcal{P}_1$ includes linear polynomials, $\mathcal{P}_2$ second-order polynomials, etc.

The *degrees of freedom* (dof) of each element will be given by the order of the piecewise polynomials p and the number of nodal variables. This means that every function $v \in \mathcal{P}_p(K)$ is uniquely determined by dof coefficients.

For instance, in a triangulation of a two-dimensional domain, the degrees of freedom of the Lagrange elements will be given by $dof = \frac{1}{2}(p+1)(p+2)$, that is, linear Lagrange elements $(p = 1)$ will have three degrees of freedom, quadratic elements $(p = 2)$ will have six dof, etc.

Numerical quadrature

Once we know the degrees of freedom of the chosen element family, we can calculate the stiffness and mass matrices, and the load vector[36] by means of a numerical (Gaussian) quadrature on each element of the triangulation T_h

$$\int_\Omega f(x)dx = \sum_K \int_K f(x)dx.$$

The integral on the element K is approximated by the numerical quadrature

$$\int_K f(x)dx \approx \sum_{i=1}^{nq} w_i f(x_i),$$

[36] And afterwards solve the system $A\mathbf{u} = \mathbf{f}$.

where nq denotes the order of the quadrature formula (in general $nq > dof$), and the weights w_i and points x_i are given by the Gauss formula.

This process is called *assembly process*, since it has to be done for each element K in the triangulation T_h.[37]

A.2.6 Error estimates

The use of piecewise polynomials as basis of V_h makes it easy to compute the mass and stiffness matrices. This section will give estimates on how the error of the Galerkin approximation is related to the degree of these piecewise polynomials.

We have shown in section A.2.4 that it is possible (by using appropriate norms) to estimate the error of the finite element approximation. The Cea's theorem tells us that the error of the finite element approximation is bounded as

$$\|u - u_h\|_V \leq C\|u - v\|_V \qquad \forall v \in V_h.$$

This estimate does not tell us much about how the error is related to the degree of the piecewise polynomials used as a basis for V_h.

Let us choose $v \in V_h$ such that it is an appropriate interpolant of u, i.e. $v = \pi_h u$. To find an estimate for the interpolation error $(u - \pi_h u)$ is equivalent to find an estimate of the Galerkin approximation, since

$$\|u - u_h\|_V \leq C\|u - \pi_h u\|_V.$$

Defining h as the diameter of the biggest element given by the triangulation T_h, it is possible to estimate[38] the error of the interpolation $(u - \pi_h u)$ when using piecewise polynomials of degree $p \geq 1$

$$\|u - \pi_h u\|_{L^2} \leq Ch^{p+1}\|u\|_{H^{p+1}},$$

$$\|u - \pi_h u\|_{H^1} \leq Ch^{p}\|u\|_{H^{p+1}},$$

$$\|u - \pi_h u\|_{H^2} \leq Ch^{p-1}\|u\|_{H^{p+1}}.$$

[37] For a faster computational implementation, one could define an *isoparametric mapping* into a standard element defined in a peculiar coordinate system, and then calculate the mapping into each element K by means of the *Jacobian matrix* of the transformation. We will not discuss how to implement the assembly process, for references, see Refs. 189,190,191.

[38] In terms of the norms $L^2(\Omega)$ and $H^k(\Omega)$. See derivation in Refs. 190 Chap. 4 and 189 Chap. 4.

This means, for instance, that if we use linear polynomials ($p = 1$) for defining the basis ϕ_i, the finite element solution will be second order accurate, or equivalently $\mathrm{O}(h^2)$.

In general, raising the degree of the piecewise polynomials[39] will raise the accuracy of the finite element approximation u_h, but it will require higher regularity on the weak solution u.

For instance, if we use higher order polynomials, i.e. $p \to p + q$, the error will be reduced in a factor h^q, but it will require q-times more regularity on the weak solution u. It will also reduce the sparsity of the mass and stiffness matrices.

On the other hand, if we split every element of the triangulation,[40] so $h \to h/\alpha$, the error will be reduced in a factor α^{-p}. For instance, if the elements K are segments, refining the mesh will split each element in two.[41] If the elements K are triangles, refining the mesh will also reduce h in a factor of two, but it will create four triangles per each refined triangle. This will increase the sizes of the mass and stiffness matrices from $N \times N$ to $4N \times 4N$, but it will keep their sparsity.

For tree-dimensional problems, reducing h to its half will imply to split each tetrahedral element in eight, so the mass and stiffness matrices will increase their sizes from $N \times N$ to $8N \times 8N$.

More sophisticate methods will use a combination of both techniques, and will preferably refine the elements in regions whit high local errors.

A.3 Final remarks

In this chapter we have shown that given a partial differential equation with suitable boundary conditions, the finite element method can approximate its weak solution (as close as possible) in a given finite-dimensional space of functions. The existence and uniqueness of the obtained solution is guarantied by the Lax-Milgram theorem, and the stability of the numerical implementation by the Céa theorem. In this sense, we can prove that our numerical scheme is well-posed. The strength of the method is such, that it is possible to find error estimates for describing the error of the numerical implementation. These estimates relate the error to the size of the grid and to the order of the piecewise polynomials. The error tolerance defined by the user can also be confirmed.

[39] This is called the p-method.

[40] This is called the h-method

[41] Therefore, $\alpha = 2$, the error will be reduce in a factor of 2^{-p}, and the mass and stiffness matrices will increase their sizes from $N \times N$ to $2N \times 2N$.

We can summarize the steps of the finite element method as follow:

1. Write the weak (variational) formulation of the original PDE $a(u, v) = F(v)$ (verify whether it is symmetric or not).
2. Discretize the domain Ω, by means of a triangulation algorithm.
3. Define the type of elements (lagrangian, hermitian, etc.), and the degree of the piecewise polynomials (linear, second order, third order, etc.)
4. Assemble the mass and stiffness matrices, load vector, etc.
5. Solve the (linear/nonlinear symmetric/unsymmetric) system $A\mathbf{u} = \mathbf{f}$ with a direct or iterative method (use preconditioning if necessary).
6. Verify whether the numerical error satisfied the required tolerance, if not, refine the mesh and/or increase the order of the piecewise polynomials (h-method, p-method, adaptive method, etc.).
7. Visualize the results (streamlines, isosurfaces, contours, etc.)

We have used the software[42] COMSOL MULTIPHYSICS 3.2 for implementing the numerical results shown in Chaps. 2, 4, and 6. This software uses the Delaunay triangulation algorithm for the discretization of the computational domain. We have used triangular second-order Lagrange elements, for the 2D simulations; and tetrahedral second-order Lagrange elements for the 3D case. In both cases, the numerical solvers were required a relative tolerance of $< 10^{-6}$. For the result visualization, the function `postplot` has been ran on MATLAB 7.0.4.

[42] http://www.comsol.se

Vector identities

B

$$\nabla \times \nabla \times \mathbf{E} = -\nabla^2 \mathbf{E} + \nabla\nabla \cdot \mathbf{E} \tag{B.1}$$

$$\nabla \times \nabla \times \mathbf{B} = -\nabla^2 \mathbf{B} + \nabla\nabla \cdot \mathbf{B} = -\boldsymbol{\nabla^2 \mathbf{B}} \tag{B.2}$$

$$\nabla\nabla \cdot \mathbf{A} = \nabla \times \nabla \times \mathbf{A} + \boldsymbol{\nabla^2 \mathbf{A}} = \nabla \times \mathbf{B} + \boldsymbol{\nabla^2 \mathbf{A}} \tag{B.3}$$

$$\nabla(\mathbf{v} \cdot \mathbf{A}) = (\mathbf{v} \cdot \nabla)\mathbf{A} + \mathbf{v} \times \nabla \times \mathbf{A} \tag{B.4}$$

$$\nabla \mathbf{p} \cdot \mathbf{E} = (\mathbf{p} \cdot \nabla)\mathbf{E} + \mathbf{p} \times \nabla \times \mathbf{E} \tag{B.5}$$

$$\nabla \times (\mathbf{v} \times \mathbf{B}) = \mathbf{v}\nabla \cdot \mathbf{B} - (\mathbf{v} \cdot \nabla)\mathbf{B} \tag{B.6}$$

$$\dot{\mathbf{B}} = \frac{\partial}{\partial t}\mathbf{B} + (\mathbf{v} \cdot \nabla)\mathbf{B} \tag{B.7}$$

$$\nabla \mathbf{v} \cdot (\mathbf{d} \cdot \nabla)\mathbf{A} = (\mathbf{v} \cdot \nabla)(\mathbf{d} \cdot \nabla)\mathbf{A} + \mathbf{v} \times \nabla \times (\mathbf{d} \cdot \nabla)\mathbf{A} \tag{B.8}$$

$$\dot{\mathbf{A}} = \frac{\partial}{\partial t}\mathbf{A} + (\mathbf{v} \cdot \nabla)\mathbf{A} \tag{B.9}$$

References

[1] S. Ichimaru. *Strongly coupled plasmas: high-density classical plasmas and degenerate electron liquids.* Rev. Mod. Phys. **54**, 1017-1059 (1982)

[2] H. Ikezi. *Coulomb solid of small particles in plasmas.* Phys. Fluids **29**, 1764-1766 (1986)

[3] J.H. Chu, J.B. Du, and I. Lin. *Coulomb solids and low-frequency fluctuations in rf dusty plasmas.* J. Phys. D: Appl. Phys. **27**, 296-300 (1994)

[4] J.H. Chu and I. Lin. *Direct observation of Coulomb crystals and liquids in strongly coupled rf dusty plasmas.* Phys. Rev. Lett. **72**, 4009-4012 (1994)

[5] H. Thomas et al. *Plasma crystal: coulomb crystallization in a dusty plasma.* Phys. Rev. Lett. **73**, 652-655 (1994)

[6] Y. Hayashi and K. Tachibana. *Observation of Coulomb-crystal formation from carbon particles grown in a methane plasma.* Jpn. J. Appl. Phys. **33**, L804-L8003 (1994)

[7] A. Melzer, T. Trottenberg and A. Piel. *Experimental determination of the charge on dust particles forming Coulomb lattices.* Phys. Lett. A **191**, 301-307 (1994)

[8] J. B. Pieper, J. Goree, and R. A. Quinn. *Experimental studies of two-dimensional and three-dimensional structure in a crystallized dusty plasma.* J. Vac. Sci. Technol. A **14**, 519-524 (1996)

[9] G. E. Morfil et al. *The physics of complex plasmas and the microgravity programme on plasma crystal (PK) research.* 55^{th} International Astronautical Congress. Vancouver (2004)

[10] S. V. Vladimirov and M. Nambu. *Interaction of a rodlike charged macroparticle with a flowing plasma.* Phys. Rev. E **64**, 026403 (2001)

[11] B. M. Annaratone et al. *Levitation of cylindrical particles in the sheath of an rf plasma.* Phys. Rev. E **63**, 036406 (2001)

[12] A. V. Ivlev, et al. *Rodlike particles in gas discharge plasmas: Theoretical model.* Phys. Rev. E **68**, 026403 (2003)

[13] R. Marcus et al. *Experiments with microrods in a radio- frequency plasma sheath.* Phys. Plasmas **13**, 063502 (2006)

[14] V. Springel et al. *Simulations of the formation, evolution and clustering of galaxies and quasars.* Nature **435**, 629-636 (2005)

[15] N. Goldenfeld and L. P. Kadanoff. *Simple lessons from complexity.* Science **284**, 87-89 (1999)

[16] G. E. Morfill and H. Thomas. *Plasma crystal.* J. Vac. Sci. Technol. A **14**, 490-495 (1996)

[17] G. Praburam and J. Goree. *Experimental observation of very low-frequency macroscopic modes in a dusty plasma.* Phys. Plasmas **3**, 1212-1219 (1996)

[18] D. Samsonov and J. Goree. *Instabilities in a dusty plasma with ion drag and ionization.* Phys. Rev. E **59**, 1047-1058 (1999)

[19] R. P. Dahiya et al. *Evolution of a dust void in a radio-frequency plasma sheath.* Phys. Rev. Lett. **89**, 125001 (2002)

[20] H. Rothermel et al. *Gravity compensation in complex plasmas by application of a temperature gradient.* Phys. Rev. Lett. **89**, 175001 (2002)

[21] E. Thomas et al. *Measurements of forces acting on suspended microparticles in the void region of a complex plasma.* Phys. Rev. E **66**, 016405 (2002)

[22] M. Mikikian and L. Boufendi. *Experimental investigations of void dynamics in a dusty discharge.* Phys. Plasmas **11**, 3733-3737 (2004)

[23] H. Feng et al. *Voids in an experimental dusty plasma system.* Chinese Phys. Lett. **21**, 121-124 (2004)

[24] G. E. Morfill et al. *Condensed plasmas under microgravity.* Phys. Rev. Lett. **83**, 1598-1602 (1999)

[25] H. M. Thomas et al. *Complex plasmas under microgravity conditions: Parabolic flights.* Phys. Scripta T**89**, 16-19 (2001)

[26] M. Mikikian et al. *Formation and behaviour of dust particle clouds in a radio-frequency discharge: results in the laboratory and under microgravity conditions.* New J. Phys. **5**, 19 (2003)

[27] V. E. Fortov et al. *Dynamics of macroparticles in a dusty plasma under microgravity conditions (First experiments on board the ISS).* J. Exp. Theor. Phys. **96**, 704-718 (2003)

[28] A. P. Nefedov et al. *PKE-Nefedov: plasma crystal experiments on the International Space Station.* New J. Phys. **5**, 33 (2003)

[29] V. E. Fortov et al. *Transport of microparticles in weakly ionized gas-discharge plasmas under microgravity conditions.* Phys. Rev. Lett. **90**, 245005 (2003)

[30] A. V. Ivlev et al. *Decharging of complex plasmas: First kinetic observations.* Phys. Rev. Lett. **90**, 055003 (2003)

[31] M. Kretschmer et al. *Force field inside the void in complex plasmas under microgravity conditions.* Phys. Rev. E **71**, 056401 (2005)

[32] J. Goree et al. *Theory of dust voids in plasmas.* Phys. Rev. E **59**, 7055-7067 (1999)

[33] K. Avinash. *"Voids" and phase separation in complex (dusty) plasmas.* Phys. Plasmas **8**, 2601-2604 (2001)

[34] V. N. Tsytovich et al. *Theory of collision-dominated dust voids in plasmas.* Phys. Rev. E **63**, 056609 (2001)

[35] M. R. Akdim and W. J. Goedheer. *Modeling of voids in colloidal plasmas.* Phys. Rev. E **65**, 015401 (2001)

[36] B. M. Annaratone et al. *Complex plasmas boundaries.* Phys. Rev. E **66**, 056411 (2002)

[37] G. E. Morfill and V. N. Tsytovich. *Modeling of complex plasmas under micro-gravity conditions.* Phys. Plasmas. **9**, 4-16 (2002)

[38] A. A. Mamun, P. K. Shukla, R. Bingham. *Plasma voids (holes) in a dusty plasma.* Phys. Lett. A **298**, 179-184 (2002)

[39] K. Avinash, A. Bhattacharjee and S. Hu. *Nonlinear theory of void formation in colloidal plasmas.* Phys. Rev. Lett. **90**, 075001 (2003)

[40] D. Jovanovic and P. K. Shukla. *Nonlinear theory for dust voids in plasmas.* Phys. Lett. A **308**, 369-374 (2003)

[41] M. R. Akdim and W. J. Goedheer. *Modeling the effect of dust on the plasma parameters in a dusty argon discharge under microgravity.* Phys. Rev. E **67**, 066407 (2003)

[42] V. N. Tsytovich et al. *Collision-dominated dust sheaths and voids–observations in micro-gravity experiments and numerical investigation of the force balance relations.* New J. Phys. **5**, 66 (2003)

[43] V. N. Tsytovich, S. V. Vladimirov and G. E. Morfill. *Theory of dust and dust-void structures in the presence of the ion diffusion.* Phys. Rev. E **70**, 066408 (2004)

[44] P. M. Bryant. *The structure of the complex plasma boundary.* New J. Phys. **6**, 60 (2004)

[45] J. Jovanovic and P. K. Shukla. *Dust voids in magnetized dusty plasmas.* Phys. Scripta T**107**, 188-191 (2004)

[46] A. A. Mamun and P. K. Shukla. *Dust voids due to dust-phase-space vortices in plasmas.* Phys. Plasmas **11**, 1757-1761 (2004)

[47] S. V. Vladimirov, V. N. Tsytovich and G. E. Morfill. *Stability of dust voids.* Phys. Plasmas **12**, 052117 (2005)

[48] M. Tribeche et al. *Nonlinear plasma voids (holes) in a charge-varying dusty plasma.* Phys. Plasmas **12**, 092309 (2005)

[49] M. S. Barnes et al. *Transport of dust particles in glow-discharge plasmas.* Phys. Rev. Lett. **68**, 313-316 (1992)

[50] C. Zafiu, A. Melzer and A. Piel. *Ion drag and thermophoretic forces acting on free falling charged particles in an rf-driven complex plasma.* Phys. Plasmas **9**, 4794-4803 (2002)

[51] S. A. Khrapak et al. *Ion drag force in complex plasmas.* Phys. Rev. E **66**, 046414 (2002)

[52] C. Zafiu, A. Melzer and A. Piel. *Measurement of the ion drag force on falling dust particles and its relation to the void formation in complex (dusty) plasmas.* Phys. Plasmas **10**, 1278-1282 (2003)

[53] S. A. Khrapak et al. *Comment on "Measurement of the ion drag force on falling dust particles and its relation to the void formation in complex (dusty) plasmas" [Phys. Plasmas **10**, 1278 (2003)].* Phys. Plasmas **10**, 4579-4581 (2003)

[54] C. Zafiu, A. Melzer and A. Piel. *Response to "Comment on 'Measurement of the ion drag force on falling dust particles and its relation to the void formation in complex (dusty) plasmas' " [Phys. Plasmas **10**, 4579 (2003)].* Phys. Plasmas **10**, 4582-4583 (2003)

[55] A. V. Ivlev et al. *Ion drag force in dusty plasmas.* Plasma Phys. Control. Fusion **46**, B267-B279 (2004)

[56] S. A. Khrapak et al. *Hybrid approach to the ion drag force.* Phys. Plasmas **12**, 042308 (2005)

[57] V. Yaroshenko et al. *Determination of the ion-drag force in a complex plasma.* Phys. Plasmas **12**, 093503 (2005)

[58] A. V. Ivlev et al. *Kinetic approach for the ion drag force in a collisional plasma.* Phys. Rev. E **71**, 016405 (2005)

[59] M. R. Akdim and W. J. Goedheer. *Modeling of self-excited dust vortices in complex plasmas under microgravity.* Phys. Rev. E **67**, 056405 (2003)

[60] W. J. Goedheer and M. R. Akdim. *Vortices in dust clouds under microgravity: A simple explanation.* Phys. Rev. E **68**, 045401 (R) (2003)

[61] O.S. Vaulina et al. *Formation of vortex dust structures in inhomogeneous gas-discharge plasmas.* Plasma Phys. Rep. **30**, 918-936 (2004)

[62] O. S. Vaulina et al. *Analysis of dust vortex dynamics in gas discharge plasma.* Phys. Scripta. Vol. T**107**, 224-228, (2004)

[63] M. Tribeche, K. Aoutou, and T. H. Zerguini. *Nonlinear dust phase-space vortices (holes) in charge-varying dusty plasmas.* Phys. Plasmas **12**, 032305 (2005)

[64] V. N. Tsytovich. *Dust plasma crystals, drops, and clouds.* Phys. Usp. **40**, 53-94 (1997)

[65] P. K. Shukla. *A survey of dusty plasma physics.* Phys. Plasmas **8**, 1791-1803 (2001)

[66] I. Lin et al. *Fine particles in dusty plasmas.* Vacuum **66**, 285-291 (2002)

[67] G. E. Morfill et al. *A review of liquid and crystalline plasmas–New physical states of matter?.* Plasma Phys. Control. Fusion **44**, B263-B277 (2002)

[68] V. N. Tsytovich, G. E. Morfill and H. Thomas. *Complex Plasmas I. Complex plasmas as unusual state of matter.* Plasma Phys. Rep. **28**, 623-651 (2002)

[69] G. E. Morfill, V. N. Tsytovich and H. Thomas. *Complex Plasmas II. elementary processes in complex plasmas.* Plasma Phys. Rep. **29**, 1-30 (2003)

[70] S. V. Vladimirov and K. Ostrikova. *Dynamic self-organization phenomena in complex ionized gas systems: new paradigms and technological aspects.* Phys. Rep. **393**, 175-380 (2004)

[71] R. L. Merlino and J. A. Goree. *Dusty Plasmas in the Laboratory, Industry, and Space.* Phys. Today **57**, 32-39 (2004)

[72] V. E. Fortov et al. *Dusty plasmas.* Phys. Usp. **47**, 447-492 (2004)

[73] A. V. Ivlev et al. *Complex (dusty) plasmas: Current status, open issues, perspectives.* Phys. Rep. **421**, 1-103 (2005)

[74] A. M. Ignatov. *Basics of Dusty Plasma.* Plasma Phys. Rep. **31**, 46-56 (2005)

[75] H. M. Thomas et al. *PKE-Nefedov - Complex plasma research on the international space station.* Microgravity Sci. Technol. **XVI**, 317-321 (2005)

[76] O. Heaviside. *Electromagnetic theory*, 3rd ed. (Chelsea Publ., New York, 1971)

[77] W. Gibbs. *The collected works of J. W. Gibbs, vol. 2.* (Yale Univ. Press, New Haven, 1957)

[78] I. V. Lindell. *Differential Forms in Electromagnetics.* (Wiley, New York, 2004)

[79] W. D. Niven. *The scientific papers of J. C. Maxwell.* (Dover, New York, 1890)

[80] R. P. Feynman. *The Feynman lectures on physics vol. 2: Mainly electromagnetism and matter.* (Addison-Wesley, Massachusetts, 1964)

[81] J. D. Jackson. *Classical electrodynamics*, 3rd ed. (Wiley, New York, 1999)

[82] B. Agdur and B. Enander. *Resonances of a microwave cavity partially filled with a Plasma.* J. Appl. Phys. **33**, 575-581 (1962)

[83] R. Eaves, T. Twardeck and S. Morin. *Determination of plasma electron-density distribution from the resonant frequencies of a parallel-plate cavity.* IEEE T. Antenn. Propag. **19**, 221-226 (1971)

[84] J. C. Maxwell. *A treatise on electricity and magnetism (vol. 1).* (Dover, New York, 1954)

[85] J. A. Stratton. *Electromagnetic theory.* (McGraw-Hill, New York, 1941)

[86] H. Mott-Smith and I. Langmuir. *The theory of collectors in gaseous discharges.* Phys. Rev. **28**, 727-763 (1926)

[87] D. A. Law et al. *Probe-induced particle circulation in a plasma crystal.* Phys Rev. Lett. **80**, 4189-4192 (1998)

[88] E. Thomas, K. Avinash and R. L. Merlino. *Probe induced voids in a dusty plasma.* Phys. Plasmas **11**, 1770-1774 (2004)

[89] M. Klindworth et al. *Dust-free regions around Langmuir probes in complex plasmas under microgravity.* Phys. Rev. Lett. **93**, 195002 (2004).

[90] D. J. Griffiths. *Introduction to electrodynamics.* (Prentice-Hall, New Jersey, 1999)

[91] L. D. Landau and E. M. Lifshitz. *Electrodynamics of continuous media.* (Pergamon, Oxford, 1960)

[92] H. H. Woodson and J. R. Melcher. *Electromechanical dynamics vol. 3: Elastic and fluid media.* (Wiley, New York, 1968)

[93] R. Courant and F. John. *Introduction to calculus and analysis, vol. II/1.* Reprint of the 1989 ed. (Springer, Berlin, 2000)

[94] H. Goldstein, C. Poole and J. Safko. *Classical mechanics.* (Addison Wesley, New York, 2000)

[95] R. Shankar. *Principles of quantum mechanics.* (Plenum, New York, 1994)

[96] W. Greiner. *Classical mechanics: Systems of particles and Hamiltonian dynamics.* (Springer, New York, 2003)

[97] L. N. Hand and J. D. Finch. *Analytical mechanics.* (Cambridge Univ. Press, Cambridge, 1998)

[98] J. R. Ellis. *Force and couple exerted on a moving electromagnetic dipole.* J. Phys. A **3**, 251-262 (1970)

[99] A. Engel and R. Friedrichs. *On the electromagnetic force on a polarizable body.* Am. J. Phys. **70**, 428-432 (2002)

[100] H. A. Pohl. *The motion and precipitation of suspensoids in divergent electric fields.* J. Appl. Phys. **22**, 869-871 (1951)

[101] H. A. Pohl. *Some effects of nonuniform fields on dielectrics.* J. Appl. Phys. **29**, 1182-1188 (1958)

[102] H. A. Pohl. *Dielectrophoresis.* (Cambridge Univ. Press, Cambridge, 1978)

[103] T. B. Jones. *Electromechanics of particles.* (Cambridge Univ. Press, New York, 1995)

[104] H. Morgan and N. G. Green. *AC electrokinetics: colloids and nanoparticles.* (Research Studies Press, Hertfordshire, 2003)

[105] H. Morgan, M. P. Hughes, and N. G. Green *Dielectrophoretic trapping of single sub-micrometre scale bioparticles.* J. Phys. D **31**, 2205-2210 (1998)

[106] A. Ramos et al. *AC electrokinetics: a review of forces in microelectrode structures.* J. Phys. D **31**, 2338-2353 (1998)

[107] H. Morgan, M. P. Hughes, N. G. Green. *Separation of submicron bioparticles by dielectrophoresis.* Biophys. J. **77**, 516-525 (1999)

[108] M. P. Hughes. *AC electrokinetics: applications for nanotechnology.* Nanotechnology **11**, 124-132 (2000)

[109] J. P. Huang et al. *Dielectrophoresis of charged colloidal suspensions.* Phys. Rev. E **67**, 021403 (2003)

[110] L. Dong, J. P. Huang, and K. W. Yu. *Theory of dielectrophoresis in colloidal suspensions.* J. Appl. Phys. **95**, 8321-8326 (2004)

[111] E. Salonen et al. *Dielectrophoresis of nanocolloids: A molecular dynamics study. Eur.* Phys. J. E **18**, 133-142 (2005)

[112] R. Hölzel et al. *Trapping single molecules by dielectrophoresis.* Phys. Rev. Lett. **95**, 128102 (2005)

[113] A. Ashkin. *Acceleration and trapping of particles by radiation pressure.* Phys. Rev. Lett. **24**, 156-159 (1970)

[114] A. Ashkin and J. Dziedzic. *Optical levitation by radiation pressure.* Appl. Phys. Lett. **8**, 283-285 (1971)

[115] A. Ashkin. *Trapping of atoms by resonance radiation pressure.* Phys. Rev. Lett. **40**, 729-732 (1978)

[116] S. Chu et al. *Experimental observation of optically trapped atoms.* Phys. Rev. Lett. **57**, 314-317 (1986)

[117] S. Chu. *Nobel Lecture: The manipulation of neutral particles.* Rev. Mod. Phys. **70**, 685-706 (1998)

[118] M. Wolter and A. Melzer. *Laser heating of particles in dusty plasmas.* Phys. Rev. E **71**, 036414 (2005)

[119] S. G. Brush. *Kinetic Theory vol. 2: Irreversible processes.* (Pergamon, Oxford, 1966)

[120] S. G. Brush. *Kinetic theory vol. 3: The Chapman-Enskog solution of the transport equation for moderately dense gases.* (Pergamon, Oxford, 1972)

[121] S. Chapman and T. G. Cowling. *The mathematical theory of non-uniform gases.* (University Press, Cambridge, 1970)

[122] C. Cercignani. *Mathematical methods in kinetic theory*, 2nd ed. (Plenum, New York, 1990)

[123] C. Cercignani. *The Boltzmann equation and its applications.* (Springer, New York, 1988)

[124] R. L. Liboff. *Introduction to the theory of kinetic equations.* (Wiley, New York, 1961)

[125] E. M. Lifshitz and L. P. Pitaevskii. *Physical kinetics.* (Pergamon, Oxford, 1981)

[126] Y. L. Klimontovich. *The statistical theory of non-equilibrium processes in a plasma.* (Pergamon, Oxford, 1967)

[127] Y. L. Klimontovich. *Kinetic theory of nonideal gases and nonideal plasmas.* (Pergamon, Oxford, 1982)

[128] J. Hirschfelder, C. Curtiss and R. Bird. *Molecular theory of gases and liquids*, 4th ed. (Wiley, New York, 1967)

[129] J. G. Kirkwood. *The statistical mechanical theory of transport processes II. Transport in gases.* J. Chem. Phys. **15**, 72-76 (1947)

[130] A. A. Vlasov. *Many-particle theory and its application to plasma.* (Gordon and Breach, New York, 1961)

[131] E. H. Holt and R. E. Haskell. *Foundations of plasma dynamics.* (Macmillan, New York, 1965)

[132] S. de Groot and P. Mazur. *Non-equilibrium thermodynamics.* (North-Holland, Amsterdam, 1963)

[133] A. E. Lifschitz. *Magnetohydrodynamics and spectral theory.* (Kluwer, Dordrecht, 1989)

[134] J. Goedbloed and S. Poedts. *Principles of magnetohydrodynamics.* (Cambridge Univ. Press, Cambridge, 2004)

[135] H. Alfvén. *Existence of electromagnetic-hydrodynamic waves.* Nature **150**, 405-406 (1942)

[136] H. Alfvén. *Cosmical electrodynamics*, 2nd ed. (Clarendon, Oxford, 1963)

[137] A. Brown, C. Smith, and A. Rennie. *Pumping of water with ac electric fields applied to asymmetric pairs of microelectrodes.* Phys. Rev. E **63**, 016305 (2001)

[138] N. G. Green et al. *Fluid flow induced by nonuniform ac electric fields in electrolytes on microelectrodes. III. Observation of streamlines and numerical simulation.* Phys. Rev. E **66**, 026305 (2002)

[139] A. Ramos et al. *Pumping of liquids with ac voltages applied to asymmetric pairs of microelectrodes.* Phys. Rev. E **67**, 056302 (2003)

[140] M. Karttunen, I. Vattulainen, and A. Lukkarinen. *Novel methods in soft matter simulations.* (Springer, Berlin, 2004)

[141] B. Spain. *Tensor calculus.* (Oliver and Boyd, Edinburgh, 1953)

[142] N. Rott. *Note on the history of the Reynolds number.* Annu. Rev. Fluid Mech. **22**, 1-11 (1990)

[143] J. E. Allen, R. Boyd and P. Reynolds. *The collection of positive ions by a probe immersed in a plasma.* Proc. Phys. Soc. **B70**, 297-304 (1956)

[144] I. B. Bernstein and I. N. Rabinowitz. *Theory of electrostatic probes in a low-density plasma.* Phys. Fluids **2**, 112-121 (1959)

[145] S. H. Lam. *A general theory for the flow of weakly ionized gases.* AIAA J. **2**, 256-262 (1964)

[146] S. H. Lam. *Unified theory for the Langmuir probe in a collisionless Plasma.* Phys. Fluids **8**, 73-87 (1965)

[147] F. F. Chen. *Numerical computations for ion probe characteristics in a collisionless plasma.* Plasma Phys. **7**, 47-67 (1965)

[148] J. G. Laframboise and L. W. Parker. *Probe design for orbit-limited current collection.* Phys. Fluids **16**, 629-636 (1973)

[149] E. C. Whipple. *Potentials of surfaces in space.* Rep. Prog. Phys. **44**, 1198-1250 (1981)

[150] J. Goree. *Charging of particles in a plasma.* Plasma Sources Sci. Technol. **3**, 400-406 (1994)

[151] D. B. Graves et al. *Charging, transport and heating of particles in radiofrequency and electron cyclotron resonance plasmas.* Plasma Sources Sci. Technol. **3**, 433-441 (1994)

[152] A. Barkan, N. D'Angelo, and R. L. Merlino. *Charging of dust grains in a plasma.* Phys. Rev. Lett. **73**, 3093-3096 (1994)

[153] T. Matsoukas and M. Russell. *Particle charging in low-pressure plasmas.* J. Appl. Phys. **77**, 4285-4292 (1995)

[154] E. Thomas and M. Watson. *Charging of silica particles in an argon dusty plasma.* Phys. Plasmas **7**, 3194-3198 (2000)

[155] S. V. Vladimirov, S. A. Maiorov and N. F. Cramer. *Dynamics of the charging and motion of a macroparticle in a plasma flow.* Phys. Rev. E **63**, 045401 (2001)

[156] R. V. Kennedy and J. E. Allen. *The floating potential of spherical probes and dust grains. Part 1: Radial motion theory.* J. Plasma Phys. **67**, 243-250 (2002)

[157] R. V. Kennedy and J. E. Allen. *The floating potential of spherical probes and dust grains. Part 2: Orbital motion theory.* J. Plasma Phys. **69**, 485-506 (2003)

[158] A. A. Samarian and S. V. Vladimirov. *Charge of a macroscopic particle in a plasma sheath.* Phys. Rev. E **67**, 066404 (2003)

[159] P. Bryant. *Floating potential of spherical probes and dust grains in collisional plasmas.* J. Phys. D **36**, 2859-2868 (2003)

[160] S. A. Khrapak et al. *Particle charge in the bulk of gas discharges.* Phys. Rev. E **72**, 016406 (2005)

[161] X. Wang and A. Bhattacharjee. *On a kinetic theory for strongly coupled dusty plasmas.* Phys. Plasmas **3**, 1189-1191 (1996)

[162] D. Z. Wang and J. Q. Dong. *Kinetics of low pressure rf discharges with dust particles.* J. Appl. Phys. **81**, 38-42 (1997)

[163] S. A. Trigger and P. Schram. *Kinetic theory of the charging process in dusty plasmas.* J. Phys. D **32**, 234-239 (1999)

[164] V. N. Tsytovich and U. de Angelis. *Kinetic theory of dusty plasmas I. General approach.* Phys. Plasmas **6**, 1093-1106 (1999)

[165] V. N. Tsytovich and U. de Angelis. *Kinetic theory of dusty plasmas II. Dust-plasma particle collision integrals.* Phys. Plasmas **7**, 554-563 (2000)

[166] P. Ricci et al. *Plasma kinetics in dusty plasmas.* Phys. Plasmas **8**, 769-766 (2001)

[167] P. Schram et al. *Statistical theory of dusty plasmas: Microscopic equations and Bogolyubov-Born-Green-Kirkwood-Yvon hierarchy.* Phys. Rev. E **63**, 016403 (2001)

[168] V. N. Tsytovich and U. de Angelis. *Kinetic theory of dusty plasmas III. Dust-dust collision integrals.* Phys. Plasmas **8**, 1141-1153 (2001)

[169] V. N. Tsytovich and U. de Angelis. *Kinetic theory of dusty plasmas IV. Distribution and fluctuations of dust charges.* Phys. Plasmas **9**, 2497-2506 (2002)

[170] P. Schram, S. A. Trigger, and A. G. Zagorodny. *New microscopic and macroscopic variables in dusty plasmas.* New J. Phys. **5**, 27 (2003)

[171] V. N. Tsytovich and U. de Angelis. *Kinetic theory of dusty plasmas V. The hydrodynamic equations.* Phys. Plasmas **11**, 496-506 (2004)

[172] V. N. Tsytovich et al. *Kinetic theory of partially ionized complex (dusty) plasmas.* Phys. Plasmas **12**, 082103 (2005)

[173] A. V. Ivlev et al. *Kinetics of ensembles with variable charges.* Phys. Rev. E **70**, 066401 (2004)

[174] U. de Angelis et al. *Stochastic heating of dust particles with fluctuating charges.* Phys. Plasmas **12**, 052301 (2005)

[175] S. K. Zhdanov, A. V. Ivlev, and G. E. Morfill. *Non-Hamiltonian dynamics of grains with spatially varying charges.* Phys. Plasmas **12**, 072312 (2005)

[176] A. V. Ivlev et al. *Generalized kinetic theory of ensembles with variable charges.* Phys. Plasmas **12**, 092104 (2005)

[177] R. Kompaneets et al. *Dust clusters with non-Hamiltonian particle dynamics.* Phys. Plasmas **13**, 072104 (2006)

[178] H. Brezis and F. Browder. *Partial differential equations in the 20th century.* Adv. Math. **135**, 76-144 (1998)

[179] R. Courant. *Variational methods for the solution of problems of equilibrium and vibrations.* Bull. Amer. Math. Soc. **49**, 1-23 (1943)

[180] J. Hadamard. *Four lectures in mathematics.* (Columbia Univ. Press, New York, 1915)

[181] P. Monk. *Finite element methods for Maxwell's equations.* (Oxford Univ. Press, Oxford, 2003)

[182] R. Gruber and J. Rappaz. *Finite element methods in linear ideal magneto-hydrodynamics.* (Springer, Berlin, 1985)

[183] J. Jianming. *The finite element method in electromagnetics.* (Wiley, New York, 1993)

[184] V. Girault and P. Raviart. *Finite element approximation of the Navier-Stokes equations.* (Springer, Berlin, 1981)

[185] J. Oden. *Finite elements of nonlinear continua.* (McGraw-Hill, New York, 1972)

[186] J. Oden. *Finite elements: an introduction, in Handbook of numerical analysis, vol 2: Finite element methods (part 1). P. Ciarlet and J. Lions eds.* (Elsevier, North-Holland, 1991)

[187] G. Strang and G. Fix. *An analysis of the finite element method.* (Prentice-Hall, Englewood Cliffs, 1973)

[188] O. Zienkiewicz and R. Taylor. *Finite Element Method: Vol. 2- Solid mechanics*, 4th ed. (Butterworth Heinemann, London, 2000)

[189] S. Brenner and L. Scott. *The mathematical theory of finite element methods.* (Springer, New York, 1994)

[190] C. Johnson. *Numerical solution of partial differential equations by the finite element method*. (Cambridge Univ. Press, Cambridge, 1987)

[191] P. G. Ciarlet. *The finite element method for elliptic problems*. - 2nd printing. (North-Holland, Amsterdam, 1980)

[192] R. Adams. *Sobolev spaces*. (Academic Press, New York, 1975)

[193] W. Ritz. *Über eine neue Methode zur Lösung gewisser Variationsprobleme der mathematischen Physik*. Z. Angew. Math Mech. **135**, 1-61 (1908)

[194] Lord Rayleigh. *The theory of sound*, 2nd ed. (Dover, New York, 1945)

[195] B. Galerkin. *Series solution of some problems in elastic equilibrium of rods and plates* (in Russian). Vestnik inzhenerov i Tekhnikov **19**, 897-908 (1915)

[196] G. Lapenta. *Dipole moments on dust particles immersed in anisotropic plasmas*. Phys. Rev. Lett. **75**, 4409-4412 (1995)

[197] A. V. Ivlev et al. *Potential of a dielectric particle in a flow of a collisionless plasma*. Phys. Plasmas **6**, 1415-1420 (1999)

[198] D. Resendes. *Dipolar interaction in a colloidal plasma*. Phys. Rev. E **61**, 793-800 (2000)

[199] O. Ishihara, S. Vladimirov and N. Cramer. *Effect of a dipole moment on the wake potential of a dust grain in a flowing plasma*. Phys. Rev. E **61**, 7246-7248 (2000)

Acknowledgements

I would like to thank Prof. Dr. Dr.h.c. Gregor Morfill for the invitation to join the theory group at the Max-Planck Institute for Extraterrestrial Physics. This gave me the opportunity to do research in the fascinating field of complex plasmas. The granted Max-Planck fellowships (first as a PhD. student and later as a researcher) are also thankfully acknowledged.

I also appreciate the motivating conversations with colleges and friends from MPE, MPA, ESO and IPP about life, physics, and a long list of etceteras.

Last but not least, I would like to express my gratitude to my family, whom even without understanding what I was doing, always gave me all their support.